UNIVERSITY *of the*
WESTERN CAPE

PETROPHYSICAL EVALUATION OF SANDSTONE RESERVOIR OF WELL E-AH1, E-BW1 AND E-L1 CENTRAL BREDASDORP BASIN, OFFSHORE SOUTH AFRICA

A Thesis in Petroleum Geology

By

Moses Magoba

Submitted in fulfillment of the requirements for the degree of
M.Sc. (Masters) in the Department of Earth Sciences,
University of the Western Cape

May 2014

Supervised by Dr. M. Opuwari

Key Words

Permeability

Porosity

Hydrocarbon

Facies

Reservoirs

Petrophysics

Sandstone

Abstract

The Bredasdorp basin is a sub-basin of the greater Outeniqua basin. It is located off the south coast, Southeast of Cape Town, South Africa. This basin is one of the largest hydrocarbon (mainly gas) producing basins within Southern Africa. The petrophysical characteristic of the E-block sandstone units within the Bredasdorp basin has been studied to evaluate their hydrocarbon potential. The data sets used in this research were wireline logs (Las format), core data, and geological well completion reports. The three studied wells are E-AH1, E-BW1 and E-L1. The evaluated interval ranges from 2000.33m to 3303.96m in depth with reference to Kelly bushing within the wells. The sandstone reservoirs of the Bredarsdorp basin are characterized by a range of stacked and amalgamated channels. They originated from materials eroded from pre-existing high stand shelf sandstone and transported into the central Bredarsdorp basin by turbidity current. These sandstones are generally in both synrift and drift section. The basin is thought to have developed from fan deltas and stream overwhelmed to water dominated delta. River dominated deltaic system progresses southward over the Northern edge of the central Bredasdorp basin. The Interactive Petrophysics (IP) software has been used extensively throughout the evaluation and development of interpretation model. The lithofacies of the rock units were grouped according to textural and structural features and grain sizes of well (E-AH1, E-BW1 and E-L1). Four different facies (A, B, C and D) were identified from the cored intervals of each well. Facies A was classified as a reservoir and facies B, C and D as a non-reservoir. Detailed petrophysical analyses were carried out on the selected sandstone interval of the studied wells. The cut-off parameters were applied on the seven studied sandstone interval to distinguish between pay and non-pay sand and all intervals were proved to be producing hydrocarbon. Volume of clay, porosity, water saturation and permeability were calculated within the pay sand interval. The average volume of clay ranged from 23.4% to 25.4%. The estimated average effective porosity ranged from 9.47% to 14.3%. The average water saturation ranged from 44.4% to 55.6%. Permeability ranged from 0.14mD to 79mD. The storage and flow capacity ranged from 183.2scf to 3852scf and 2.758mD-ft to 3081mD-ft respectively. The geological well completion reports classify these wells as a gas producing wells. E-L1 is estimated to have a potential recoverable gas volume of 549.06 cubic feet, E-BW1 is estimated to have 912.49 cubic feet and E-AH1 is estimated to have 279.69 cubic feet.

Declaration

I declare *The petrophysical evaluation of sandstone reservoir of well E-AH1, E-BW1 and E-L1 of Central Bredasdorp Basin, Offshore south Africa* is my own work, that it has not been submitted before for any degree or examination in any other university, and that all the sources I have used or quoted have been indicated and acknowledged by means of complete references.

Moses Magoba May 2014

……

Signature

Acknowledgements

I wish to express my deepest gratitude to my supervisor DR M.OPUWARI for his patience, assistance and guidance throughout this study. Special thanks also goes to Petroleum Agency of South Africa (PASA) for making the data available to conduct this study.

I would like to thanks my big brother DR REMBULUWANI MAGOBA for taking his time to review this work, his input and also the motivation he gave me throughout this study.

A special thanks to all my fellow Masters students in geology department at the University of the Western Cape for their encouragement and support. I give my heartfelt thanks to HAKUNDWI MANDENDE, SEDZANI NETHENZHENI, HAAJIERAH MOSAVEL, ENERST, AYODELE LASISI, LIZEKA SIKUTSHWA and ROZWIVHONA MAGOBA for the very supportive role they have played during my study at the University of Western Cape. Lastly, I dedicate this work to my parents ALFRED and ELISA MAGOBA without them this would not have been possible.

TO GOD BE THE GLORY.

Table of contents

Key words…….. ... i
Abstract……. ii
Declaration…… iv
Acknowledgements……... v
List of Figures……ix
List of Tables……...… xii
List of Appendices…….. xiii

Chapter 1: Introduction.....……..... 1
1.1 Background Information..... 1
1.2 Basics..... 1
1.2.1 Thesis Outline 1
1.2.2 Chapter 2 2
1.2.3 Chapter 3, 4, and 5 2
1.2.4 Chapter 6, 7 and 8 2
1.3 Location and description of the study area..... 2
1.4 Research Aims..... 5
1.5 Literature Review 5
Chapter 2: Geological background of the Bredasdorp basin…… 7
2.1 Offshore Basins 7
2.2 Tectonic Setting of the Outeniqua Basin..... 10
2.3 Depositional Environment..... 11
2.4 Sequence Stratigraphy of the Bredasdorp Basin 12
2.5 Structural development of the Bredasdorp basin..... 14
2.6 Hydrocarbon plays of the Bredarsdorp Basin..... 15
2.6.1 Source Rocks..... 15
2.6.2 Reservoir rock 15
2.6.3 Seal and Trap..... 16
Chapter 3: Methodology…… 17
3.1 Log editing..... 18
3.1.1 Environmental Correction 18
3.1.2 Log splicing..... 19
3.2 Identification of possible sandstone Reservoir..... 20

3.3 Determination of m, a, n and Rw parameters from standalone picket plots 21
Chapter 4: Wireline logging 23
4.1 Introduction 23
4.2 Characteristics of the selected wireline logs 23
4.2.1 Gamma Ray Log (GR) 23
4.2.2 Neutron Log 24
4.2.3 Density Log 24
4.2.4 Combination of Neutron-Density Logs 25
4.2.5 Resistivity Log 25
4.2.6 Sonic Log 25
4.2.7 Caliper Log 25
Chapter 5: Conventional core analysis and interpretation of well logs 27
5.1 Introduction 27
5.2 Conventional core analysis 27
5.2.1 Intervals cored 28
5.3 Lithofacies Description 33
5.3.1 Analysis and Interpretation of Results 33
5.4 Analysis and Interpretation of Results 37
5.4.1 Grain Density 37
5.4.2 Porosity Interpretation 41
5.4.3 Core permeability Interpretation 47
5.5 Porosity versus permeability relationship 54
5.5.1 Well E-AH1 POROPERM relationship 55
5.5.2 Well E-BW1 POROPERM relationship 56
5.5.3 Well E-L1 POROPERM relationship 57
5.6 Fluid Saturation Interpretation 58
5.6.1 Well E-AH1 fluid saturation 58
5.6.2 Well E-BW1 fluid saturation 59
5.6.3 WellE-L1 fluid saturation 60
5.7 Interpretation of Geophysical wireline logs 61
5.7.1 Well E-AH1 wireline logs interpretation 66
5.7.2 Well E-BW1 wireline logs interpretation 66
5.7.3 Well E-L1 wireline logs interpretation 67
Chapter 6: Petrophysical models 68

6.1 Volume of shale determination 68
6.2 Porosity and Water saturation determination 70
6.3 Determination of initial fluid saturation parameters 74
6.3.1 Water saturation exponent (n) 74
6.3.2 Tortuosity factor (a) 74
6.3.3 Cementation exponent (m) 75
6.3.4 Formation water resistivity 75
6.4 Permeability determination from well logs 75
Chapter 7: Cut-off determination 84
7.1 Porosity and permeability cut-off determinations 84
7.2 Volume of shale cut-off determination 87
7.3 Water saturation cut-off determination 88
7.4 Net-pay determination 89
7.5 Storage capacity, flow capacity and reservoir hydrocarbon volume calculations 96
7.5.1 Storage and flow capacity calculations 96
7.5.2 Recoverable hydrocarbon volume determination 97
7.6 General trend of petrophysical properties of pay sand within the field in 3-D view 98
Chapter 8: Conclusion 102
8.1 Deductions 102
8.2 Recommendations 103
References 105
Appendices 108

List of Figures

Figure 1.1 Map showing the location of the study area (modified from the Petroleum Agency SA Brochure, 2004)..... 3
Figure 1.2 Well location map (UTM Co-ordinates) generated in PETREL..... 4
Figure 2.1 Formation of a half-graben from a series of normal faults dipping in the same direction (modified from Houston, 1986) 8
Figure 2.2: Western, eastern and southern offshore zones of South Africa (Modified from Broad, 2004)..... 9
Figure 2.3: Oblique rift half-grabens sub-basins of Outeniqua Basin: Bredasdorp, Pletmos, Gamtoos, and Algoa (modified from Broad, 2004). 10
Figure 2.4: The rift phase in the Late Jurassic – Lower Valanginian showing the break -up of Africa, Madagascar and Antarctica (modified from Broad, 2004). 11
Figure 2.5: Prograding complex terminating canyon filling episode (Modified from Broad, 2004)..... 13
Figure 2.6: Basin floor fan (Lowstand fan) on canyon floor (Modified from Broad, 2004) ... 13
Figure 2.7: Channel-Levee complex deposited on basin floor fan (Modified from Broad, 2004)..... 14
Figure 3.1: Flow chat summarising the methodology..... 17
Figure 3.2: Example of Gamma ray log before splicing 19
Figure 3.3: Example of Gamma ray log after splicing..... 20
Figure 3.4: Example of the selected potential sandstone reservoir. 21
Figure 3.5: Standalone picket plot used to determine the above mentioned parameters. 22
Figure 5.1: Log plot showing two distinctive lithofacies (Track 4) identified. 34
Figure 5.2: Log plot showing the identified lithofacies (track 4) of the cored interval. 35
Figure 5.3: Log plot showing three distinctive lithofacies (Track 4) identified. 36
Figure 5.4: Grain density histogram plot of well E-AH1..... 38
Figure 5.5: Grain density histogram plot of well E-BW1. 39
Figure 5.6: Grain density histogram plot of well E-L1. 40
Figure 5.7: Multi well density histogram plot for E-AH1, E-BW1 and E-L1. 41
Figure 5.8: Core porosity histogram plot for E-AH1 well. 43
Figure 5.9: Well E-AH1 core porosity plot (Track 4)..... 43
Figure 5.10: Core porosity histogram plot. 44

Figure 5.11: Core porosity plot (Track 3). 45
Figure 5.12: Core porosity histogram plot. 46
Figure 5.13: Core porosity versus plot (Track 3). 46
Figure 5.14: Multi-well core porosity distribution. 47
Figure 5.15: Core permeability histogram plot. 49
Figure 5.16: Core permeability (Core KL) plot (Track 3). 50
Figure 5.17: Core Permeability plot (Track 4). 51
Figure 5.18: Core permeability histogram plot. 52
Figure 5.19: Core permeability plot (Track 4). 52
Figure 5.20: Core permeability histogram plot. 53
Figure 5.21: Core permeability distribution histogram plot. 54
Figure 5.22: Poroperm relationship cross plot (Glover 2009). 55
Figure 5.23: Porosity versus permeability cross-plot of E-AH1. 56
Figure 5.24: Porosity versus permeability cross-plot of E-L1. 56
Figure 5.25: Porosity versus permeability cross-plot. 57
Figure 5.26: Well E-AH1 fluid saturation plot (track5). 58
Figure 5.27: Well E-BW1 fluid saturation plot (track 3). 59
Figure 5.28: Well E-L1 fluid saturation plot (Resistivity rack). 61
Figure 5.29: Log plot showing different log curves of well E-AH1 in different tracks 63
Figure 5.30: First reservoir interval of E-BW1. 64
Figure 5.31: Second reservoir interval of E-BW1 64
Figure 5.32: Third reservoir interval of E-BW1. 65
Figure 5.33: First and second reservoir interval of well E-L1. 65
Figure 5.34: Third reservoir interval of well E-L1 66
Figure 6.1: Multi-well gamma-ray histogram plot 69
Figure 6.2: Comparison of different methods used for volume of shale determination (Irfan Saputra, 2008) 70
Figure 6.3: Example of the calibration of log curves with the core data. 72
Figure 6.4: Example of the selected log curves that best fit the core data trend. 72
Figure 6.5: Porosity versus Permeability cross plot for well E-L1. 77
Figure 6.6: Porosity versus Permeability cross plot of well E-BW1. 78
Figure 6.7: Porosity versus Permeability cross plot of well E-AH. 79
Figure 6.8: Log curves plot displaying predicted (track 5) permeability of well E-AH1. 80

Figure 6.9: Log curves plot displaying predicted permeability (track11) of well E-BW1, reservoir 1. 80
Figure 6.10: Log curves plot displaying predicted permeability (track11) of well E-BW1, reservoir 2. 81
Figure 6.11: Log curves plot displaying predicted permeability (track11) of well E-BW1, reservoir 3. 81
Figure 6.12: Log curves plot displaying predicted permeability (track11) of well E-L1, reservoir 1 and 2. 82
Figure 6.13: Log curves plot displaying predicted permeability (Track 11) of well E-L1, zone 3. 83
Figure 7.1: Porosity versus permeability cross plot for cut-off determination. 85
Figure 7.2: Core permeability histogram plot for all study wells. 85
Figure 7.3: Core porosity histogram plot for all wells. 86
Figure 7.4: Volume of shale versus porosity and gamma ray plot. 87
Figure 7.5: Multi-well porosity versus water saturation cross plot for cut-off determination. 88
Figure 7.6: Multi-well water saturation frequency distribution cross plot. 89
Figure 7.7: Well E-AH1 showing calculated reservoir and pay flags. 91
Figure 7.8: Well E-BW1 showing calculated reservoir and pay flags of reservoir 1. 92
Figure 7.9: Well E-BW1 showing calculated reservoir and pay flags of reservoir 2. 92
Figure 7.10: Well E-BW1 showing calculated reservoir and pay flags of reservoir 3. 93
Figure 7.11: Well E-L1 showing calculated reservoir and pay flags of reservoir 1. 94
Figure 7.12: Well E-L1 showing calculated reservoir and pay flags of reservoir 2. 94
Figure 7.13: Well E-L1 showing calculated reservoir and pay flags of reservoir 3. 95
Figure 7.14: 3-D parameter view showing average volume of clay pay within the field. 99
Figure 7.15: 3-D parameter view showing average pay porosity within the field. 100
Figure 7.16: 3-D parameter view showing average water saturation clay within the field.... 101

List of Tables

Table 5.1: Results obtained from the conventional core analysis of well E-AH1. 29
Table 5.2: Results obtained from the conventional core analysis of well E-BW1..... 31
Table 5.3: Results obtained from the conventional core analysis of well E-L1..... 32
Table 5.4: Matrix density of common lithology (Source: Schlumberger, 2013) 37
Table 5.5: Classification of the permeability of a reservoir 48
Table 6.1: Parameters used to calculate volume of clay within the reservoir intervals. 69
Table 6.2: Basic log analysis parameters calculated from the standalone picket plots..... 75
Table 7.1: Predicted permeability of the evaluated reservoirs for each study well 86
Table 7.2: Petrophysical reservoir averages report 90
Table 7.3: Petrophysical reservoir averages report. 91
Table 7.4: Petrophysical reservoir averages report. 93
Table 7.5: Summary results of the calculated flow and storage capacity 96
Table 7.6: Calculated reservoir hydrocarbon volume of each reservoir 97

List of Appendices

Appendix A: Standalone pickets plot for wells

Appendix B: Gamma ray histogram plots

Appendix C: Calculated volume of clay, porosity and Water saturation curves

Appendix D: Wells correlation

Appendix E: Storage and flow capacity calculations

Appendix F: Reservoir hydrocarbon volume in acre foot of rock calculations

Appendix G: Core photographs

Chapter 1

1 Introduction

1.1 Background Information

Petrophysics is regarded as the process of characterizing the physical and chemical properties of the rock-pore-fluid system through the integration of geological environment, geophysical well logs, reservoir rock and fluid sample analyses and their production histories. In simple terms petrophysics is about the study of well logs, including rock principles and their interactions with the fluids (gaseous or liquid hydrocarbons) (Rider, 2002). Geophysical well logs are a continuous recording of a geophysical parameter along a borehole. A reservoir rock is a porous and permeable rock that contains interconnected pores or holes that occupy the areas between the mineral grains of the rock (Rider, 2002). Depending on their geological origin these rocks are usually sandstone or carbonate rocks (Rider, 2002).

A petrophysicist is the authorized user of the well log, and his interest is strictly quantitative. The logs are used for the calculation of porosity, water saturation, moveable hydrocarbon, hydrocarbon density and other factors related to quantification of the amount of hydrocarbons in a reservoir for estimates of reserves (Rider, 2002). Most of the reservoir rocks contain only a small percentage (approximately 15%) of a typical well, and out of this 15% only a small fraction contains hydrocarbons and is therefore very crucial to the petrophysicist. Petrophyisics is widely used in the oil and gas industry during the evaluation of hydrocarbons within the reservoirs.

1.2 Basics

1.2.1 Thesis Outline

This thesis embodies the written report of the study work carried out to assess the petrophysical evaluation of sandstone reservoir of well E-AH1, E-BW1 and E-L1 in the central part of the Bredasdorp Basin and consist of eight chapters.

1.2.1.1 Chapter 1

Chapter one gives the broad overview of what the thesis is all about and presents the research framework background, aims and the location of the study area. Consulted publications

relating to general geology, stratigraphy and characterization of reservoir rocks in the study area were discussed under literature review.

1.2.2 Chapter 2

Chapter two is all about the presentation of the general description and a broader general perspective of the area.

1.2.3 Chapter 3, 4, and 5

Chapter three lay out the methodologies which were used to obtain the results and in writing up the thesis. Chapter four is focused on the theory of the selected wireline logs used in the study. Chapter five is focused on the core descriptions and interpretation of the wireline logs within the cored and non-cored intervals of the studied wells.

1.2.4 Chapter 6, 7 and 8

Chapter 6 discussed the petrophysical models used to obtain the volume of shale/clay, porosity, water saturation and permeability results. Chapter 7 discussed the determination of the cut-off values used to attain the desired results. Chapter 8 gives the conclusion of the work and the recommendations.

1.3 Location and description of the study area

The study range is located inside the central Bredasdorp Basin which covers roughly 18,000 km^2 underneath the Indian Ocean along the South Coast of South Africa, Southwest of Mossel Bay. The basin is basically filled with upper Jurassic, lower Cretaceous, marine strata, post Cretaceous and Cenozoic unique rocks (Schalkwyk, 2005).

The study area is bounded in the East and West (Latitude) by geographical co-ordinates with reference to meridian whereas the North and South (Longitude) is bounded by geographical coordinates with reference to the equator. Well E-AH1 is located at 35^0 11’ 13. 40” South and 21^0 08’ 37.07” East. E-BW1 borehole is located 93km southwest of the F-A platform at a geographically coordinates of 35^0 09’ 12. 04” S and 21^0 11’ 25. 85” E. E-L1 is situated in the west central part of the basin, 84km South-South-West of Stilbaai, off the central coast of South Africa at a geographical coordinates of 35^0 06’ 08. 20’’ S and 21^0 11’ 43.46” E.

Figure 1.1 and 1.2 shows the location of the Bredasdorp Basin and the position of the studied wells.

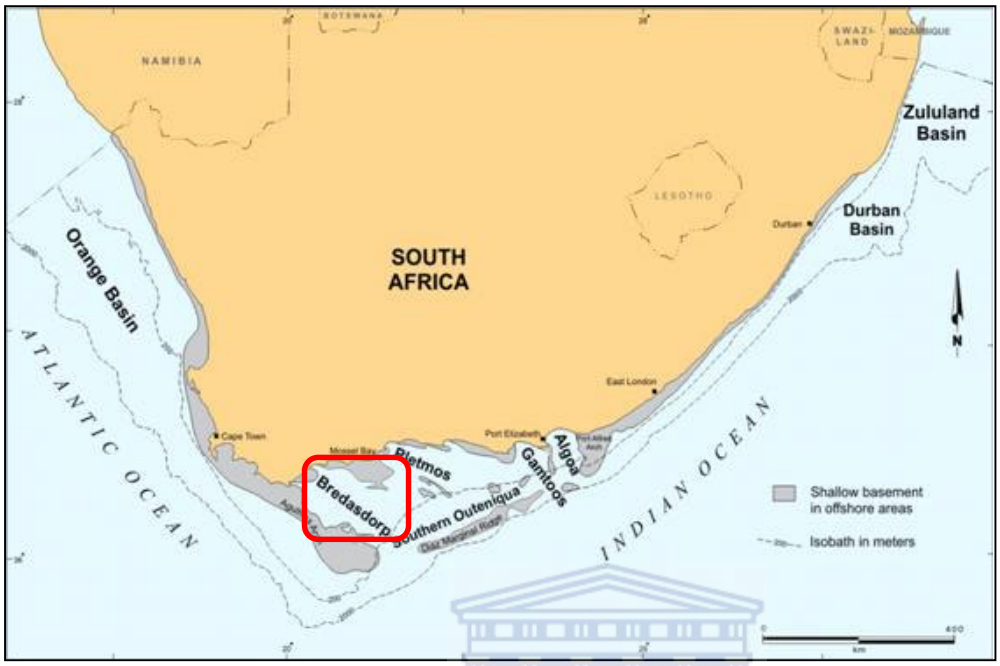

Figure 1.1 Map showing the location of the study area (modified from the Petroleum Agency SA Brochure, 2004)

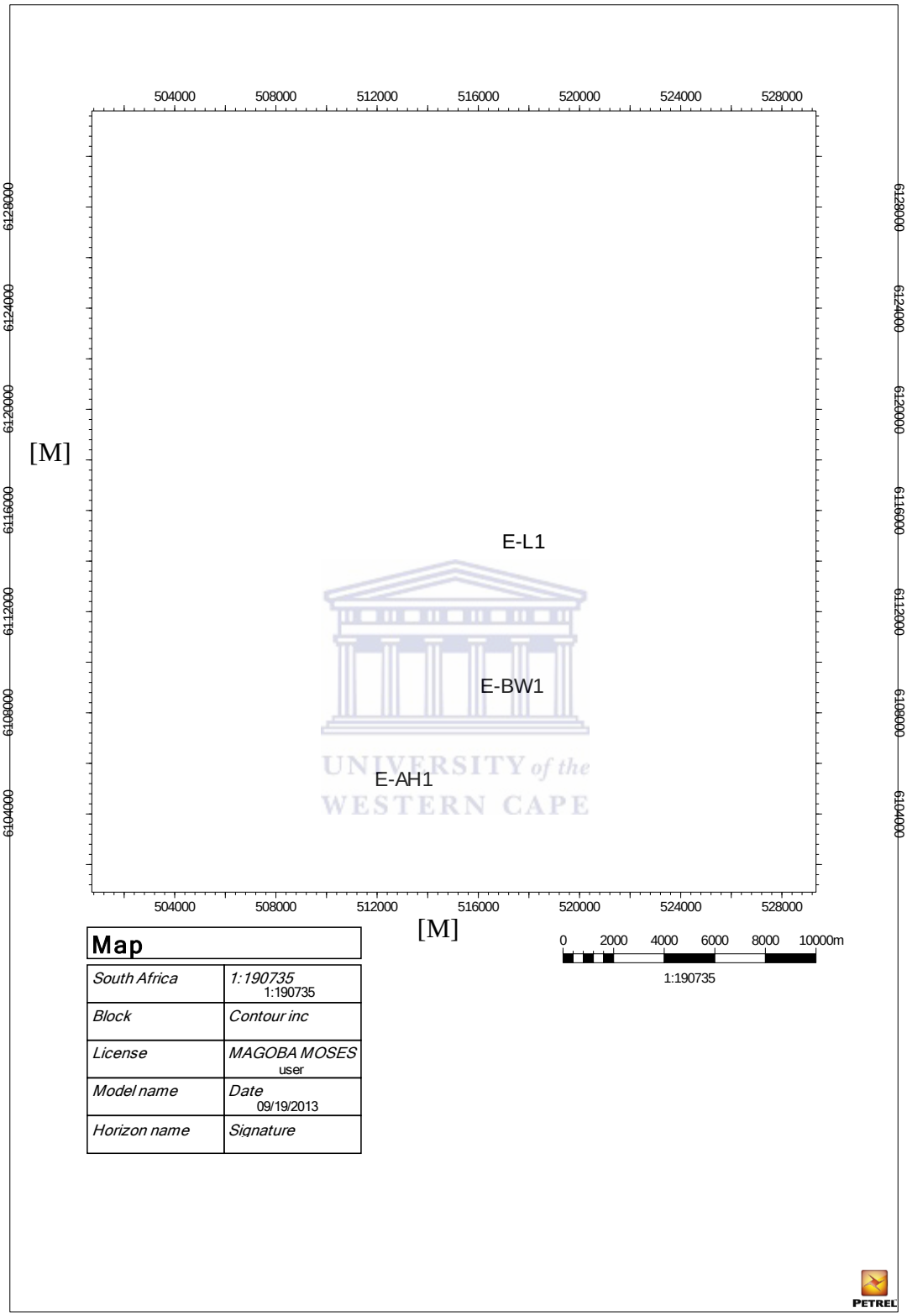

Figure 1.2 Well location map (UTM Co-ordinates) generated in PETREL.

1.4 Research Aims

The research is aimed at employing the expansive use of petrophysical analysis in the evaluation of the selected sandstone reservoirs of central Bredasdorp Basin. The physical rock properties, for example, lithology, fluid type, facies classification and hydrocarbon bearing zone are qualitatively characterized while different parameters, for example, porosity, permeability, water saturation and hydrocarbon saturation have been assessed for selected reservoir intervals. Wireline log data provided by the Petroleum Agency South Africa (PASA) was further used to recognize permeable zones, to determine depth and thickness of zones and to estimate generation potential.

The strategic aims of this research were to:

- Identify sandstone reservoirs- from Gamma ray logs
- Calculate volume of clay from gamma ray log within the studied reservoirs
- Calculate porosity and water saturation of the studied reservoirs by means of calibrating core data with the wireline logs
- Facies classification of the selected cored interval within the wells
- Estimate permeability of the studied reservoirs by using multiple variable regression method
- Calculate storage and flow capacity of the hydrocarbon producing intervals
- Estimate recoverable hydrocarbon of the producing intervals

1.5 Literature Review

The Bredasdorp Basin has been well studied and the literature is readily available relating to geology, stratigraphy, structural features and hydrocarbon potential of reservoir rocks.
Sandstone reservoirs in the Bredasdorp Basin are portrayed by a reach of stacked and amalgamated channels and projections, started from materials disintegrated from prior high stand rack sandstones and transported into the central basin turbidity current (Petroleum Agency of South Africa Brochure, 2005). Generally, the presence of sandstone reservoirs is seen in both Synrift and drift section (PASA, 2005).

The principal marine sandstones transpire inside the synrift progression, where they are interbedded with lagoonal and fluvial claystones (PASA, 2005). A thick marginal marine

sandstone complex caps the sequence. The complex is well known boreholes on the flanks of the basin and is of promptly Cretaceous age. These sandstones are believed to have formed the main gas reservoirs of the North flank gas field where the F-A gas field has been established by SOEKOR (now Petroleum South Africa). The fracture fill truncated by the rift/drift (1At1) which is most erosive on the basin flanks. The synrift progression is broadly faulted and folded in places (Burden, 1992).

The particular ocean-level falls throughout promptly Aptian and mid-Albian brought about material eroded from previous highstand rack sandstones and transported into the central basin by turbidity momentums from the west-southwest (Turner et al., 2000).

Mcaloon et al. (2000) investigated core, well logs and dip information and reasoned that the enormous amalgamated profound marine sandstone, which make up a bigger part of sandstone reservoirs, represent extensive mass flow deposit.

Global sea level changes overlaid on regional tectonism has largely controlled the pattern of the sediment distribution in the Bredasdorp Basin (Haq et al., 1987) such tectonic control on the sediment distribution is of great importance because some of the sediments in the basin are potential source rocks for hydrocarbons and others are possible reservoir rocks (Davies, 1997)

Chapter 2

2 Geological Background of the Bredasdorp Basin

The Bredasdorp Basin is a sub-basin of the Outeniqua Basin located in Southeast of Cape Town and West Southwest of Port Elizabeth, South coast of the Republic of South Africa. From various geological studies, the Bredasdorp Basin is said to have been shaped as a consequence of extensional scenes throughout the introductory phases of rifting in the Jurassic. The basin acted as a neighborhood depocentre and was at first infilled with Late Jurassic and Early Cretaceous shallow -marine and continental sediments (Turner et al., 2000).

2.1 Offshore Basins

The seaward basins of South Africa have been separated into three different tectonostratigraphic zones: western, southern and eastern seaward and have been created in the Permo-Triassic –Jurassic period or prior (Petroleum Agency SA Handbook, 2004/2005). Bredasdorp Basin comprises of an arrangement of Eclon sub-basin which all comprises of half grabens and is of a combination of thicknesses.

Half-graben feature is shaped when normal faults inside a sedimentary basin are dipping in the same bearing making adjacent fault blocks to descend and tilt with respect to the fault next to it (Figure 2.1).

The southern edge, known as the Outeniqua Basin, is essentially exchange of pullapart basins and transformed edges. The Bredasdorp, Pletmos, Gamtoos and Algoa basins are the sub-basins of the Outeniqua Basin (Figure 2.2). They show rift halfgraben characteristic overlaid by variable thicknesses of drift sediments.

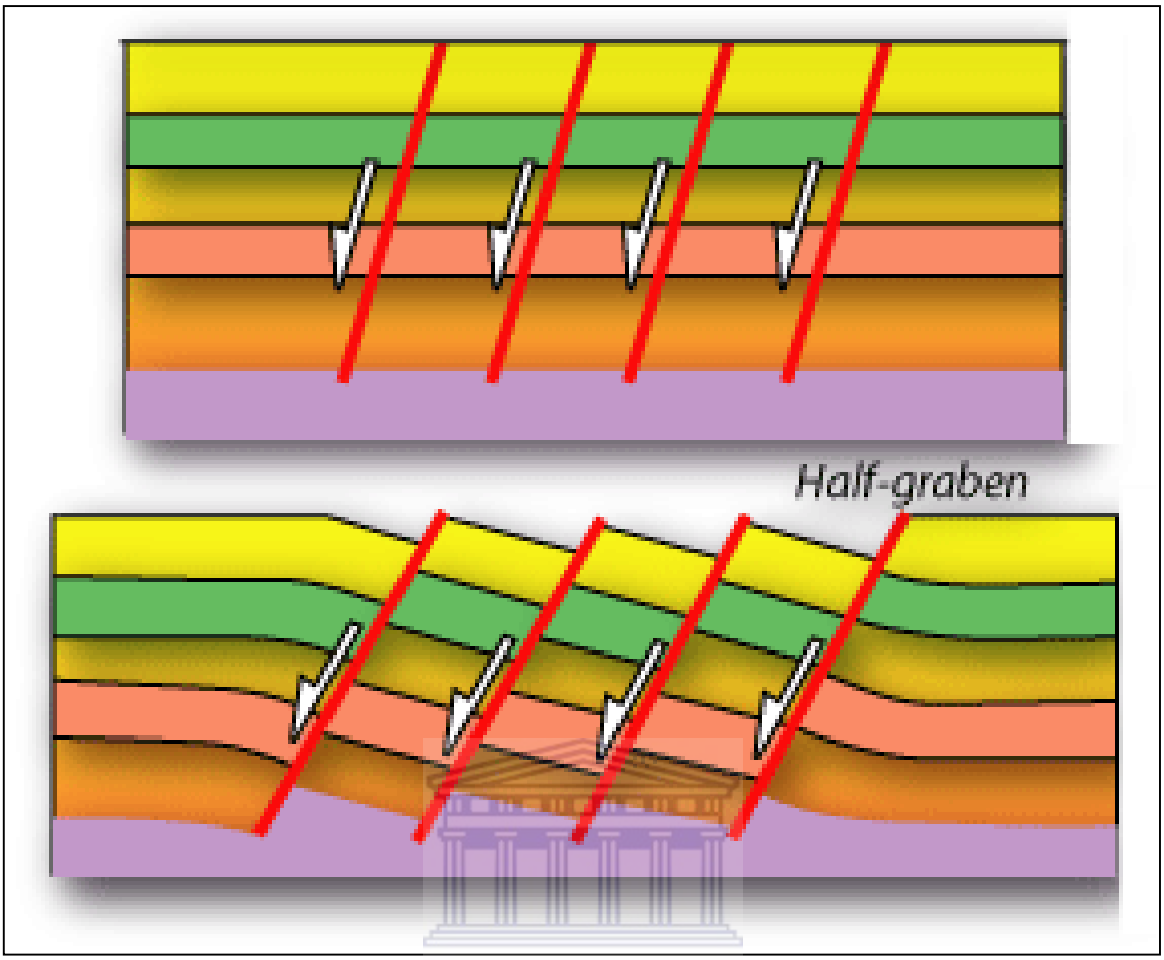

Figure 2.1 Formation of a half-graben from a series of normal faults dipping in the same direction (modified from Houston, 1986)

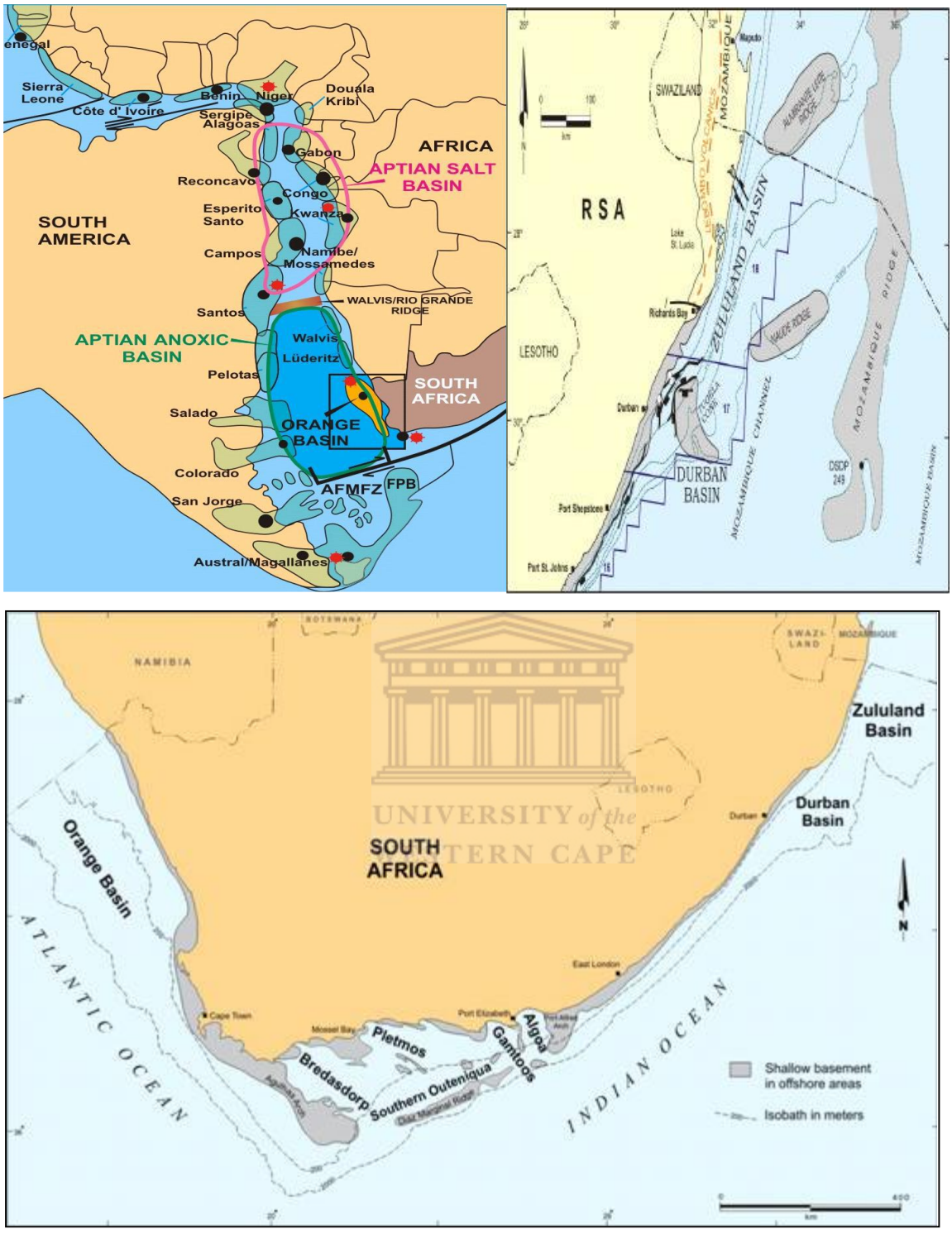

Figure 2.2: Western, eastern and southern offshore zones of South Africa (Modified from Broad, 2004).

2.2 Tectonic Setting of the Outeniqua Basin

The Outeniqua Basin is embodying four sub-basins (Bredasdorp, Pletmos, Gamtoos and Algoa) and was structured from dextral shearing procedures of the South African edge, which started in the Early to Mid-Cretaceous (Petroleum Agency Brochure 2004/2005). The rift period of the south coast finished in the Lower Valanginian, this is associated with drift-onset unconformity (Petroleum Agency Brochure 2004/2005). The drift-onset unconformity is synchronous to the soonest oceanic crust in the South Atlantic. A complex arrangement of micro plates, for example, the Falkland Plateau progressively moved south-westwards, past the southern bank of Africa (Figure 2.3). These developments made some slanted rift half-graben sub-basins including the Bredasdorp Basin which may be viewed as fizzled fractures. It is most youthful in the west and most established in the east (Figure 2.3). Succeeding to the rift stage was a transitional rift-drift stage emphasizing no less than three periods of reversal identified with nonstop shearing. Transitional rift-drift finished in the mid Albian as the Falkland Plateau at last differentiated from Africa and was trailed by the improvement of a genuine aloof edge (Figure 2.4).

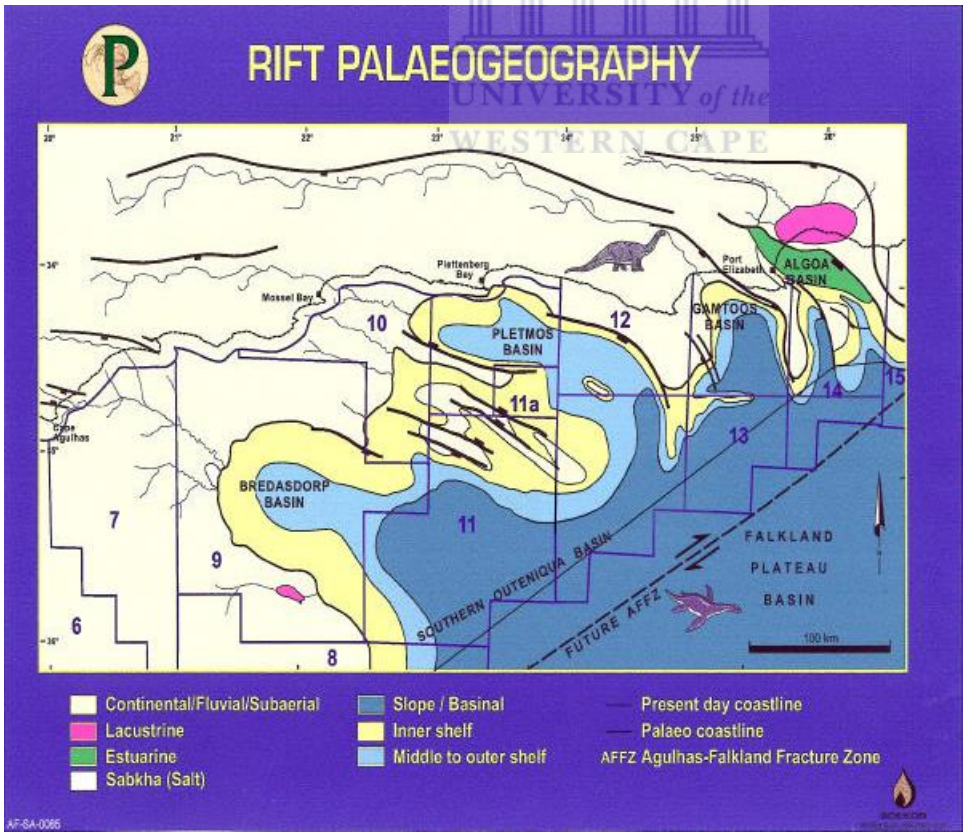

Figure 2.3: Oblique rift half-grabens sub-basins of Outeniqua Basin: Bredasdorp, Pletmos, Gamtoos, and Algoa (modified from Broad, 2004).

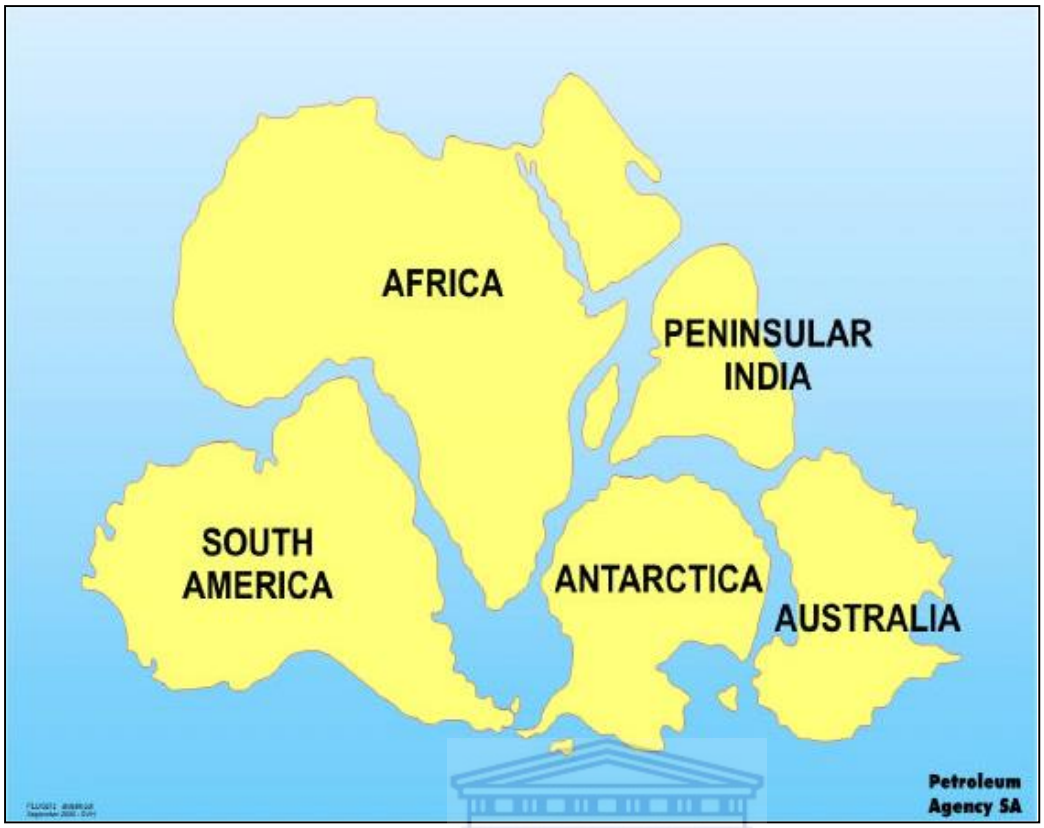

Figure 2.4: The rift phase in the Late Jurassic – Lower Valanginian showing the break - up of Africa, Madagascar and Antarctica (modified from Broad, 2004).

2.3 Depositional Environment

The Bredasdorp Basin developed from fan deltas and stream overwhelmed to wave dominated deltas and likewise coastal systems (PASA brochure 2004/2005). Slope and basin frameworks developed from fine-grained thickness and suspended deposits to leveed incline and basin floor turbidite fans has also been identified with the fine-grained turbidite frameworks. The progressions is because of the reaction to second order tectonic episode which brought about the variety in sediment supply rates and subsidence or settlement rates and expanding untamed sea forms (PASA brochure 2004/2005). Four relative separated fault sub basins making the Bredasdorp Basin throughout supercycle 1-5 (126-117.5 Ma) were supplied with sediments by high angle fluvial frameworks. River dominated deltaic frameworks progrades southward over the northern edge of the central sub basin (PASA brochure 2004/2005).

2.4 Sequence Stratigraphy of the Bredasdorp Basin

Sequence-stratigraphic concepts have been applied to the Lower Cretaceous post rift successions of the Bredasdorp Basin to upgrade the association of depositional frameworks tracts and related facies all around the basin. Lessening rift tectonics, thermal cooling, and eustatic varieties in global sea level prompted the advancement of a different arrangement of redundant cycle depositional sequences.

Different units of lowstand framework tracts inside these successions seem to hold potential hydrocarbon reservoirs. Lowstand framework tracts are created on erosional unconformity (also referred to as type 1 unconformity), which resulted from relative sea level fall beneath the shelf edge. Type 1 unconformities, which usually display incised valleys and gullies, give surfaces on which the accompanying is deposited:

(1) Mounded and sheet like submarine/basin-floor fans
(2) Submarine channel fill and associated mounds and fans
(3) Prograding deltaic/coastal lowstand wedges

These characteristics structured contemporaneously with the disintegration of etched valleys and submarine ravines, followed channelized slope fans and deltaic/seaside lowstand wedges that prograded throughout a relative sea level ascent (Figures 2.5, 2.6 and 2.7). These fans, channel fills, and wedges are top fixed and sourced by shales and marine dense segments created throughout the transgressive stage deposited during a period of regional transgression of the shoreline. Resulting flooding of the shelf as relative sea level ascent rise brought about defectively characterized transgressive framework tracts. Broadly created deltaic/seaside frameworks prograded basinward, therefore showing decently characterized clinoforms; the relative ocean level at a highstand (Broad, 2004).

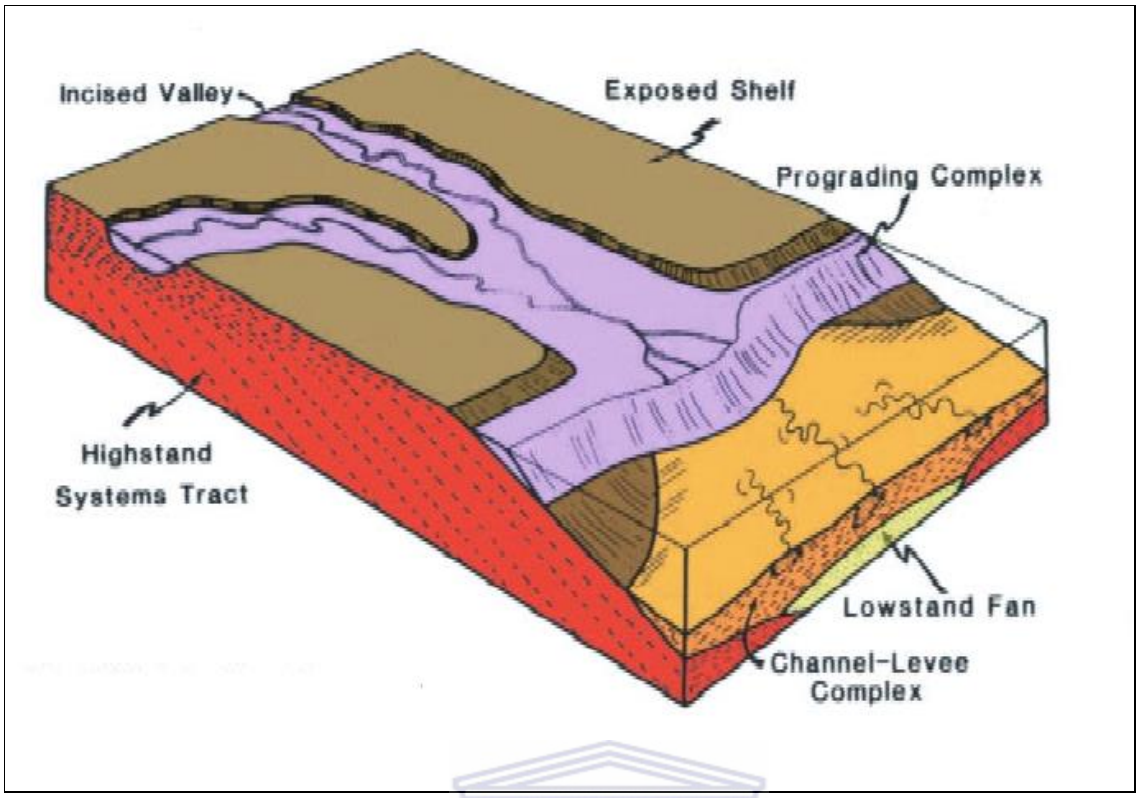

Figure 2.5: Prograding complex terminating canyon filling episode (Modified from Broad, 2004)

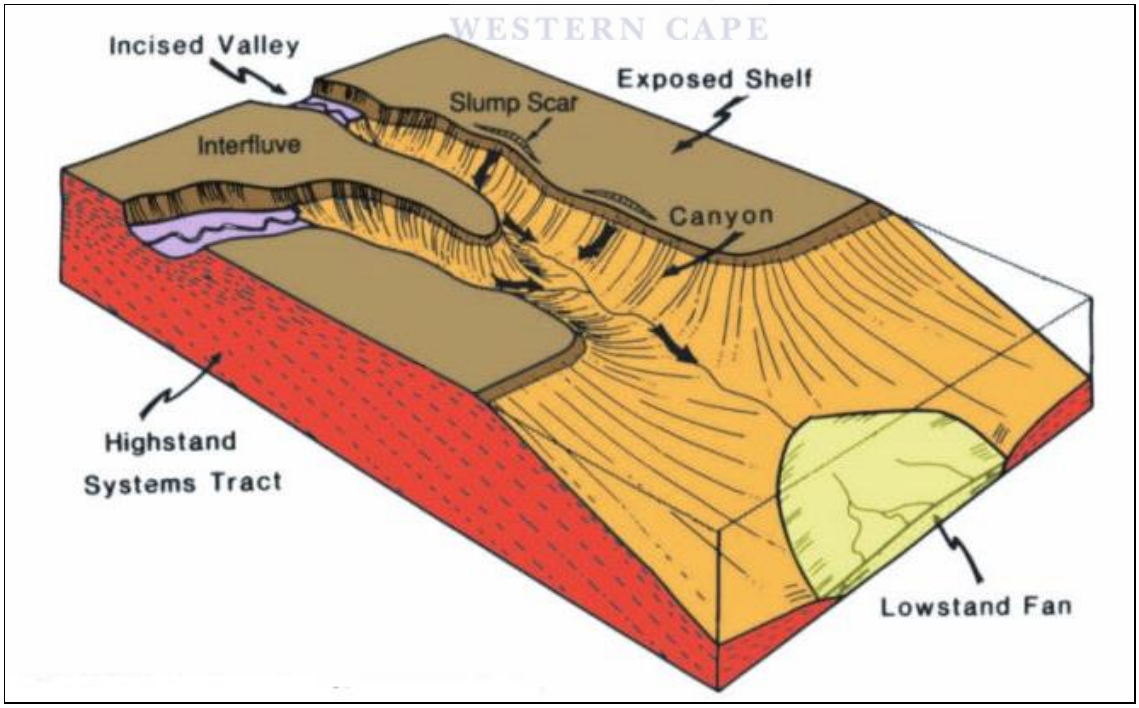

Figure 2.6: Basin floor fan (Lowstand fan) on canyon floor (Modified from Broad, 2004)

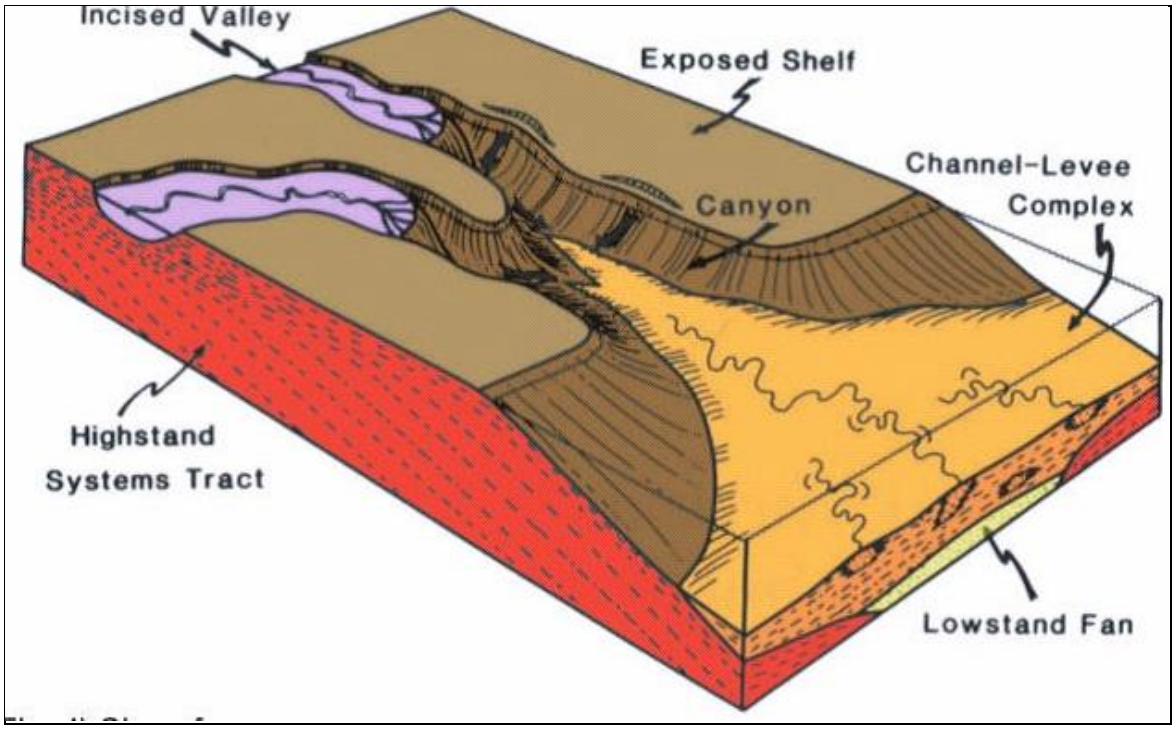

Figure 2.7: Channel-Levee complex deposited on basin floor fan (Modified from Broad, 2004)

2.5 Structural development of the Bredasdorp Basin

Bredasdorp basin had undergone the following four structural developments over the years:

I. Mid-Jurassic to Valangian (Basement to 1At1)

Synrift I stage -Extension-driven subsidence and synrift basin fill. Both sides of the graben have been isostically inspired bringing about erosional truncation of synrift sediments. Extreme bordering uplift and denudation of the northern side disengaged the in place synrift 1 progression in places (PASA, 2009).

II. Late Valangian to Hauterivian (1At1 to 6At1)

Synrift II stage -Rapid subsidence and far reaching flooding. Continuous elevation brings about auxiliary of structural highs. Source rock deposition of deep water sequences inside rift depocenters (Arniston half graben and southern sub basin (PASA, 2009).

III. Hauterivian to Aptian (6At1 to 13Amfs)

Transitional (Early Drift) stage- Progradational development of shelf in the northern part over the Arniston half-graben, joined with a ceaseless development of the southern sub-basin (PASA, 2009).

IV. Albian to Maastrichtian (13Amfs to 15At1)

Drift stage-Regional subsidence determined by the thermal cooling and subsidence stacking. Continuous development on the Arniston shortcoming (PASA, 2009).

2.6 Hydrocarbon plays of the Bredarsdorp Basin

2.6.1 Source Rocks

A source rock is a sedimentary rock that holds sufficient organic matter such that when it is buried and heated it will produce hydrocarbon (Gluyas and Swarbrick, 2004). Gas inclined source rocks of the Bredasdorp Basin occur in some north flank wells where F-A gas field is built and are likely to be available in the center of the basin but have not been traversed (Burden, 2002). In the Northern edge of the basin, sedimentation happened throughout the Barremian and mid-Aptian and is marked by solid shelf progradation around the region (Burden, 2002). Marine claystones are discovered to be interbedded with shelf shoal sandstones around the Northern edge and profound marine fan projection and channel sandstones are found in the central basin (Burden, 2002). Gas accumulations in the Bredasdorp Basin has been obtained as a consequence of low sedimentation rates initiating the deposition of the dry to wet gas inclined and adjacent oil inclined organic shales throughout the Barremian, and these shales are the thickest and best quality source rocks in the Bredasdorp Basin (Burden, 2002). Sediment starvation happened simply after the mid-Aptian unconformity (13At1) over an expansive part of the basin and throughout this time organic rich shales were deposited in the central basin area.

2.6.2 Reservoir rock

A reservoir rock is a permeable and porous rock that holds interconnected pores or openings that occupy the areas between the mineral grains of the rock (Rider, 2002). The principal marine sandstones of the Bredarsdorp Basin happen inside the synrift progression, where they are interbedded with lagoonal and fluvial claystones. A thick minor marine sandstone

complex tops the arrangement. The complex is well known boreholes on the flanks of the basin and is of promptly Cretaceous age. These sandstones are accepted to have shaped the major gas reservoirs of the North flank gas field where the F-A gas field has been created by SOEKOR (now PETROSA). The rift truncated by the rift/drift (1At1) which is most erosive on the basin flanks. The synrift progression is widely faulted and folded in places (Burden, 1992).

2.6.3 Seal and Trap

Seals are rocks which are able to stop or retard fluid migration. They are fine-grained rocks with no porosity and permeability. The strength of the seal is determined by the capacity to hold the hydrocarbon column. Marine shales of the Bredasdorp Basin that were developed during transgressive phase act as seals. Traps were created from the Late Cretaceous to promptly Tertiary. Both structural and truncational traps are available inside the shallow marine to fluvial synrift reservoir while different sorts of traps, for example, compactional trap anticlines, stratigraphic pinch-out traps and reversal related closures trapped the drift reservoirs (PASA Brochure, 2004/2005)

Chapter 3

3 Methodology

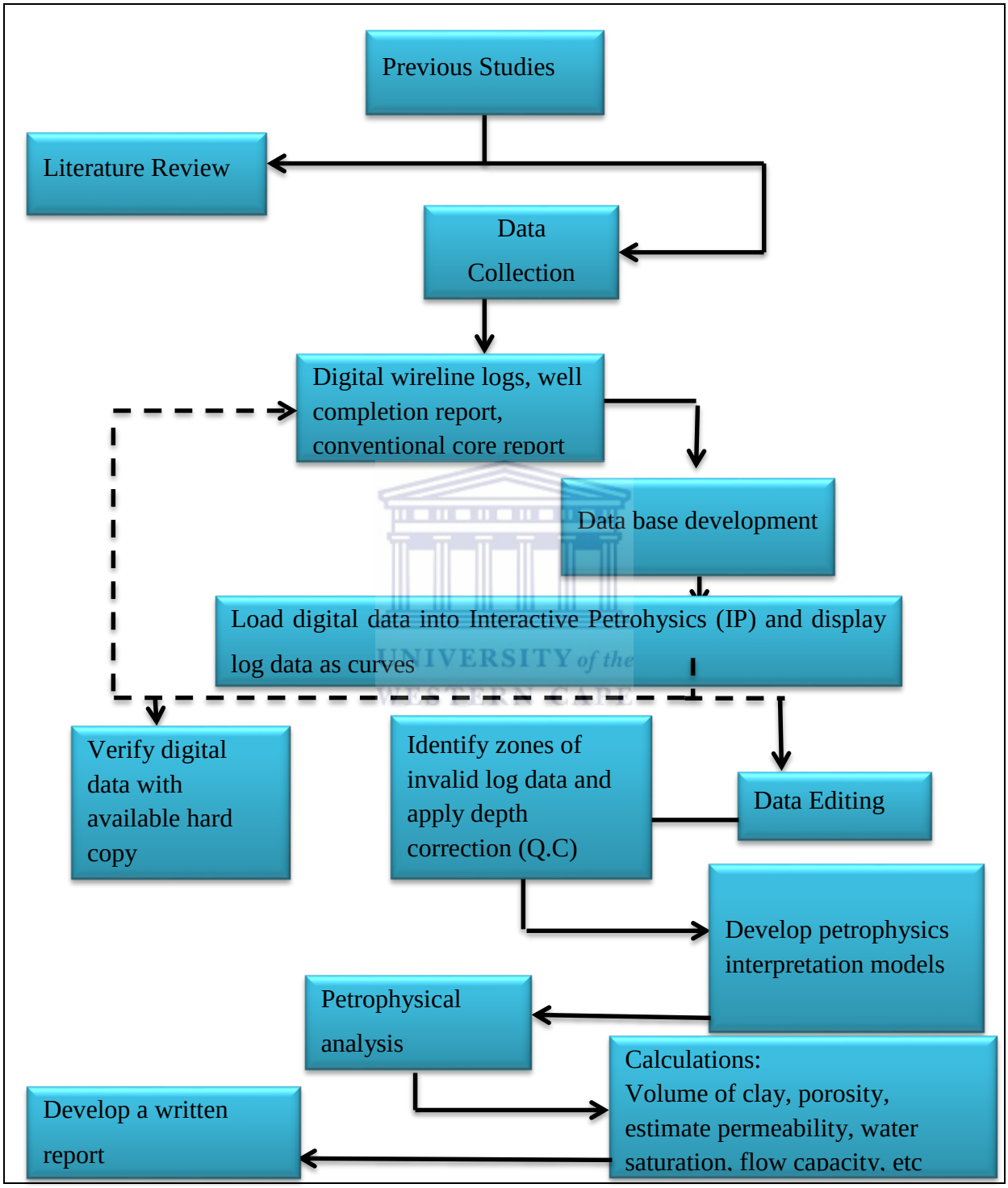

Figure 3.1: Flow chart summarizing the methodology

The flow chart in figure 3.1 outlines steps taken in completing this study. The procedure begins with the audit of past studies and literature in comparable oil and gas basin to understand the geology of the area.

The data was collected by Schlumbeger Service Company and was provided for this study by the Petroleum Agency South Africa (PASA). Data was carefully arranged, sorted, and prepared for easy access and quality controlled (QC) before being loaded into Interactive Petrophysics (IP) software to be displayed as log Curves. IP software was used to carry out data quality control (QC), interpretation, modelling and analysis of the available digitized wireline logs (LAS format) data.

The following data types were used:

a) Digital geophysical wireline logs

b) Conventional core analysis data reports

c) Geological well completion reports

After the data has been displayed as log curves in the IP, the log Interpretation took place it was at this stage where the evaluation of sandstone reservoirs took place and also calculation of porosity, permeability, water saturation, clay volume, flow capacity, and storage capacity. Once the petrophysical evaluation was done, the hydrocarbon generation potential was estimated.

3.1 Log editing

3.1.1 Environmental Correction

Environmental corrections are applied to wireline logs using computer programs because they are affected by borehole size and the environment (Opuwari, 2010). The effect of environment disturbance to the logs is caused by stress, mud weight, temperature etc. The borehole environment corrections have been applied to one log only using mud/borehole properties identity from the log headers. The corrections were only applied to gamma ray log of well E-AH1 due to the absence of the required properties for other wells to perform the corrections. The properties needed to perform the gamma ray corrections obtained from the well log headers are hole size, mud weight and tool position.

3.1.2 Log splicing

Log splicing is a process of bringing together all the runs logged in a well to form a continuous LAS file. The logs run at different depth were spliced into a continuous log. Figures 3.2 and 3.3 show the example of the logs before and after splicing.

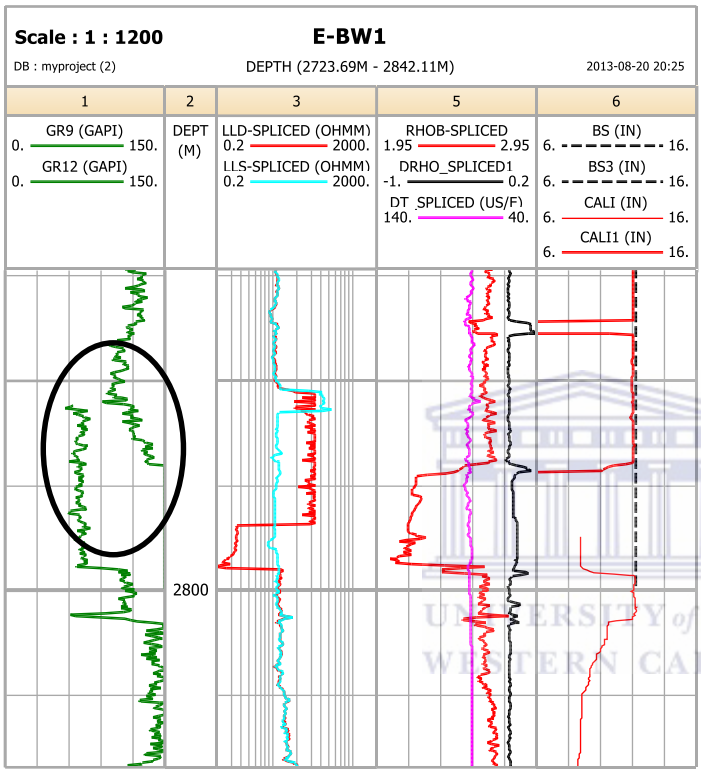

Figure 3.2: Example of Gamma ray log before splicing

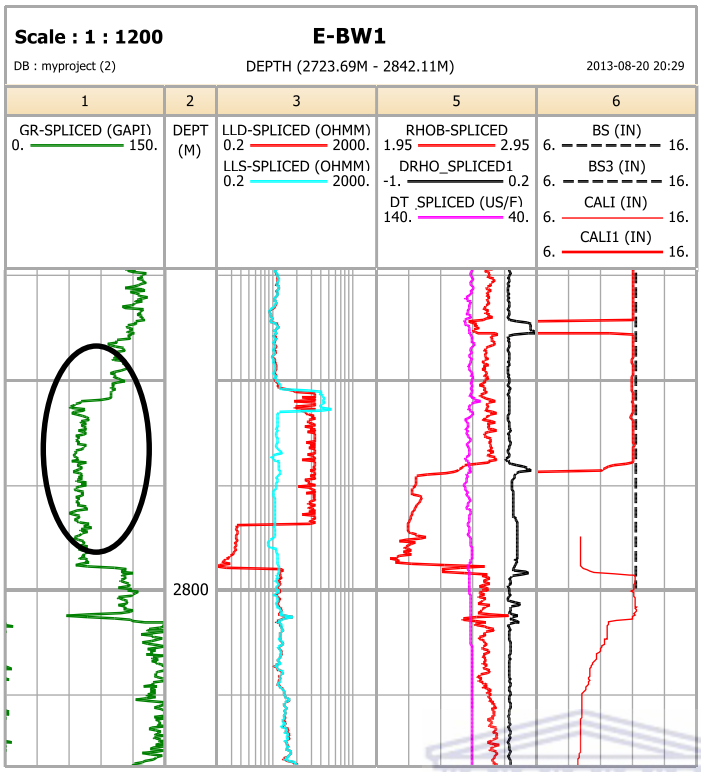

Figure 3.3: Example of Gamma ray log after splicing.

3.2 Identification of possible sandstone Reservoir

The first step in a log interpretation is to identify zones of interest or potential sandstone reservoirs (clean zones with hydrocarbon) and define a clean and shale baseline on the gamma ray (GR) logs (Figure 3.4). This is achieved by observing the behavior of the gamma ray log, maximum deflection to the right indicate a shale formation and maximum deflection to the left indicate clean sandstone (Jensen et al., 2013).

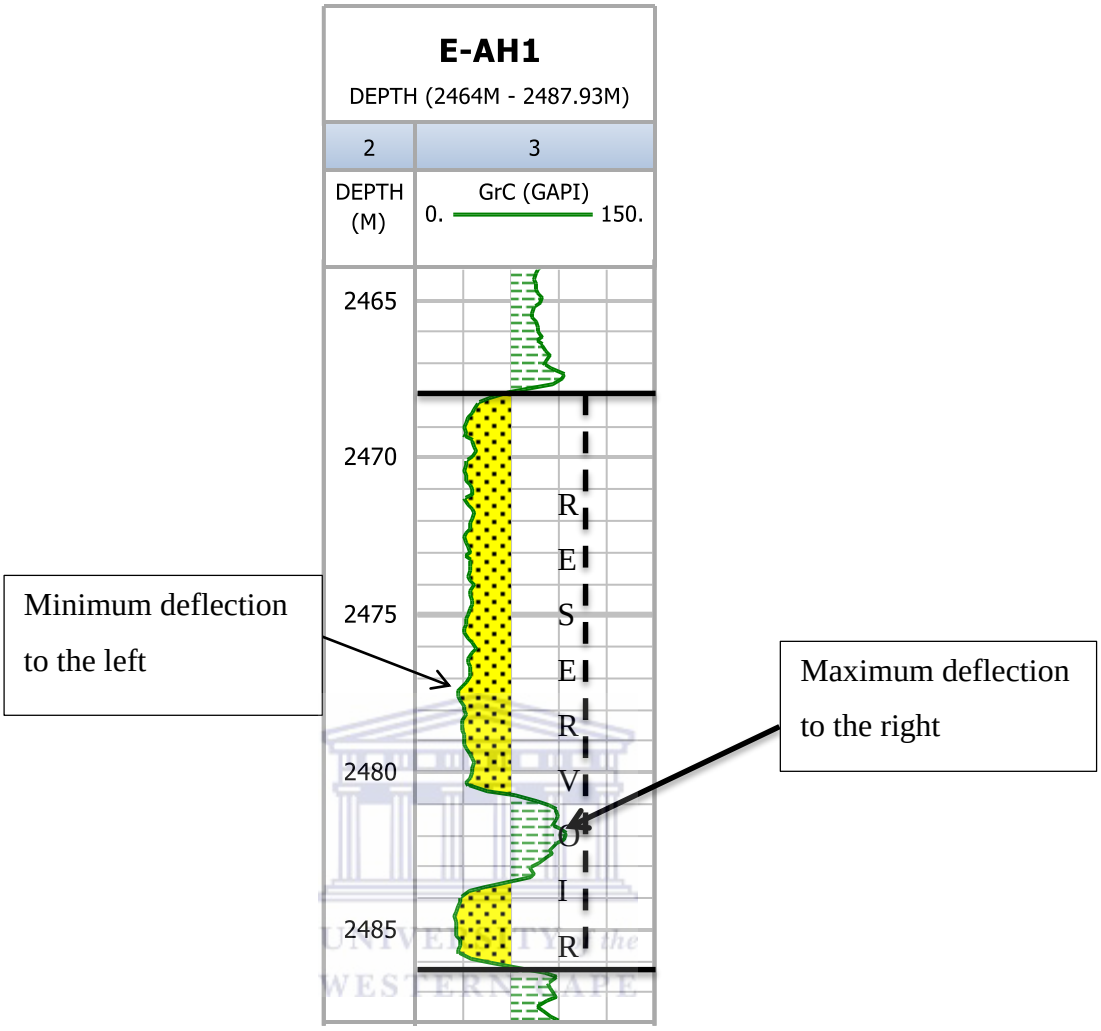

Figure 3.4: Example of the selected potential sandstone reservoir.

3.3 Determination of m, a, n and Rw parameters from standalone picket plots

A meaningful determination of tortuosity factor (a), cementation factor (m), water saturation factor (n) and water resistivity factor (Rw) is pivotal in log interpretation. Resistivity versus porosity was plotted against each other in a water bearing intervals using a standalone picket plot to determine these parameters. Figure 3.5 below shows the multi-well standalone picket plot for all three wells (E-AH1, E-BW1 and E-L1) and the determined values of each parameter. The straight lines in the cross-plot represent the amount of water saturation; the red line represents 100% water saturation, 0.5 line represents 50%, 0.3 line represents 30% and line 0.2 represents 20% water saturation.

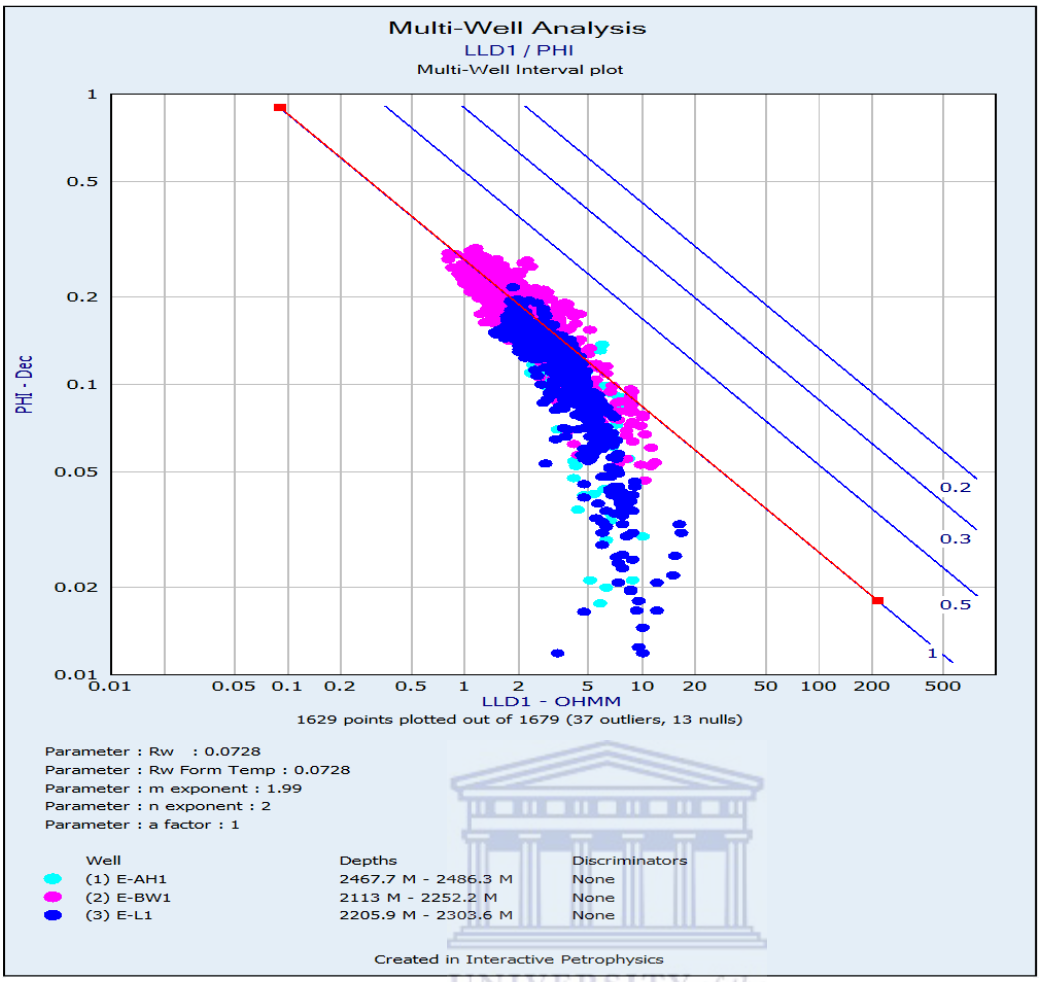

Figure 3.5: Standalone picket plot used to determine the above mentioned parameters.

Chapter 4

4 Theory of well and logs

4.1 Introduction

A well log or wireline log in the oil and gas industry is alluded to as a recording against depth of any of the aspects of the rock formations crossed by a measuring apparatus in the well bore (Serra, 1984). These wireline logs are gotten when logging instruments are brought down on cable (wireline) into the well; the measurements are transmitted up a cable to a surface laboratory or machine unit. An extensive number of logs might be run on simultaneously each one recording an alternate property of the rocks infiltrated by the well. Through logging various physical parameters are identified with both the topographical and petrophysical properties of the rock formation that have been drilled.

4.2 Characteristics of the selected wireline logs

Wireline logging tools are numerous and new models are being designed to handle specific logging restrictions. In this manner with purpose of this study, a couple of logging apparatuses have been chosen for short portrayal of their peculiarity.

4.2.1 Gamma Ray Log (GR)

Gamma ray logs are intended to measure the characteristic radioactivity in formation. The amount of vitality of the naturally occurring gamma ray in the formation was measured and distinguished between elements of parents and daughter product of the three principle radioactive families: uranium, thorium and potassium (Rider, 2002). In sediments, the log mostly reflects clay content because clay contains the radioisotopes of potassium, uranium, and thorium. Potassium feldspars, volcanic ash, granite wash, and some salt rich deposits containing potassium (e.g. potash) might likewise give critical gamma-ray readings. Shale-free sandstones and carbonates have low concentrations of radioactive materials and give low gamma ray readings. The standard unit of measurement is API (American Petroleum Institute). High gamma ray might frequently not indicate shaliness, however an impression of radioactive sands, for example, potassium rich feldspathic, glauconitic, or micaceous sandstones (Rider, 2002). Gamma ray log is normally preferred to spontaneous potential logs

for correlation purposes in open holes non-conductive borehole liquids, for thick carbonate interval, and to correlate cased-hole logs with open–hole logs.

4.2.2 Neutron Log

Neutron logs are porosity logs that measure the hydrogen ion concentration in a formation additionally influenced by mineralogy and borehole impacts. In clean formations, where the porosity is filled with water or oil, the neutron log measures fluid filled porosity. At whatever point pores are filled with gas as opposed to oil and water, neutron peruses low values. This happens as results of less concentration of hydrogen in gas contrasted with oil or water. The lowering of neutron porosity by gas is called Gas effect. The device holds a consistently discharging neutron source and could either be a (neutron-neutron tool) or a gamma ray locator (neutron-gamma tool). High vitality neutrons from the source are backed off by impacts with atomic nuclei. The hydrogen atoms are unquestionably the best in the slowing down the process because their mass is almost equivalent to that of the neutron. Thus, the circulation of the neutrons at the time of recognition is principally dictated by the hydrogen concentration. Neutron log reactions change, contingent upon: distinction in indicator types, dividing between source and detector, and lithology (i.e. sandstone, limestone, and dolomite).

4.2.3 Density Log

This is a well log that records formation density. The logging apparatus comprises of a gamma ray source (e.g. Cs137) and a finder protected from the source with the goal that it records back-scattered gamma ray from the formation relying upon the electron density of the formation (Rider, 2002). The formation electron density is corresponding to its bulk density. Like in neutron apparatus, the source and the identifier are typically mounted on a slide which is pressed against the borehole wall. The compensated density logging device incorporates a secondary indicator which reacts more to the mud cake and little borehole irregularities. The reaction of the second tool is utilized to rectify the estimations of the primary detector. Density log is applied basically to uncased holes (Rider, 2002).

4.2.4 Combination of Neutron-Density Logs

This is a blending porosity log. Plus its utilization as a porosity tool, it is additionally used to determine lithology and to detect gas bearing zones. Both the neutron and density curves are typically recorded in limestone porosity units with every division equivalent to either two percent or three percent porosity. Limestone and dolomite porosity units can likewise be recorded. An increase in density porosity happening with a lessening in neutron porosity demonstrates a gas bearing zone typically alluded to as Gas Effect. Gas Effect is made by gas in the pores as it causes the density log to record excessively high porosity (i.e. gas is lighter than oil or water) while the neutron log record excessively low porosity reflecting lower concentration of hydrogen atoms than oil or water.

4.2.5 Resistivity Log

The resistivity log is a measurement of a formation resistivity that is its resistance to the parkage of an electric current (Rider, 2002). It is measured by resistivity devices. The resistivity logs were created to discover hydrocarbon (Rider, 2002). This is still their essential quantitative utilization; resistivity logs furnish the basic numbers for petrophysical calculations. However a formation resistivity is one of its typical geophysical characteristics and as such can contribute information on lithology, texture, facies and overpressure (Rider, 2002). The log is frequently used for correlation.

4.2.6 Sonic Log

Sonic log measures the formation capacity to transit sound waves. The capacity measured by the sonic log varies geologically with the lithology and rock texture, notably porosity (Rider, 2002). It also provides a formation's interval transit time, designated Δt. Sonic log is used to evaluate porosity in a liquid-filled hole (Rider, 2002). It can also help to identify lithology, indicate source rocks, normal compaction and overpressure.

4.2.7 Caliper Log

Mechanical Caliper measures the varieties in borehole diameter with depth. Caliper log accomplish the measurements by utilizing two enunciated arms that are pushed against the borehole wall. The arms are interfaced to the cursor along the resistance. Parallel development

of the arms is deciphered into the movements of the cursor along the resistance, and henceforth varieties in electrical yield. The contrasts in yield are deciphered into diameter varieties after a simple calibration. Caliper log is usually equipped with frequently used logging tools such as micrologs and density and neutron where it is used to apply the measuring head of the tool to the borehole wall.

Chapter 5

5 Conventional core analysis and interpretation of well logs

5.1 Introduction

The objective of coring is to bring a sample of the formation and its pore fluids (water, oil or gas) to the surface in its original state, to maintain the sample and transport it to the laboratory for analysis. This objective need to be met , because the procedure of cutting the core will, at some extent exchange the properties of both the rock and the saturation fluids in the rock itself. These cores can be obtained in different ways; conventional core, sidewall cores or plugs and cuttings (Opuwari, 2010). Great care should be in place to place the coring fluid and in the transportation and storage of cores in order to maintain the desired fluid saturations. In some cases the initial reservoir condition and the coring fluids used may cause the saturation of water, oil or gas in the core arriving at the lab considerably higher or lower than it was in the original state of the formation (Bateman, 1985)

5.2 Conventional core analysis

The conventional core analysis includes the measurement of porosity, permeability and saturations (oil, water and gas); these three measurements are made to answer three fundamental questions about a reservoir. The measurements should be made to tell whether the rock contain a fluid filled space (porosity), is there a hydrocarbon in that fluid filled space and can those hydrocarbon fluids be produced (Permeability)?. This type of analysis focuses on analyzing the portion of each interval of selected area of interest. This analysis is performed on homogeneous formations such as sandstones, carbonates and shaly sands formation at around three or four inches of each foot of the core (Opuwari, 2010).

This analysis was performed in three wells E-AH1, E-BW1 and E-L1 of the study area in order to obtain the petrophysical properties of the reservoirs. All the conventional core analysis results presented in this study were obtained from the conventional core analysis and core description reports provided by PASA.

5.2.1 Intervals cored

5.2.1.1 Well E-AH1 cored interval

Two cores were cut, but for the purpose of this study only one core was studied. The studied core was cut from 2471m to 2485m to evaluate a drilling break with associated cut and fluorescence. Core comprises grain flow sandstone with minor claystone. The core permeability was very good. The measurement of the conventional core analysis includes grain density, gas expansion (helium) porosity; air (Ka) and liquid (KL) permeability, fluid saturation (gas, water and oil) and calcimetry (calcite and dolomite).

The Table below represents the results obtained from the conventional core analysis of well E-AH1.

Table 5.1: Results obtained from the conventional core analysis of well E-AH1.

Depth (M)	Permeability(KL) (mD)	Permeability(Ka) (mD)	Porosity (%)	Sg (%)	So (%)	Sw (%)	Calcite (%)	Dolomite (%)	Grain density (g/cc)
Core 1									
2471.08	35	33	13.4	40	16	44	0.5	2.5	2.64
2471.95	45	38	13.9	29	17	54	1.0	2.0	2.65
2472.00	35	33	14.9	26	15	59	0.5	0.5	2.68
2473.98	28	23	14.1	25	0	75	0.5	5.5	2.67
2475.00	13	10	11.1	35	0	65	1.0	9.0	2.67
2476.00	61	53	13.1	21	0	79	3.5	15.0	2.69
2476.80	39	33	12.8	21	0	79	0.5	6.5	2.66
2477.80	56	48	18.2	19	0	81	0.5	15.0	2.78
2480.80	0.037	0.02	4.8	55	0	45	0.5	6.0	2.63
2482.04	75	65	16.5	45	14	41	0.5	24.0	2.77
2483.00	94	83	18.5	27	16	57	1.0	25.0	2.81
2483.90	61	53	14.7	44	15	41	0.5	0.5	2.63

5.2.1.2 Well E-BW1 cored interval

Two cores were cut to investigate the reservoir properties of sandstones with associated high gas values and fluorescence. However, for the purpose of this study, only one core was studied.

The core was cut from 3023m to 3032m of which 8.94m was recovered, which is equivalent to 99.3%. The upper 2.87m consists of sandstone. The rest of the core consists of claystone with well-rounded claystone pebbles. Porosities range from 3% to 11% with an average of 8.1%. The average permeability is 0.14 mD. This core intersected the upper sandy interval of the 6A sequence. The sandstones were found to be clean, very fine to fine grained and lithic with claystones and metamorphic grains. Table 5.2 represents the results obtained from the conventional core analysis of well E-BW1.

5.2.1.3 Well E-L1 cored interval

One core was cut in order to evaluate a 6m drilling break (3287m to 3293) and associated hydrocarbon show. The coring was terminated at 3302m due to the very slow penetration rates (up to 127 min/m). Core recovery was 84% (7.54m) of which the upper 3m and Basal 1m interval consists of tight, fine grained sandstones separated interbedded claystone/siltstone. The coring was terminated due to the poor reservoir quality of the sandstone. Porosities range from 5-9% and permeability are less than 0.4mD. Table 5.3 represents the results obtained from the conventional core analysis report of well E-L1.

Table 5.2: Results obtained from the conventional core analysis of well E-BW1.

Depth (M)	Porosity (%)	Permeability (KL) (mD)	Permeability (Ka) (mD)	Sg (%)	So (%)	Sw (%)	Calcite (%)	Dolomite (%)	Grain density (g/cc)
3023.05	9.7	0.460	0.750	36	5	59	0.5	3.0	2.66
3023.30	10.1	0.680	1.020						2.69
3023.55	8.6	0.210	0.360						2.74
3023.80	8.3	0.180	0.320						2.73
3024.06	7.8	0.060	0.140	35	0	65	1.5	19.0	2.71
3024.35	10.5	0.760	1.070						2.75
3024.60	19.2	33.970	36.970						2.89
3024.83	6.5	0.020	0.060						2.76
3025.10				27	0	73	1.0	2.0	
3025.35	0.0	0.170	0.340						0.00
3025.60	8.9	0.270	0.470						2.66
3025.87	8.3	0.290	0.470	34	10	56	0.5	1.5	2.65
3031.86				43	0	57	18.5	3.0	

Table 5.3: Results obtained from the conventional core analysis of well E-L1.

Depth (Top) M	Depth(bottom) (M)	Porosity (%)	permeability(KL) (mD)	permeability (Ka) (mD)	Sg (%)	So (%)	Sw (%)	Calcite (%)	Dolomite (%)	Grain density (g/cc)
3293.00	3293.20	7.1	0.26	0.040	56	0	44	1	0	2.65
3293.40		8.8	0.37	0.57						2.67
3293.65		7.3	0.09	0.132						2.67
3293.90	3294.06	5.8	0.08	0.14	59	0	41	0.5	1	2.66
3294.33		7.2	0.17	0.270						2.67
3294.58		6.7	0.07	0.127						2.67
3294.78		5.0	0.03	0.061						2.68
3294.95	3295.22	4.0	0.03	0.06	35	0	65	1.5	0	2.66
3295.45		8.4	0.01	0.017						2.70
3295.71		3.2	0.01	0.019						2.68
3298.37		1.5	0.010	0.01						2.69
3298.76		1.6	0.01	0.01						2.69
3299.49	3299.73	7.6	0.08	0.14	54	0	46	0.5	0	2.65
3300.10		8.7	0.36	0.55						2.66
3300.21	3300.43	7.4	0.41	0.62	60	0	40	0.5	0	2.65

5.3 Lithofacies Description

5.3.1 Analysis and Interpretation of Results

Sedimentary facies is defined as any areally restricted part of a designated stratigraphic unit which exhibit characters significantly different from those of other parts of the units (Moore, 1949). The study and description of a reservoir core is fundamental in the development of petrophysical model because of the way that it serves to discover a relationship between log information, routine and special core analysis. The lithofacies of the rock units were grouped according to textural and structural features and grain sizes with reference to the approach of lithofacies groupings adopted by Nieto and Rojas (1998). In this study, different facies were identified from the cored intervals of each well. In well E-AH1, two facies (A and B) were identified; in well E-BW1, four facies (A, B, C and D) were identified and in well E-L1, three facies were identified. The description of each facies is provided below.

5.3.1.1 Well E-AH1 Description

Two distinct facies were identified, facies A and facies B in the cored interval (Figure 5.1). Lithofacies A consists of massive dark-greyish black deep-marine claystone with minor siltstone interbeds. The claystones are found to be non-calcareous and carbonaceous with abundant radiolarian (see appendix G). The claystones are characterized by near horizontal bedding and sedimentation injection features (sandstones into clay near contact with the sandstone). Lithofacies B consist of massive well sorted, fine to medium grained glauconitic sandstone with good porosity-permeability characteristics (see appendix G). Large fragments of bivalve shells derived from the shells are found to be concentrated in the intervals 2475.50m to 2476.07m and 2477.50m to 2744.86m. The upper sandstone (7.5m thick) is generally massive with some high angle bedding towards the base where it overlies deep-marine claystone. Sandstone of the low 2.61m unit is found to be also glauconitic and well sorted. Facies B was identified as reservoir facies and facies A as a non-reservoir facies.

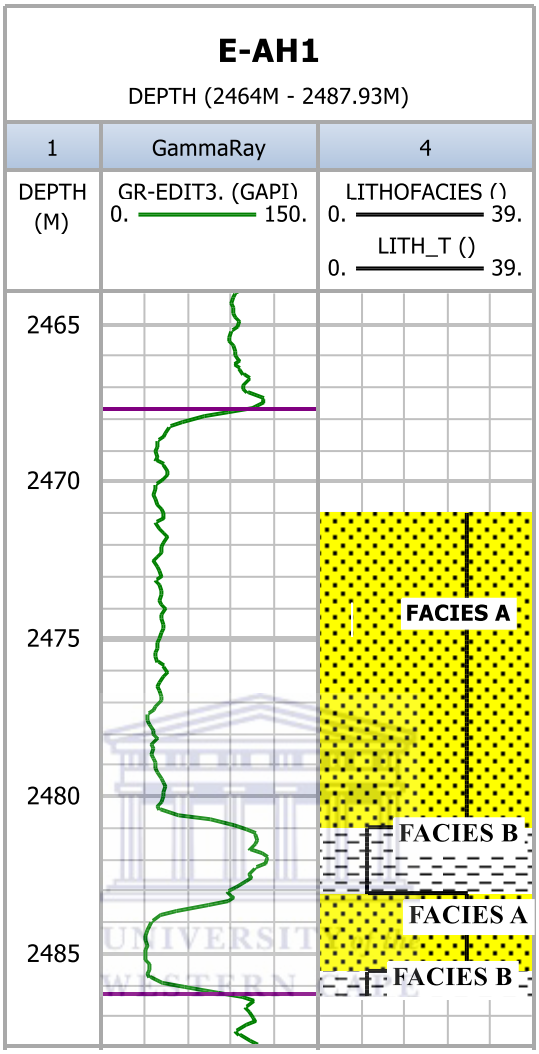

Figure 5.1: Log plot showing two distinctive lithofacies (Track 4) identified.

5.3.1.2 Well E-BW1 Description

Four facies (A, B, C and D) were identified from the studied cored interval (Figure 5.2). Facies A was described as a predominantly massive, upward fining sandstone unit. It is slightly graded with small, minor pebbles or granules occurring at the base of the sandstone beds. The sandstone in general, is porous, fine to medium grained, clean to slightly argillaceous, moderately to highly calcareous in places. Glauconite and carbonaceous detritus occur in minor amounts throughout the unit.

Facies B was described as medium darkgrey, to greyish black, non-calcareous to slightly calcareous (in places) claystone. The claystone contains laminations of siltstone and occasional sandstone lenses.

Facies C was found to be consisting of claystone matrix and polymitic conglomerate. Pebbled sizes vary between 10mm-30mm. Pebbles are well rounded, poorly sorted and consist mainly of quartz, sandstone and shale fragments. The amount of pebbles gradually decreases towards the base of this facies unit. Facies D was described as light grey, medium grained, clean, porous and very calcareous sandstone unit. The sandstone is marked by wavy, irregular laminations. Minor carbonaceous material, glauconite and pyrite were also, recognized in this facies. Facies A was identified as reservoir and facies B, C and D as a non-reservoir. No core photographs were presented for this well.

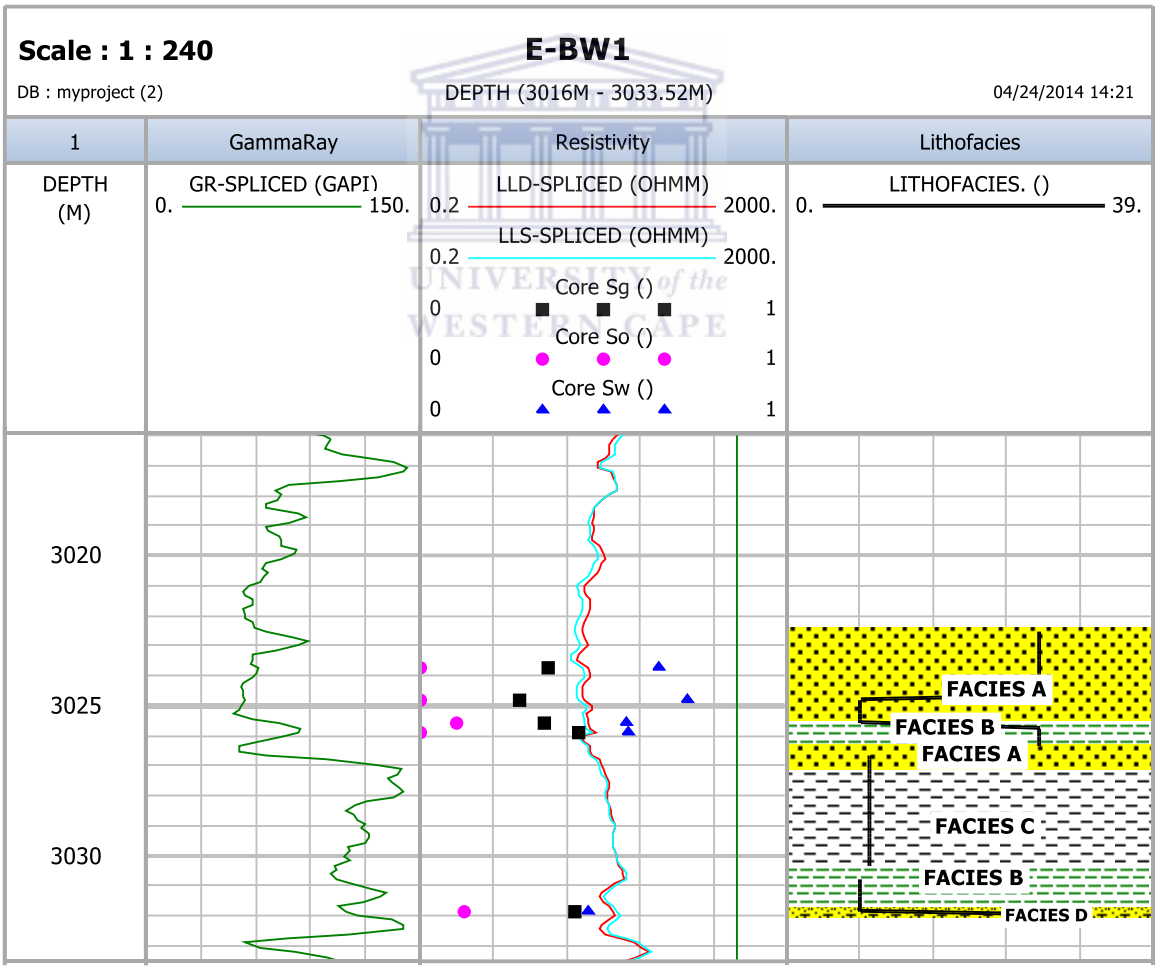

Figure 5.2: Log plot showing the identified lithofacies (track 4) of the cored interval.

5.3.1.3 Well E-L1 description

Three distinctive facies (A, B and C) were identified from the cored interval (Figure 5.3). Facies A was described as calcareous sandstone, tight, with some irregular clay partings (Appendix G). Facies B was identified as massive sandstone with clay inclusions and also include few mm-cm bedded claystone and siltstone (Appendix G). Facies C was found to be a coarsening upwards cycles of claystone, with siltstone and sandstone. Claystone is predominant, non-calcareous and the sandstone is tight and argillaceous (Appendix G).

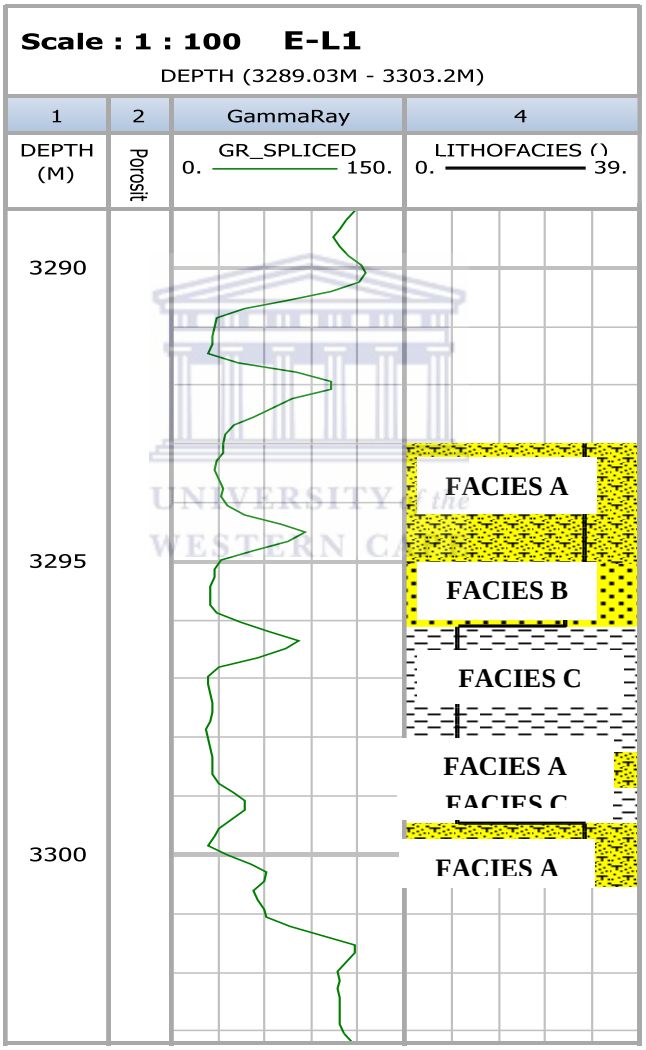

Figure 5.3: Log plot showing three distinctive lithofacies (Track 4) identified.

The best facies for this well is facies A because it has a slightly high porosity and permeability values as compared to facies B and C respectively.

5.4 Analysis and Interpretation of Results

5.4.1 Grain Density

Grain density is a density of a rock or mineral with no porosity, it is usually given in units of g/cm^3. Regarding formation evaluation, grain density is characterized as the density of the grains in a formation or core sample (Schlumberger, 2013). As it is utilized within log and core analysis, the term grain alludes to all the solid material in the rock, because when interpreting the measurement no exertion is made to recognize grains from other robust material. This grain density is figured from the measured dry weight partitioned by the grain volume. It is likewise ascertained from the density logs utilizing an appraisal of porosity and information of the fluid content (Schlumberger, 2013).

The matrix densities of some common lithology are given in the table below.

Table 5.4: Matrix density of common lithology (Source: Schlumberger, 2013)

Lithology	**Matrix value (g/cm^3)**
Clay mineral	2.02-2.81
Chlorite	2.81
Illite	2.61
Kaolinite	2.55
Smectite	2.02
Coal	1.19
Halite	2.04
Sandstone (Quartz)	2.65
Limestone	2.71
Dolomite	2.85
Orthoclase	2.57
Plagioclase	2.59
Anhydrite	2.98
Siderite	3.88
Pyrite	4.99

5.4.1.1 Well E-AH1 grain density

The grain density values of well E-AH1 range from 2.64 to 2.81g/cc with a mean value of 2.686g/cc as shown in the figure 5.4 below.

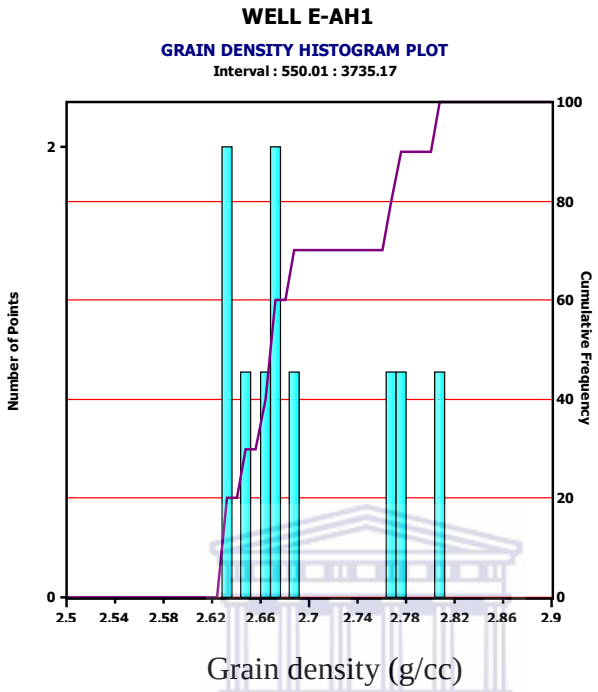

Figure 5.4: Grain density histogram plot of well E-AH1.

Clean quartz sandstone is expected at the grain density of 2.65g/cc. The standard deviation which is the value that shows approximately how far the values from the core values deviate from the mean value is found to be 0.06586 g/cc. This means that the minimum and maximum grain density values range from 2.62014 g/cc to 2.75186 g/cc.

5.4.1.2 Well E-BW1 grain density

The grain density of well E-BW1 obtained from the conventional core analysis measurement ranges from 2.65g/cc to 2.89g/cc as shown in the histogram plot below (Figure 5.5) with the standard deviation of 0.058g/cc and a mean value of 2.7081g/cc. This means that the minimum and maximum grain density values range from 2.6501g/cc to 2.7661g/cc.

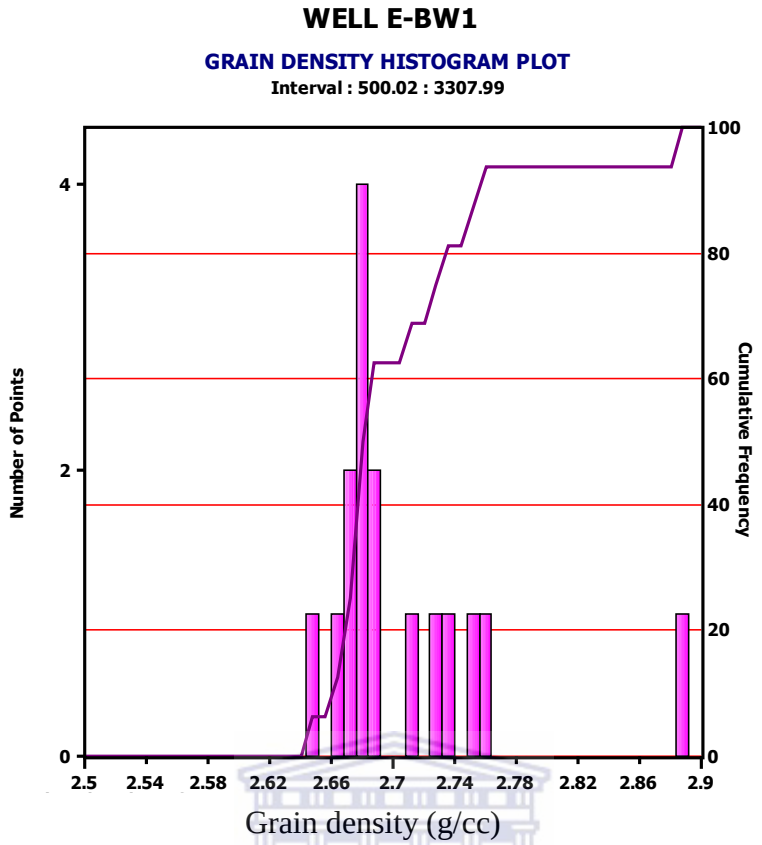

Figure 5.5: Grain density histogram plot of well E-BW1.

At depth of 3023.05m, 3024.06m, 3025.10m and 3031.86m there is a presence of carbonates minerals (calcite and dolomite). Core results do not indicate consistent carbonate cements because the presesnce of calcite and dolomite minerals is very insignificant (only found in few depths) in core analysis report. The grain density values deviate from the mean value by 0.058g/cc.

5.4.1.3 Well E-L1 grain density

In a clean quartz sandstone a grain density of 2.65g/cc is expected. The grain density of this well obtained from the conventional core analysis report and shown clearly in the histogram plot below (Figure 5.6) range from 2.65g/cc to 2.70g/cc with the mean value of 2.6677g/cc.

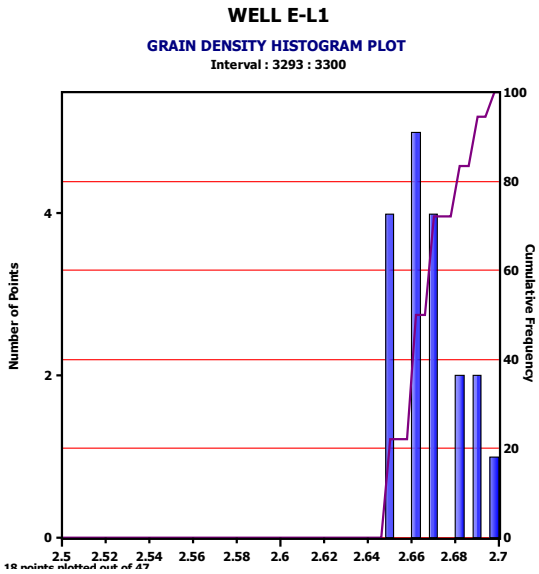

Figure 5.6: Grain density histogram plot of well E-L1.

At depth of 3293m-3293.20m, 3293.90m- 3294.06m, 3294.95m-3295.22m, 3299m-3299.73m and 3300.21m - 3300.43m there is a presence of calcite in the quartz sandstone formation (2.65g/cc). Core results do not indicate consistent carbonate cements because the presence of calcite and dolomite is very insignificant in core analysis results (Table 5.3). The standard deviation is found to be 0.015 g/cc. This simply means that the values from the core results deviated from the mean value by 0.015g/cc and range from 2.6527g/cc to 2.6827g/cc.

5.4.1.4 Comparison of the grain density distribution for all studied wells

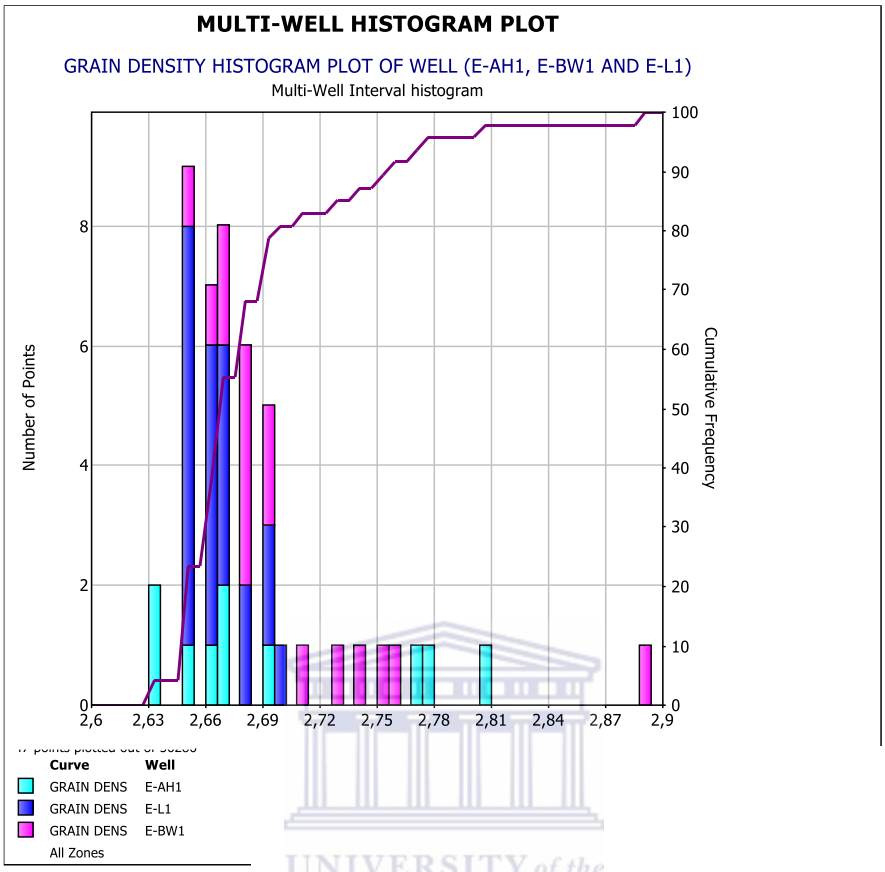

Figure 5.7: Multi well density histogram plot for E-AH1, E-BW1 and E-L1.

The grain density value for all three wells with core analysis results showed a range of 2.64g/cc to 2.89g/cc with a mean value of 2.6863g/cc and standard deviation of 0.04958g/cc. The presence of carbonate minerals (calcite and dolomite) were observed in all cored interval with relatively small proportion and only found in few depth except for the E-AH1 well in which there is persistence carbonate cements throughout the cored interval. The highest mean value of 2.7081 was obtained from well E-BW1 as compared to 2.6652g/cc and 2.695g/cc of E-L1 and E-AH1 respectively.

5.4.2 Porosity Interpretation

Porosity is described as the ability of the rock to contain fluids (oil, gas or water) in their pore spaces (Rider, 2002). It is a very important property of reservoir rocks and it also indicates

the storage capacity of the reservoir. It is used as a primary indicator of the reservoir quality and can also be combined with other factors to calculate hydrocarbon volume in place and recoverable reserves. Core porosity is usually used by Petrophysicist to help calibrate porosity derived from well log data (Crain, 2013). Two different porosities are estimated from different measurement. The gas expansion method is used to determine the effective porosity while the destruction of the sample to estimate grain volume determines the total volume (Opuwari, 2010). Effective porosity is the porosity of the interconnected pore spaces within the rock while the total porosity is the volume of the rock with which fluid filled (interconnected and non-connected). The determination of the core porosities for the wells was done using helium gas based on the Boyle's law for gas expansion ($P_1V_1=P_2V_2$). Porosity determined by gas expansion method indicates only pores that are interconnected (effective porosity) therefore providing a very good estimate of effective porosity for the purpose of reservoir evaluation. The porosities of the petroleum reservoir range from about 5% to 47.6% and geological factors that control porosity are sorting, grain packing, compaction and cementation. Grains are generally of the same size and shape. If all the grains are well rounded and are of similar size then sorting is good. Porosity of a well sorted is generally high and vice versa. Grain packing strongly affects the porosity of the rock. This factor refers to the spacing of the grain. Cubic packing can yield a porosity of 47.6% and Rhombohedral packing can yields approximately 26%. Compaction affects porosity by reducing the amount of the interconnected pore space. Cementation is the crystallization or precipitation of soluble minerals in the pore spaces between clastic particles. Common cementation agents include $CaCO_3$. Porosity and permeability can be reduced significantly due to cementation.

5.4.2.1 Well E-AH1 core porosity

The core porosity value of well E-AH1 ranges from 0.048 to 0.185 at the cored interval. It showed the average porosity of 0.1165 and a standard deviation value of 0.039 from the histogram plot below, Figure 5.8. Core porosity is plotted together with resistivity curves in figure 5.9 (Track 4). Facies A has been identified as the reservoir facies because it mostly contains a bit of high porosity as compared to facies B (Track 5)

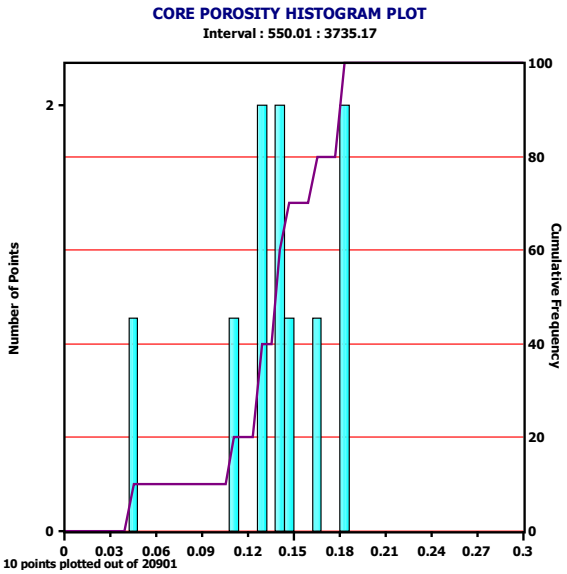

Figure 5.8: Core porosity histogram plot for E-AH1 well.

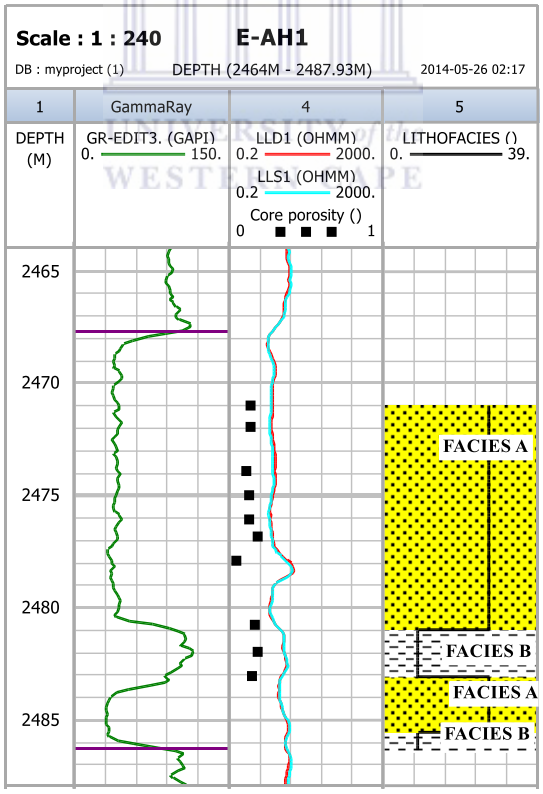

Figure 5.9: Well E-AH1 core porosity plot (Track 4).

5.4.2.2 Well E-BW1 core porosity

Core porosity ranges from 0.065 to 0.192 in the cored interval with the standard deviation of 0.03849 and mean value of 7.565 from the histogram plot (figure 5.10) below. The distribution of values on the histogram plot shows that the porosity values measured are generally low. In Figure 5.11, facies A was identified as reservoir and facies B and C as non-reservoirs, though facies A is predominantly consisted of low porosity values.

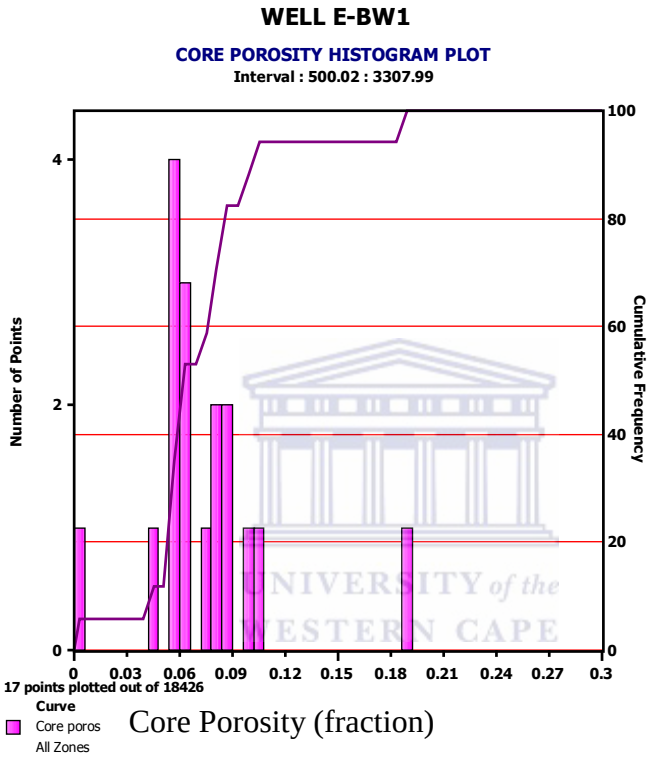

Figure 5.10: Core porosity histogram plot.

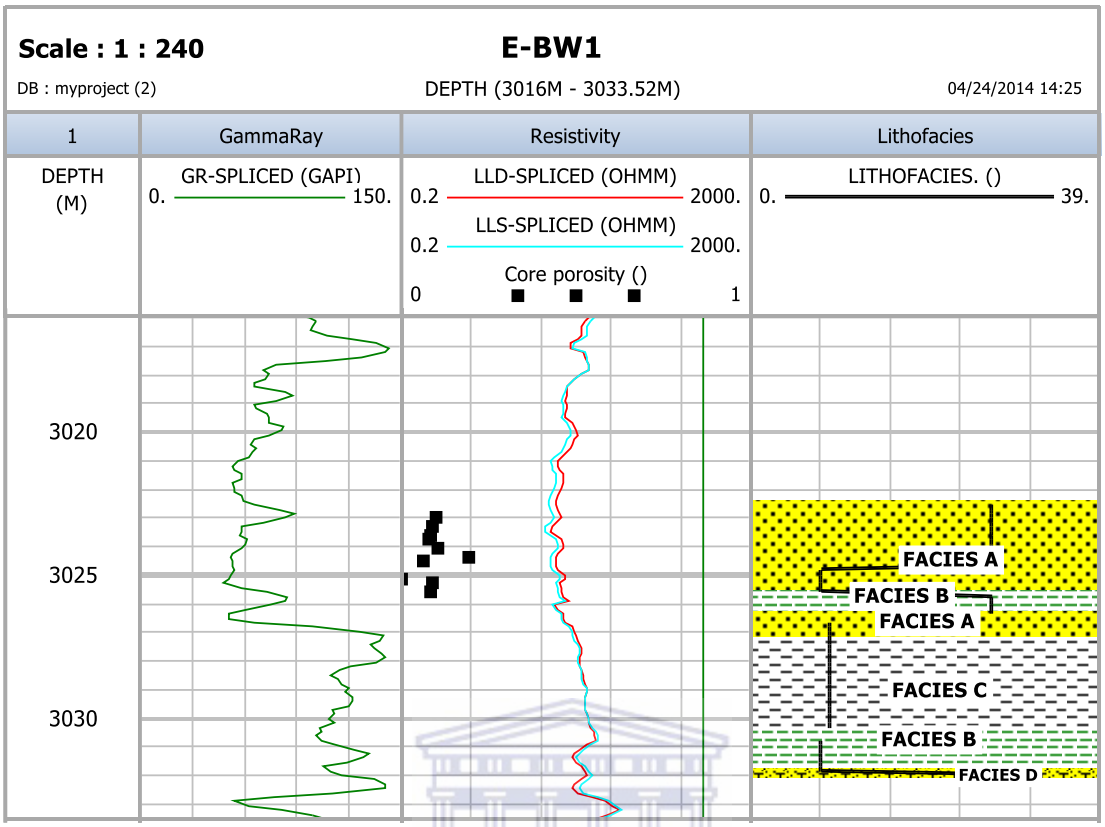

Figure 5.11: Core porosity plot (Track 3).

5.4.2.3 Well E-L1 core porosity

The core porosity of E-L1 ranges from 0.015 to 0.088 with the mean value of 0.0594 and standard deviation of 0.02134 from the histogram plot 9 (figure 5.12) below. The core porosity values are generally low as it can be seen from the distribution of values in the histogram plot and also in the core porosity versus depth plot (Figure 5.13). Facies A and B were identified as a potential sandstone reservoirs but the core porosity values proved to be too low to classify them as a reservoir. According to the measured core porosity values, facies A, B contains low porosity values and no porosity values were recorded for Facies C.

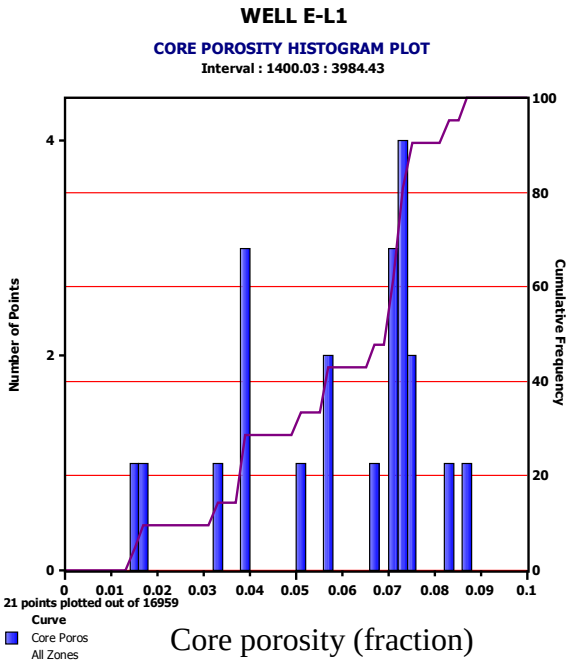

Figure 5.12: Core porosity histogram plot.

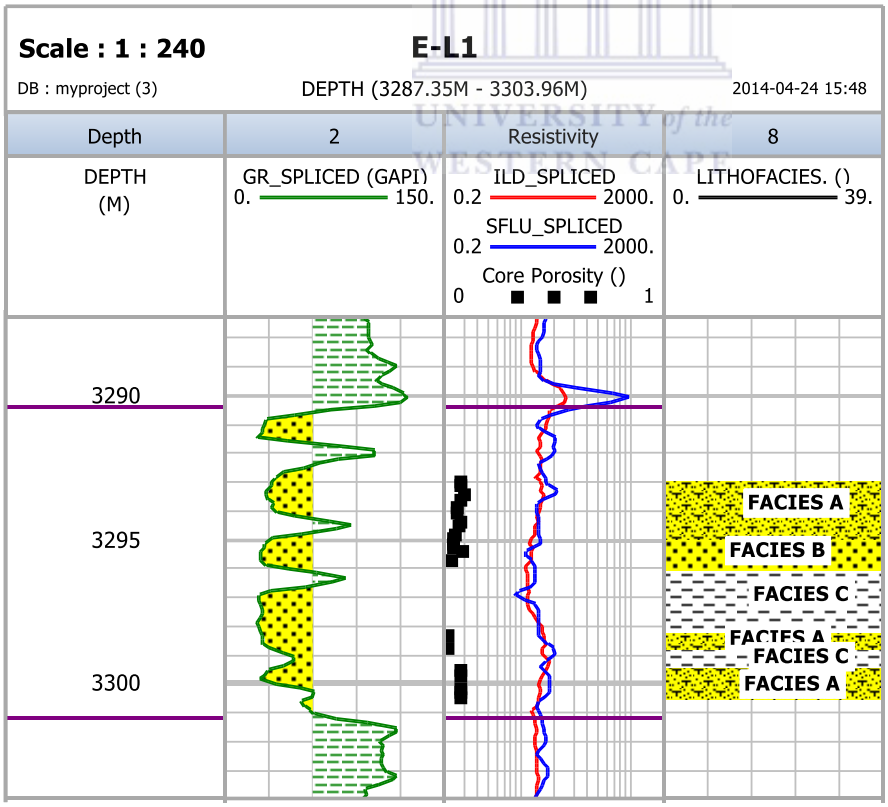

Figure 5.13: Core porosity versus plot (Track 3).

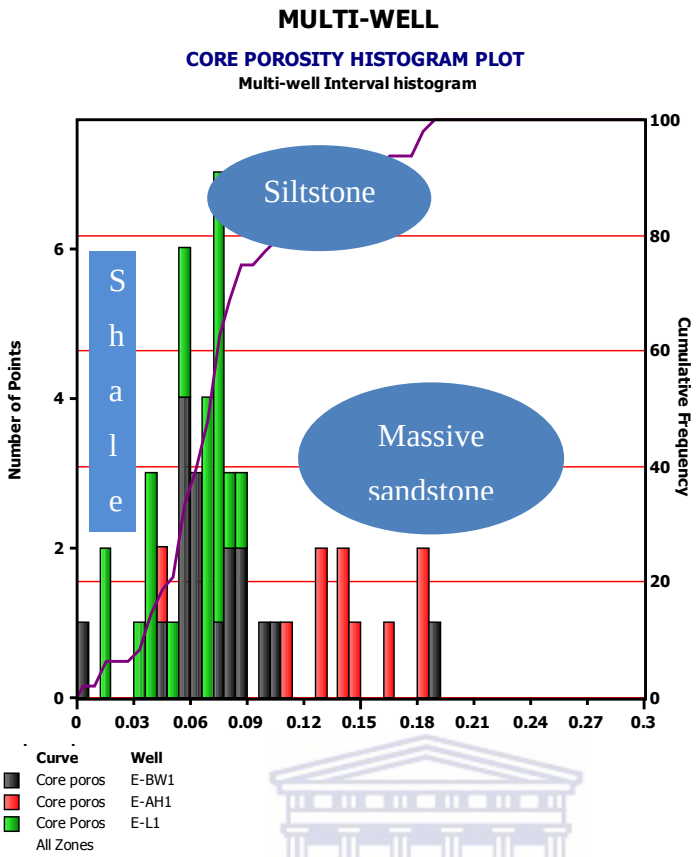

Figure 5.14: Multi-well core porosity distribution.

The histogram plot present E-AH1 well as the dominant wells in the most porous interval and well E-BW1 recorded the least value of porosity (Figure 5.14). The highest porosity value of well E-AH1 and E-BW1 were recorded in massive sandstone and lowest in shale.

5.4.3 Core permeability Interpretation

Permeability is a property of a reservoir rock which indicates the flow capacity of the reservoir. Permeability is controlled by rock grain size, grain shape, and degree of cementation, grain packing and clay. Permeability of a reservoir rocks ranges from less than 1mD to over 1000mD depending on the nature of the reservoir. Core permeability is determined by placing the plugs in a compliant sleeve within a cylinder. The injected gas or liquid on the sleeve flows parallel to the core axis due to the pressure within a cylinder (Opuwari, 2010). This core permeability is used to help calibrate permeability derived from the log curves. Darcy's law is used to determine the permeability. Because of the differences

in the flow behavior of gas and oil more specifically in a low permeable zone, a correction called Klinkenberg correction is done on gas or air permeability (Crain, 2014). The permeability is reported as air or gas (Klinkenberg correction effect). Klinkenberg discovered that permeability measured with air as the flowing fluid is different from the one measured with liquid as a flowing fluid. This is because when the measurements are made in the laboratory, liquid had a zero velocity at a grain surface whereas gases exhibited some finite velocity at the same grain surface. This results in a higher flow rate for the gas than for liquid at a given pressures (Crain, 2014). Liquid permeability values were used for this study for consistency.

The classification of the permeability of a reservoir is shown in the Table 5.5 below:

Table 5.5: Classification of the permeability of a reservoir

Permeability Values (mD)	**Classification**
Less than 1	Poor
Between 1and10	Fair
Between 10 and 50	Moderate
Between 50 and 250	Good
Above 250	Very good

(Modified after Djebber, 1999).

5.4.3.1 Well E-AH1 permeability

The permeability of well E-AH1 was measured horizontally and vertically. The horizontal measured permeability is accepted as the rock permeability because it is measured parallel to the bedding which is the major contributor to fluid flow into a typical reservoir. The permeability values of the well were presented as permeability to air and liquid. The air permeability ranges from 0.02mD to 83mD and the liquid permeability ranges from 0.037mD to 94mD (Table 5.1).

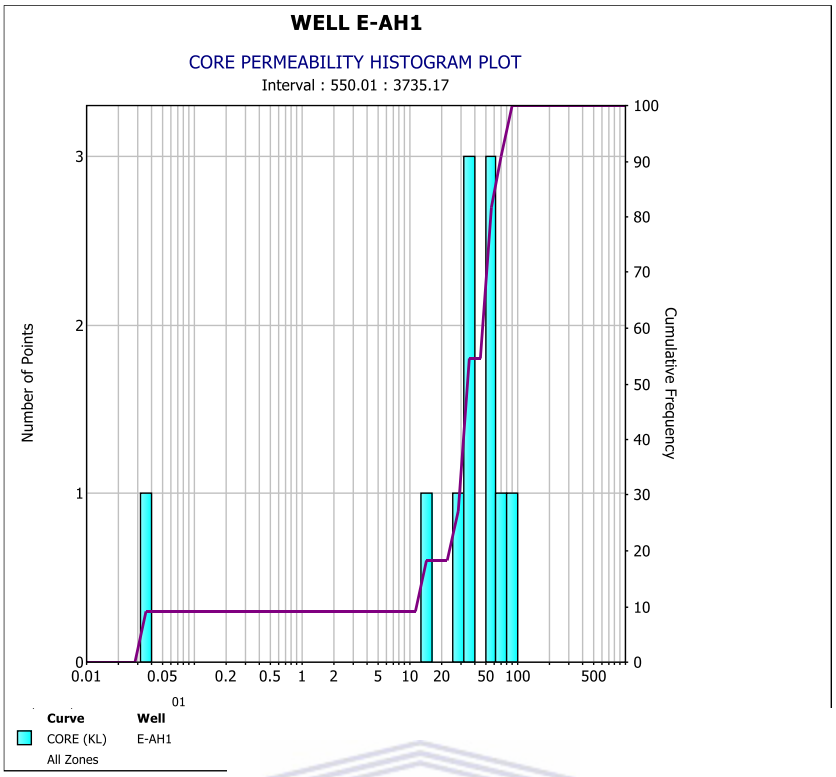

Figure 5.15: Core permeability histogram plot.

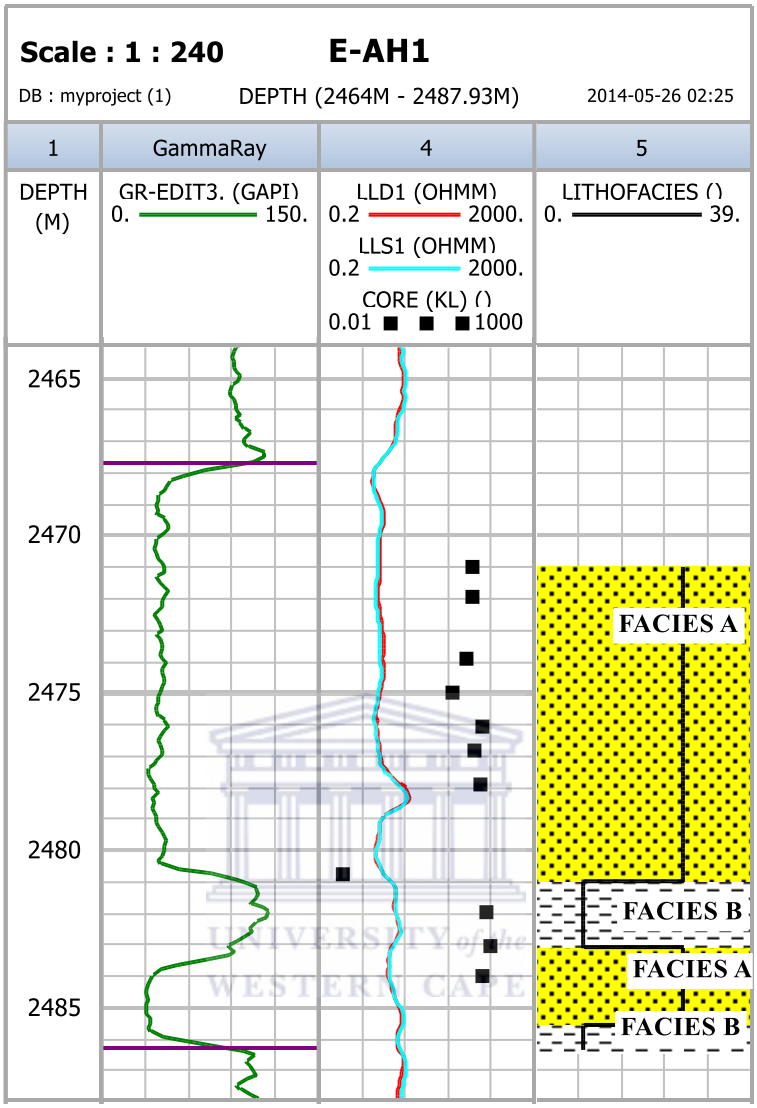

Figure 5.16: Core permeability (Core KL) plot (Track 3).

The core permeability values ranges from 0.037mD to 94mD with the mean value of 22.983mD and a standard deviation of 9.034mD obtained from the histogram plot above (Figure 5.15). The core permeability can be classified according to the standard classification of the permeability of reservoir as moderate to good (Table 5.5). The histogram plot and the core permeability show that the permeability values are concentrated between 10mD-100mD (Figure 5.15 and 5.16). Facies A has been found to support greater permeability values (Figure 5.16).

5.4.3.2 Well E-BW1 permeability

The core permeability values of well E-BW1 ranges from 0.02mD to 33.97mD with the mean value of 0.14653 and the standard deviation of 7.611mD displayed from the histogram plot below (Figure 5.17). The core permeability was generally low throughout the selected interval (Figure 5.17) and core permeability plot in track 3 (Figure 5.18). Most of the permeability values are less than 1mD except for few points that falls between 20mD- 50mD (Figure 5.15). The core permeability can be classified as poor to fair permeability. Facies A and B has been identified as the ones with measured permeability (Figure 5.14).

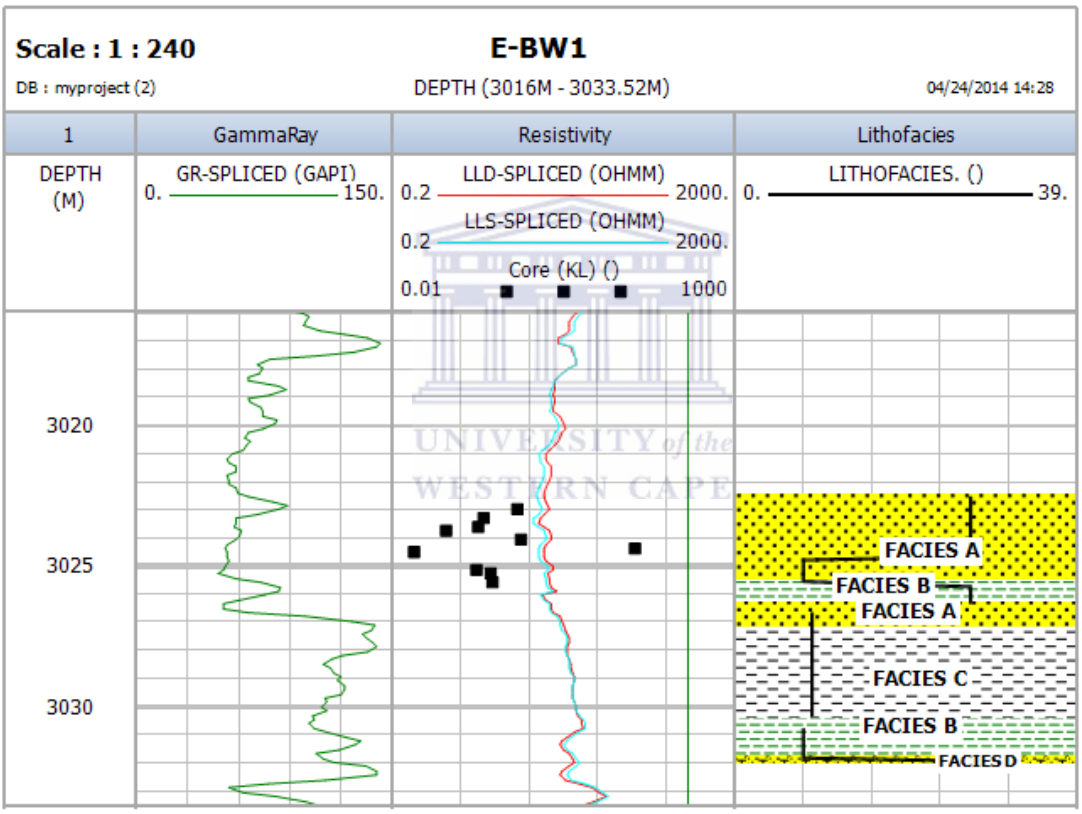

Figure 5.17: Core Permeability plot (Track 4).

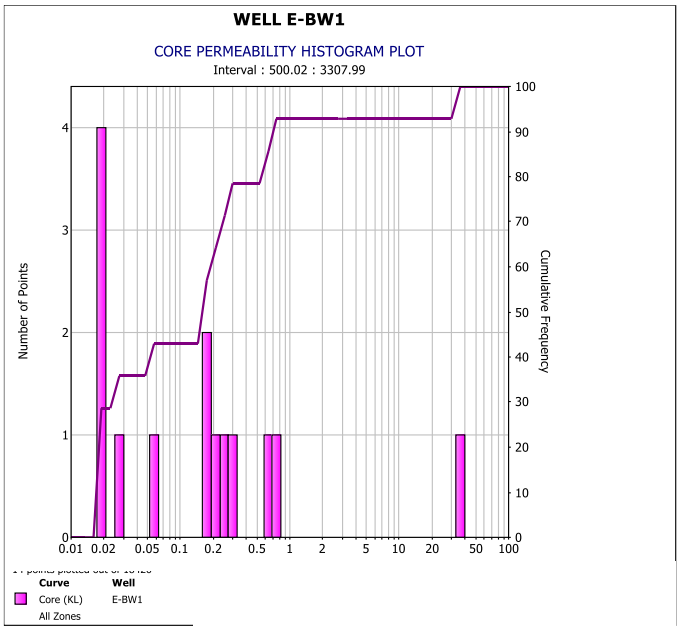

Figure 5.18: Core permeability histogram plot.

5.4.3.3 Well E-L1 permeability

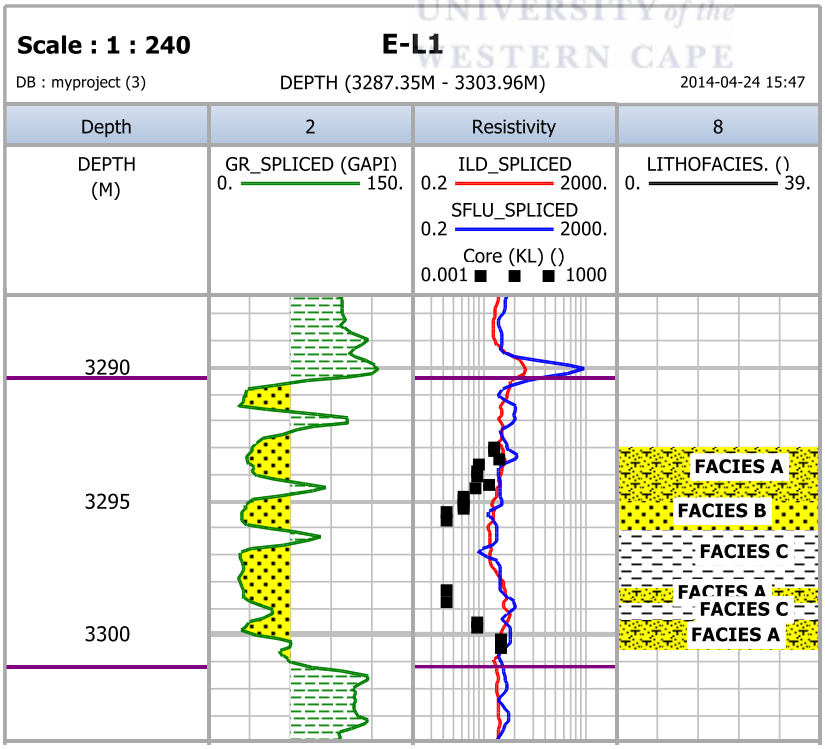

Figure 5.19: Core permeability plot (Track 4).

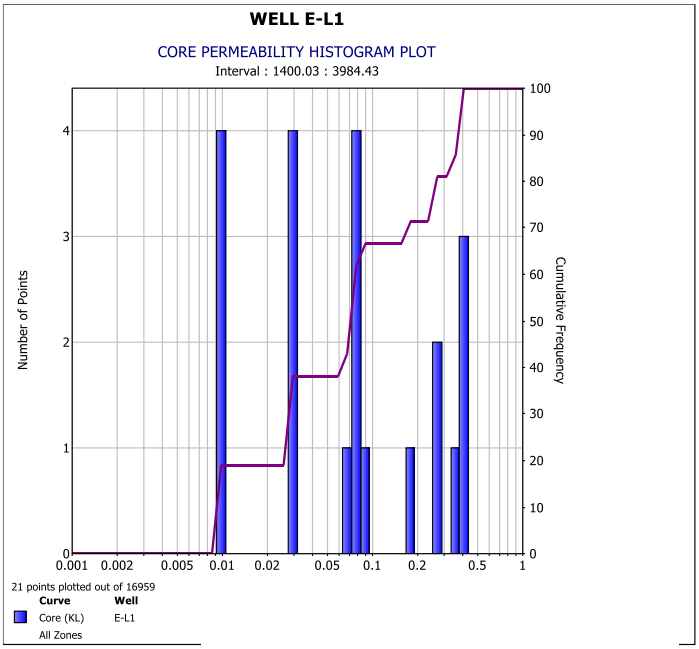

Figure 5.20: Core permeability histogram plot.

The core permeability values ranges from 0.01mD to 0.41mD with the standard deviation of 3.72mD and the mean value of 0.0703mD. Facies A and C are defined in figure 5.19 as the ones that contains the measured permeability (resistivity track). The core permeability can be classified as poor since all the permeability values were less than 1mD as it is clearly defined from the histogram plot (Figure 5.20).

5.4.3.4 Permeability distributions for all studied wells (E-AH1, E-BW1 and E-L1)

Three different areas were described in terms of permeability distribution from the histogram plot below (Figure 5.21). An area with poor permeability (less than 1.0mD) was classified as a non-reservoir rock (possibly shale). An area with permeability values of between 1mD and 10mD was classified as fair reservoir quality rocks. Another area of moderate to good permeability (greater than 10mD) was described in the histogram plot and it represents the massive sandstone. The massive sandstone area is regarded as the best sandstone reservoir because of the higher permeability. Well E-AH1 dominates the good permeability area whereas E-L1 dominates the poor permeability area.

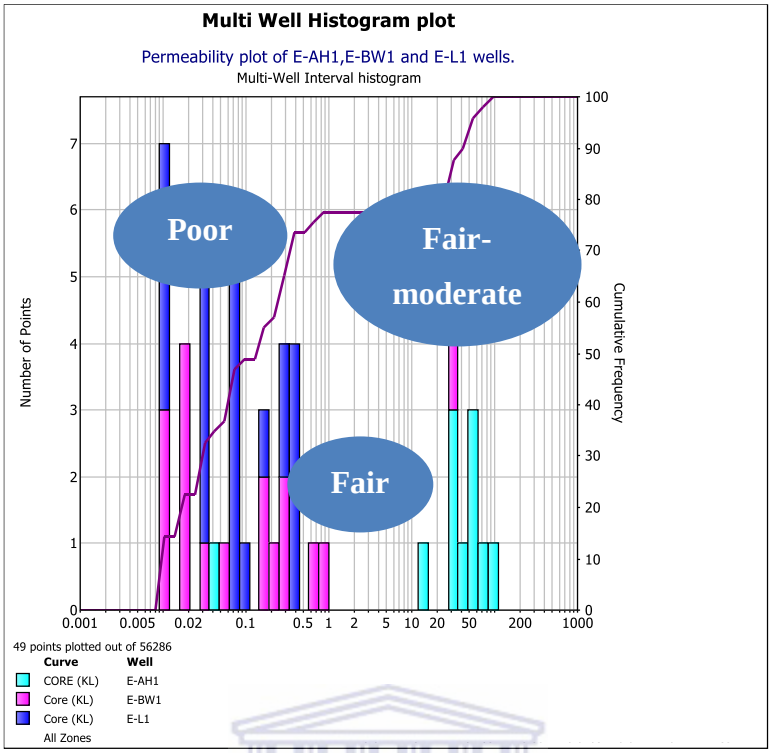

Figure 5.21: Core permeability distribution histogram plot.

5.5 Porosity versus permeability relationship

The most evident control of permeability is porosity. This is essentially this is due to the fact that the larger the porosities the more and more extensive pathways for fluid to flow. In very nearly every case, a plot of permeability introduced on logarithmic scale against porosity in direct scale for a formation, results in a clear pattern with a degree of scatter associated with the other geographical controls impacting the permeability (Glover, 2009).The porosity-permeability cross-plot should be plotted for a clearly defined lithology or reservoir zones for better results. Porosity-permeability (Poroperm) trends for different lithology can be plotted together and forms a map of poroperm relationship as shown in figure 5.22 below. The regression equation was used to determine the relationship between porosity and permeability based on the (R^2), for better results R^2 of 1 (one) or closer to one should be obtained.

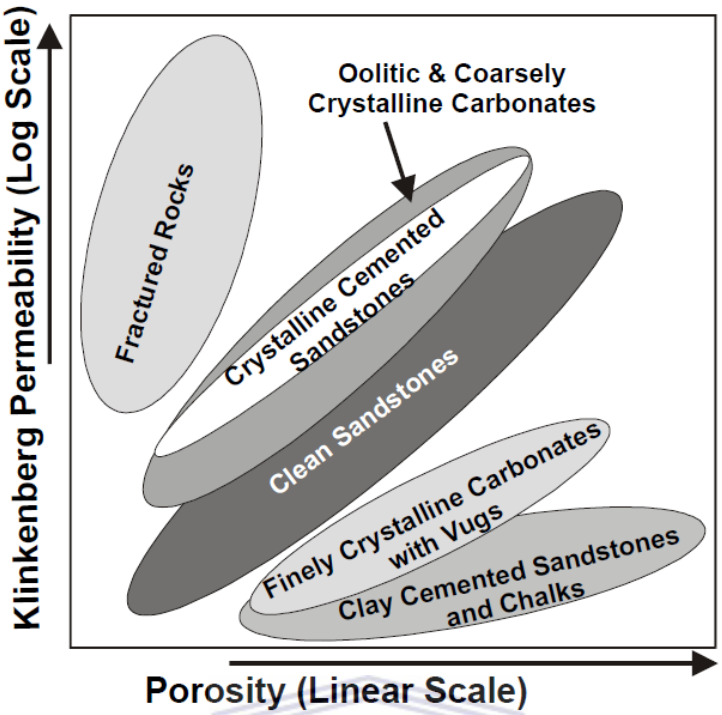

Figure 5.22: Poroperm relationship cross plot (Glover 2009).

5.5.1 Well E-AH1 POROPERM relationship

The scatter plot of well E-AH1 was not clearly defined (Figure 5.23). This was mainly because the pattern of scatter plot was like a cloud of data in which the individual trend was not clearly visible. This shows that porosity had an influence on the permeability of this reservoir but there were other major factors controlling the permeability like carbonate cements (Dolomite and Calcite) as described in Table 5.1 previously. The regression value of 0.18 just confirms the poor relationship between porosity and permeability.

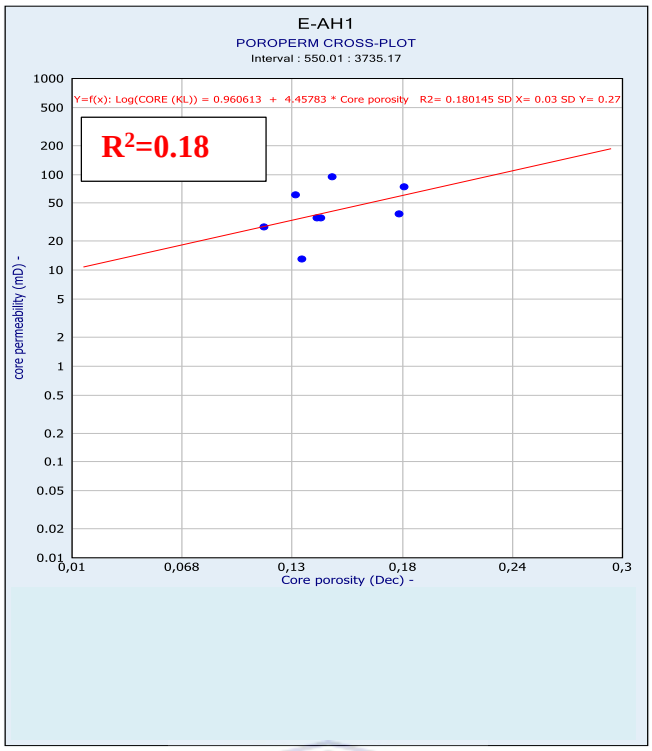

Figure 5.23: Porosity versus permeability cross-plot of E-AH1.

5.5.2 Well E-BW1 POROPERM relationship

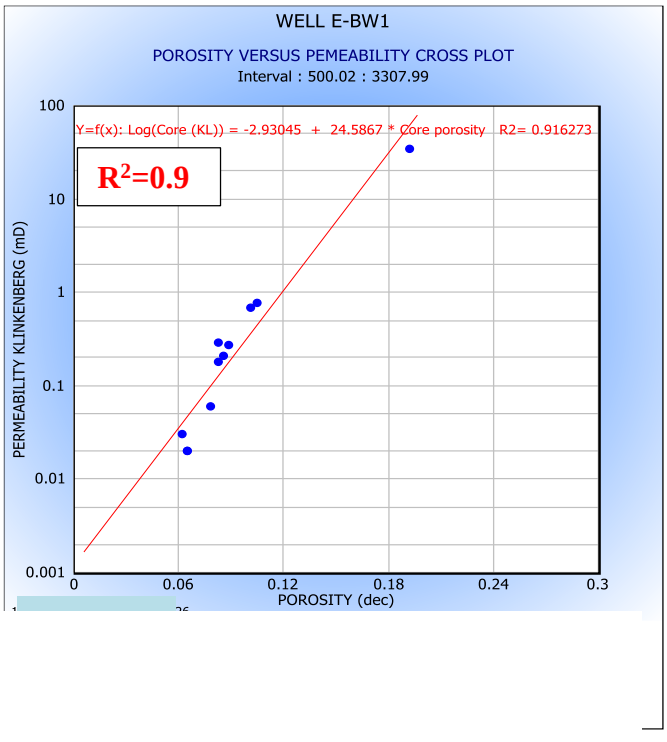

Figure 5.24: Porosity versus permeability cross-plot of E-L1.

It was clear that the permeability of the sandstone was extremely controlled by the porosity (Figure 5.24). The trend of the data was clearly visible. The regression value of 0.92 shows a strong relationship between porosity and permeability. This trend can be classified as crystalline cemented sandstones based on 5.22.

5.5.3 Well E-L1 POROPERM relationship

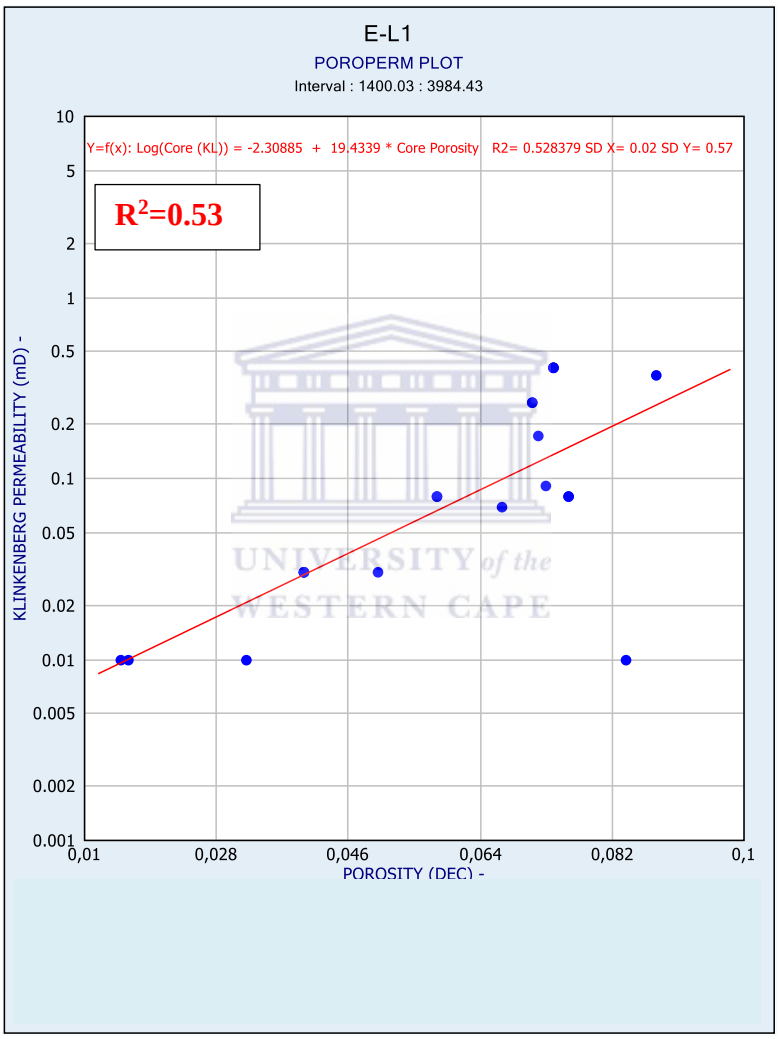

Figure 5.25: Porosity versus permeability cross-plot.

The trend of the data plots in Figure 5.25 was not clearly visible. This was mainly because the plot was like a cloud of data, more or less like those of well E-AH1 (Figure 5.23). This also shows that the porosity is not the only geological factors influencing permeability. The regression value of 0.53 indicates that the poroperm relationship is moderate.

5.6 Fluid Saturation Interpretation

Fluid saturation is the fraction of the interstitial space in a pore system occupied by oil, gas or water (Bennion et al., 1996). The pore space in the rock is never empty and is either filled with one of the fluid or by the combination of the fluids. Fluid saturation is a key factor in determining the initial reserves and also dominates the reservoir flow properties because of the influence they display on relative permeability. If fluid saturation is wrongly measured it can results in a gross over or underestimation of gas or oil in place (Bennion et al., 1996). The fluid saturation was obtained by using the plug-end trims of the core plug. Dean stark extraction method which involves the use of both heat and organic solvent was used to extract the fluid. In this study, the symbol used to represent water saturation was Sw, Oil saturation was So and Sg for Gas saturation.

5.6.1 Well E-AH1 fluid saturation

Three types of fluid saturation (Sg, So and Sw) were reported in well E-AH1. The average saturation of water (Sw) measured was 0.617, gas saturation (Sg) of 0.321 and oil saturation of approximately 0.062 was measured and presented below (Figure 5.26).

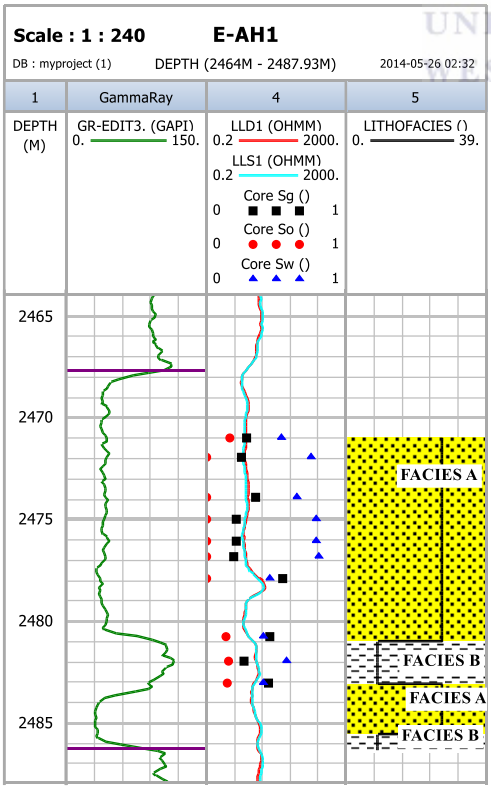

Figure 5.26: Well E-AH1 fluid saturation plot (track5).

Fluid saturation track (track 4) shows an interval of increasing hydrocarbon saturation (Sg and So) between the depth of 2475m to 2484m which correspond to facies A and B (Figure 5.26). This interval also presents the minimum water saturation obtainable in a rock. However, as water saturation increases, gas and oil saturation decreases within the depth of 2472m and 2475m which correspond to facies A at the top of the interval.

5.6.2 Well E-BW1 fluid saturation

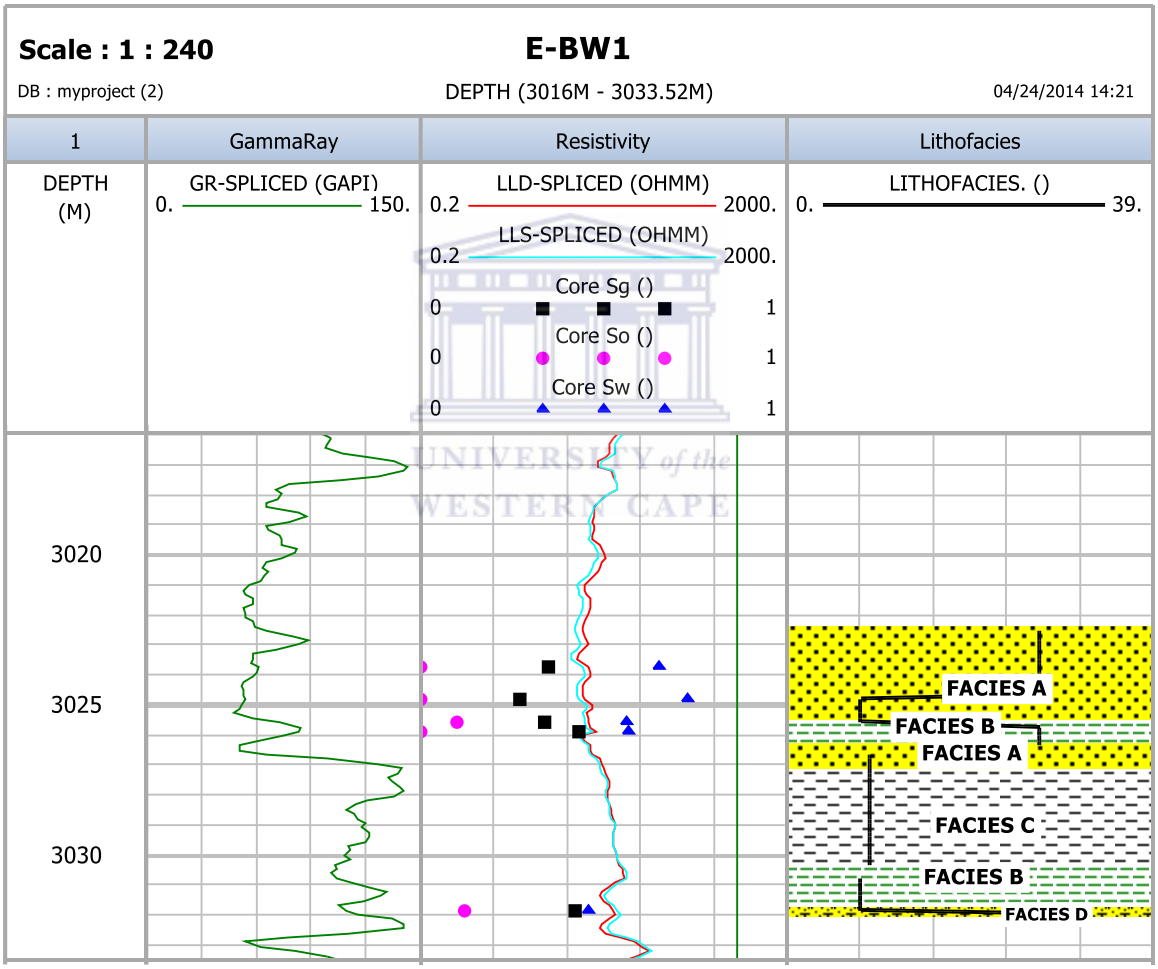

Figure 5.27: Well E-BW1 fluid saturation plot (track 3).

Three types of fluid saturation (Sg, So and So) were also recorded in well E-BW1. The reported gas saturation (Sg) was 0.39, oil saturation (So) of 0.077 and water saturation of

approximately 0.532 was measured and presented in Figure 5.27 above (track 3). Facies A represents the increasing hydrocarbon saturation from 0.20 to 0.42 between the 3022m and 3025m. Oil saturation ranges from 0% to 20% and water saturation increases from approximately 0.58 to 0.78 within the same interval.

5.6.3 WellE-L1 fluid saturation

Three types of fluid saturation (Sg, So, and Sw) were recorded in well E-L1. The reported gas saturation was 0.519 and water saturation (Sw) was approximately 0.4808 and presented in the Figure 5.25 below (track 3). The interval between 3292.17 and 3300 represent increasing gas saturation which correspond to facies A and B. This interval also presents the presence of water saturation which may be irreducible water saturation.

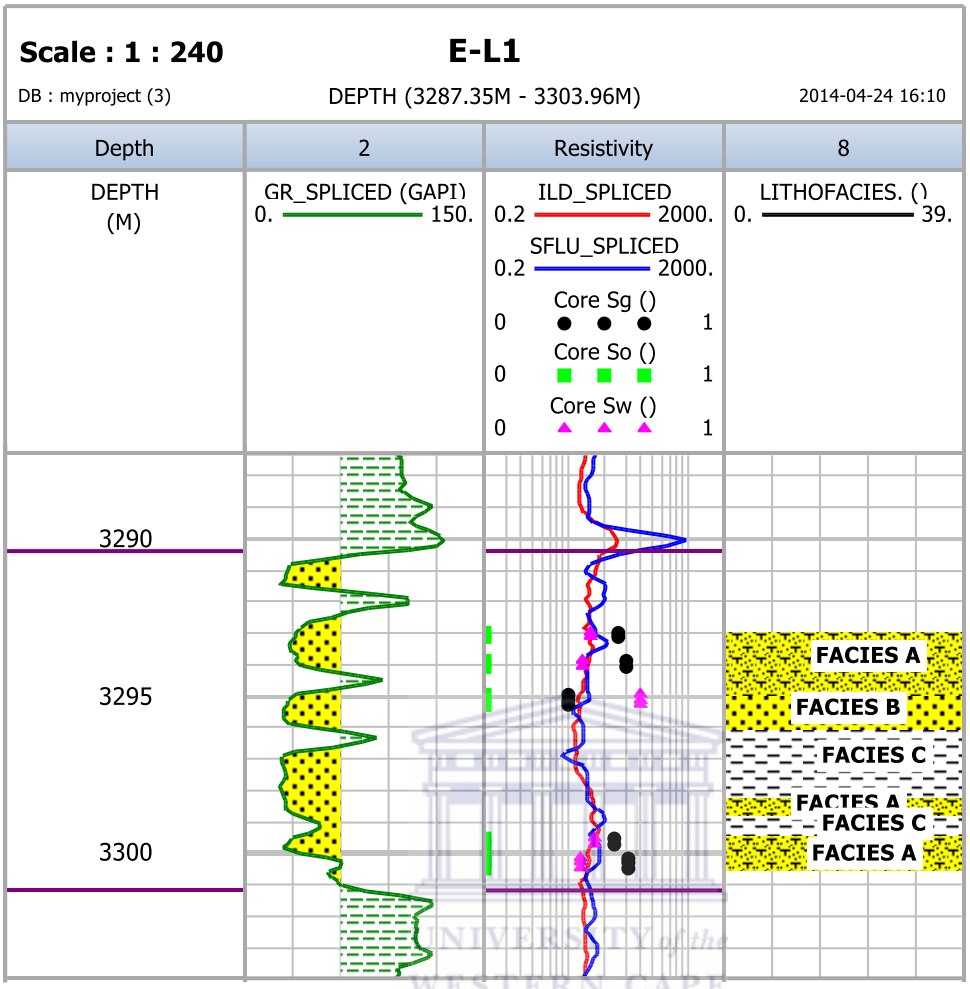

Figure 5.28: Resistivity track.

5.7 Interpretation of Geophysical wireline logs

The wireline logs give information about lithology (sandstone and shale or reservoir and non-reservoir) where sandstone with thickness of 10m or above and is controlled by a non-reservoir rock (shale) on either side is referred to as potential sandstone reservoirs and the fluids (oil and gas) in the pore spaces of the reservoirs rocks are referred to as hydrocarbon. A suite of logs from three wells in the area was provided for this study. Three wells were available (E-AH1, E-BW1, and E-L1) with a suite of logs including gamma ray (GR), Correction and Bulk density (DRHO and RHOB), neutron (NPHI), caliper (CAL), resistivity (LLD and LLS), and bit size (BS), among others. Figures 5.29- 34 show the logs for each of the three wells, over the intervals of interest. As explained in chapter 3, the first step in a log

interpretation is to identify zones of interest or potential sandstone reservoirs (clean zones with hydrocarbon) and define a clean and shale baseline on the gamma ray (GR) logs. This was achieved by observing the behavior of the gamma ray log, maximum deflection to the right indicate a shale formation and maximum deflection to the left indicate clean sandstone.

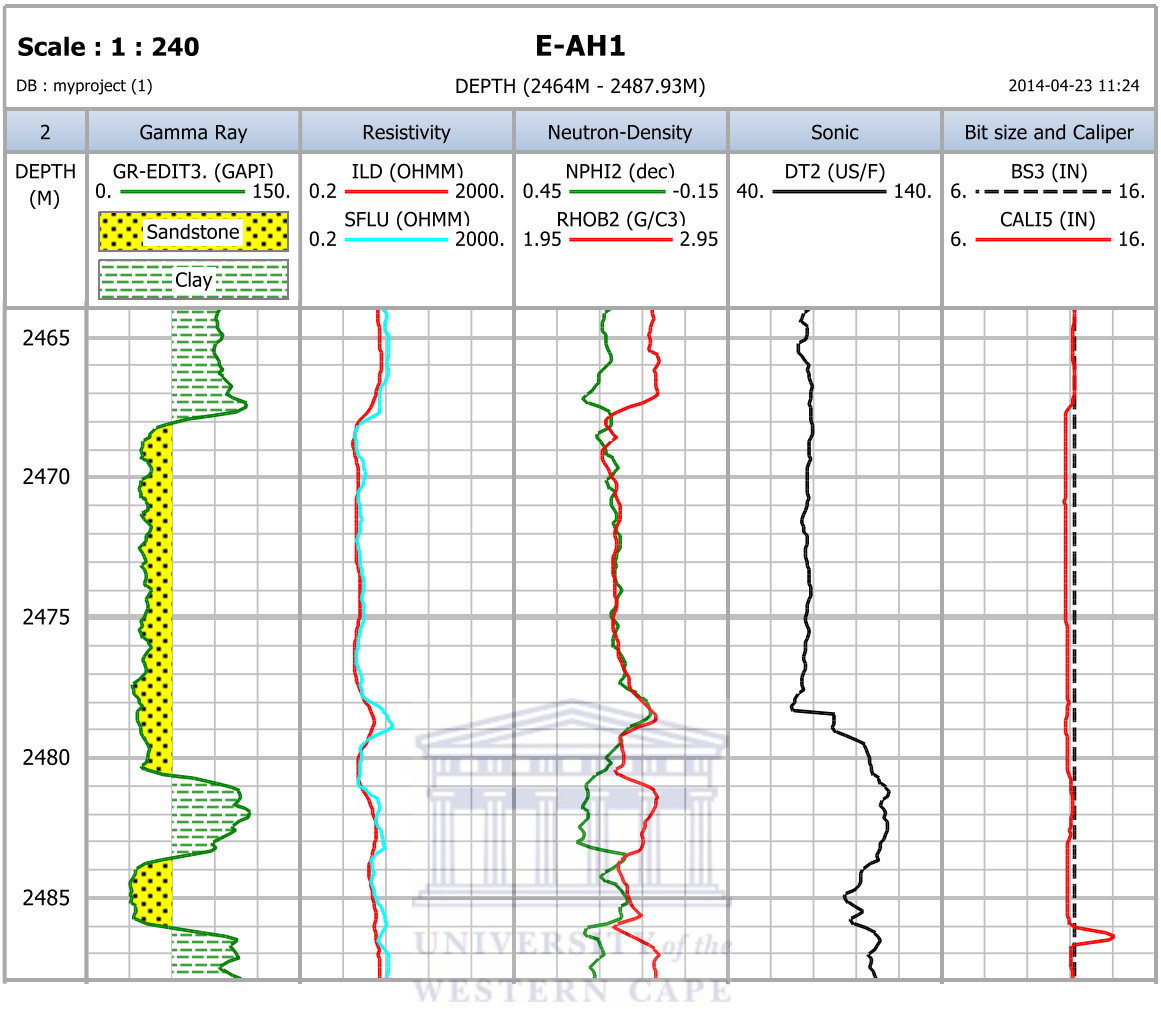

Figure 5.29: Log plot showing different log curves of well E-AH1 in different tracks.

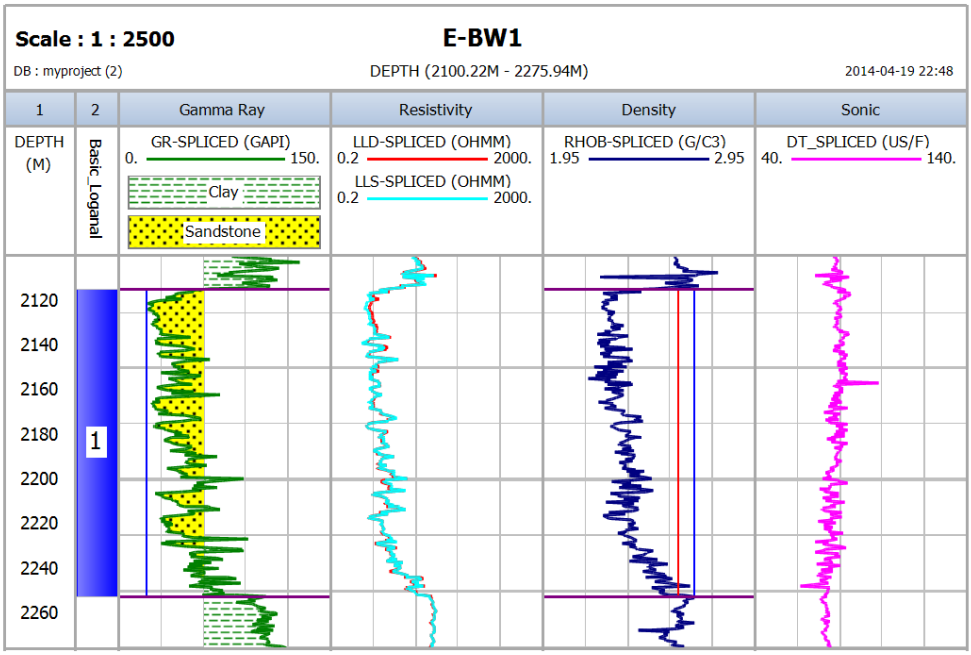

Figure 5.30: First reservoir interval of E-BW1.

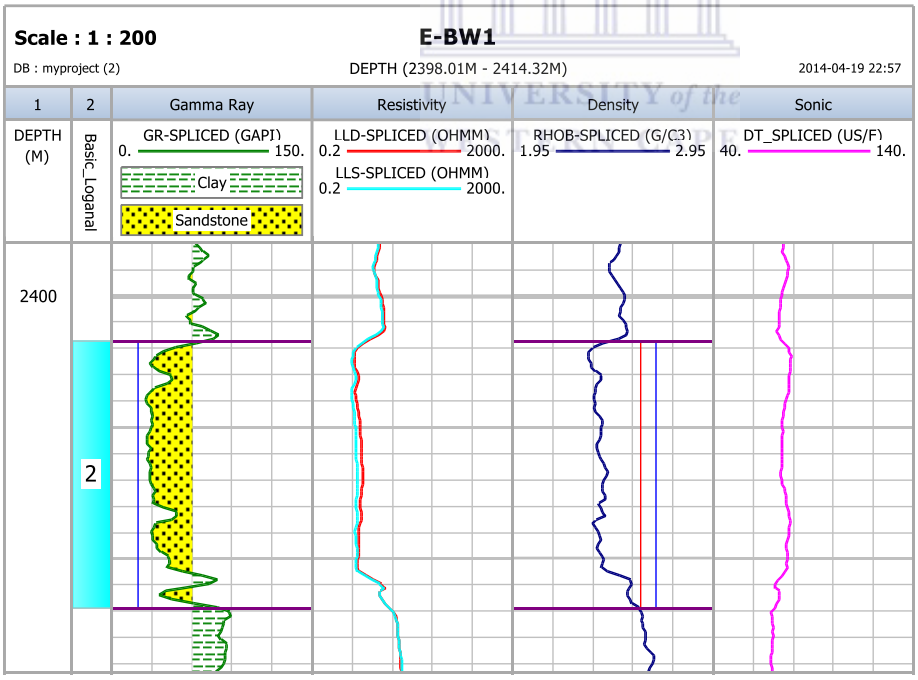

Figure 5.31: Second reservoir interval of E-BW1.

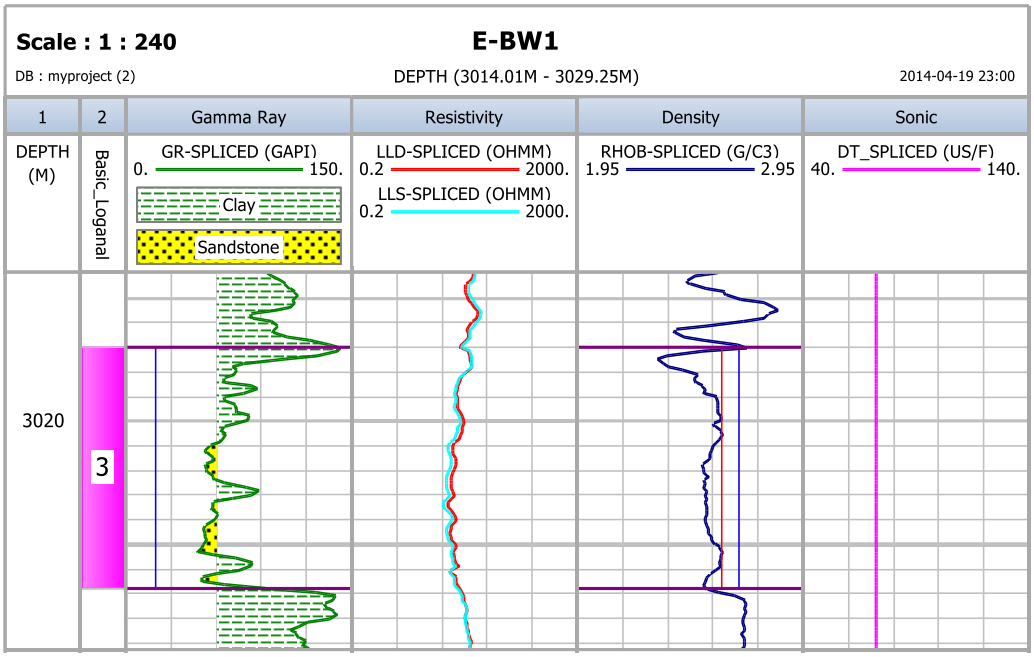

Figure 5.32: Third reservoir interval of E-BW1.

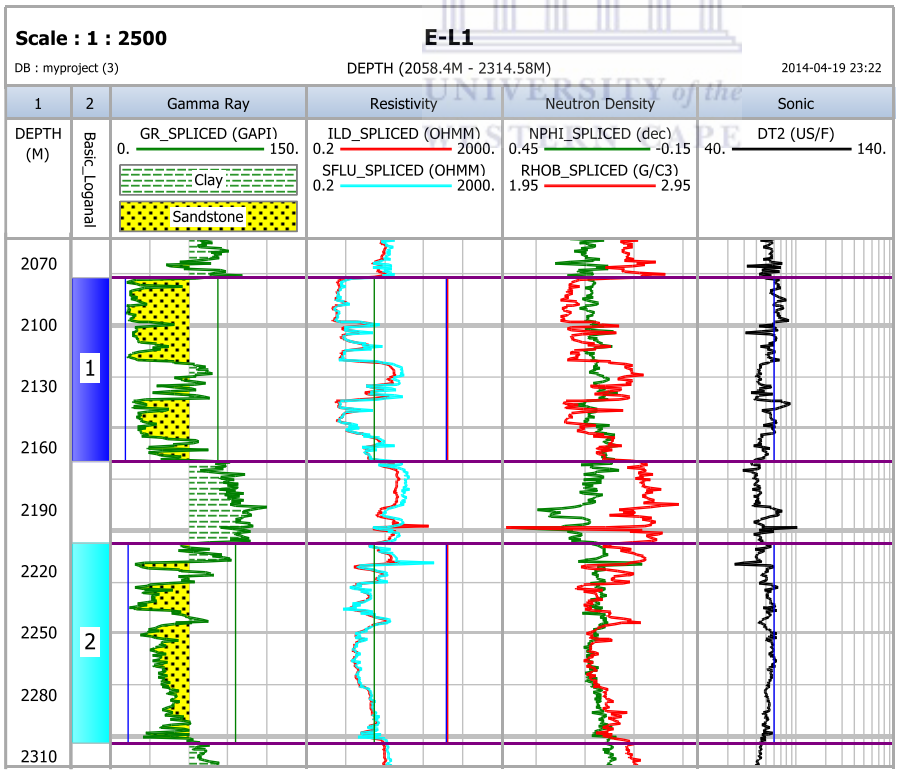

Figure 5.33: First and second reservoir interval of well E-L1.

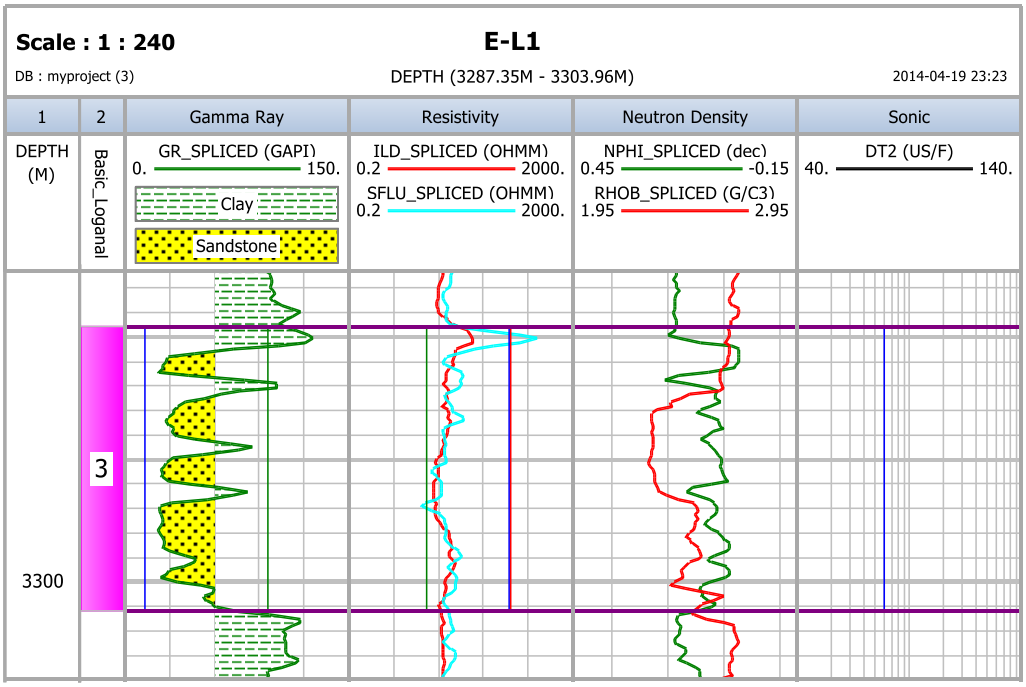

Figure 5.34: Third reservoir interval of well E-L1.

5.7.1 Well E-AH1 wireline logs interpretation

The selected potential reservoir interval (clean sand zone) of well E-AH1 selected from the gamma ray log is between 2467.70m and 2486.40m (Figure 5.29). Figure 5.29 (Track 4) shows deep (LLD1) and shallow (LLS1) resistivity log. Both resistivity log are generally low throughout the reservoir interval (indication of water within the interval) except for (4278m-2479m) depth where both resistivity tends to slightly increase, this slightly increase in resistivity indicate the possible presence of hydrocarbons at those intervals. However the possible presence of hydrocarbon is not confirmed by the (neutron porosity- density log) because there was a no cross-over between neutron and density log to indicate the presence of gas (gas effect).

5.7.2 Well E-BW1 wireline logs interpretation

Three potential reservoir intervals (clean sand zone) were selected (2114.50m-2252.50m, 2388.20m-2411.90m and 3012.00m-3033m) for analysis from the gamma ray log (Figures 5.30-32) and are shown in figures (5.30-32). Track 4 shows deep (LLD-SPLICED) and shallow (LLS-SPLICED) resistivity logs. There is no separation between the two logs

throughout the entire interval. In figures5.30 and 5.31 the reading of the resistivity logs is generally lower as compared to the readings of resistivity logs in figure 5.32. There was no neutron log available to determine the presence of gas in a reservoir.

5.7.3 Well E-L1 wireline logs interpretation

Figures 5.33 and 5.34 above show three potential reservoir intervals (sand zone) between the depths of 2077.10m-2166.10, 2205.80m-2303.20m and 3290.40m-3301.201m selected from gamma ray log (track 3). Figures 5.33 and 34 show both resistivity logs deep (ILD-SPLICED) and shallow (SFLU-SPLICED). The low resistivity readings within the reservoir intervals indicate possible presence of water and the high resistivity readings between the depths of 2116m-2134.8m, 2216.9m-2225.6m and 2239.1m-2247.2m with the cross-over in neutron-density log curves in track 5 indicate presence of gas in the reservoir. The resistivity log reading was generally high but the neutron and density log did not show any clear presence of gas within the selected interval (Figure 5.34).

Chapter 6

6 Petrophysical models

6.1 Volume of shale determination

The volume of shale (Vsh) quantity is defined as the volume of the wetted shale per unit volume of reservoir rock.

Shale volume is determined from the gamma ray log in a porous reservoir because shale is usually more radioactive than sand or carbonate (Jensen et al., 2013). The volume of shale can be expressed as decimal fraction or percentage. The first step needed to determine the volume of shale is to calculate the gamma ray index (IGR).The following linear equation is used to determine gamma ray index: $IGR = \frac{\text{GRlog}-\text{GRmin}}{\text{GRmax}-\text{GRmin}}$……(1)

Where:

IGR= Gamma-Ray Index

GRlog= Gamma-ray reading for each zone

GRmin and GRmax are the minimum (Clean sand) and maximum Gamma-ray value (shale).

The minimum and maximum values used in the equation were obtained from the gamma ray histogram plots of which one example of the multi-well histogram plot is presented below (Figure 6.1) and the rest of the histogram plots for each zone interval for all wells are presented in appendix B and their values are presented in the table below (Table 6.1). The value of (vsh) obtained have to be corrected by valid formula to obtain the optimum value usable for interpretation (Jensen et al., 2013). The volume of clay readings for each zone is obtained from the volume of clay log curves derived from the gamma ray log (See appendix C).Various non-linear (correction) equations and models used to calculate the volume of shale is presented below and the comparison of the models in Figure 6.2:

Larinov (1969) for tertiary rocks

Vsh= $0.083(2^{3.7\text{IGR}}-1)$…….... (2)

Steiber (1970) $Vsh = \frac{\text{IGR}}{3-2*\text{IGR}}$…….. (3)

Clavier (1971) Vsh= $1.7-[(3.38-(\text{IGR}+0.7)^2]^{1/2}$…….(4)

Larinov for older rocks Vsh= $0.33*(2^{2\text{IGR}}-1)$……. (5)

Table 6.1: Parameters used to calculate volume of clay within the reservoir intervals.

Well Name	Reservoir Name	Top Depth (M)	Bottom Depth (M)	GRmin (API)	GRmax (API)	GRlog (API)
E-AH1	1	2467.7	2486.3	25.603	95.198	42.167
E-L1	1	2114.5	2252.5	20.428	91.361	44.626
E-L1	2	2388.7	2411.9	25.681	86.662	53.104
E-L1	3	3017	3026.8	48.227	142.96	66.943
E-BW1	1	2077.1	2166.1	11.523	81.937	34.199
E-BW1	2	2205.8	2303.2	13.875	96.062	45.761
E-BW1	3	3289.6	3301.2	22.406	125.56	48.978

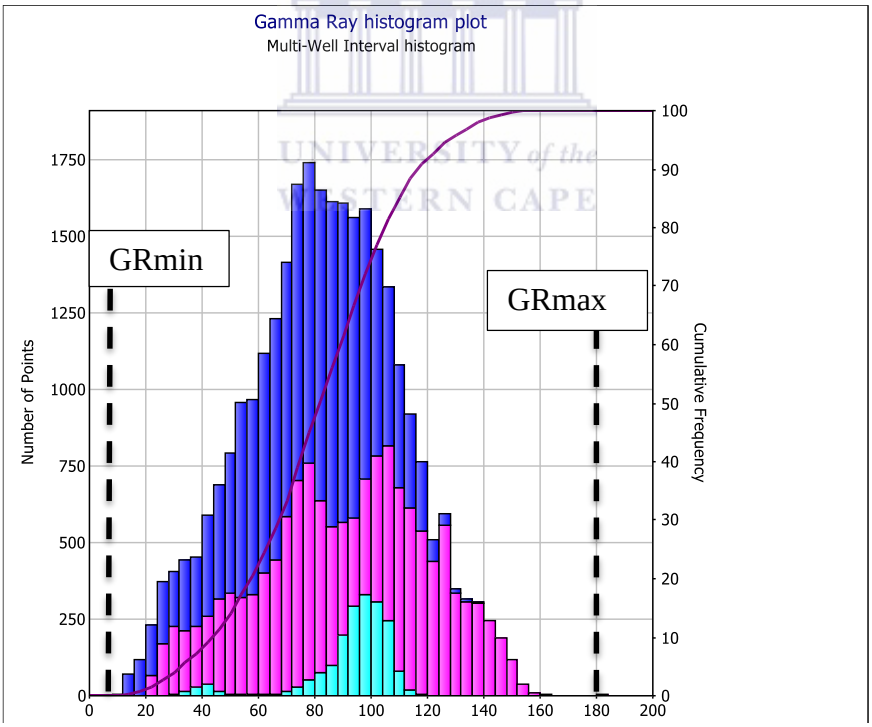

Figure 6.1: Multi-well gamma-ray histogram plot

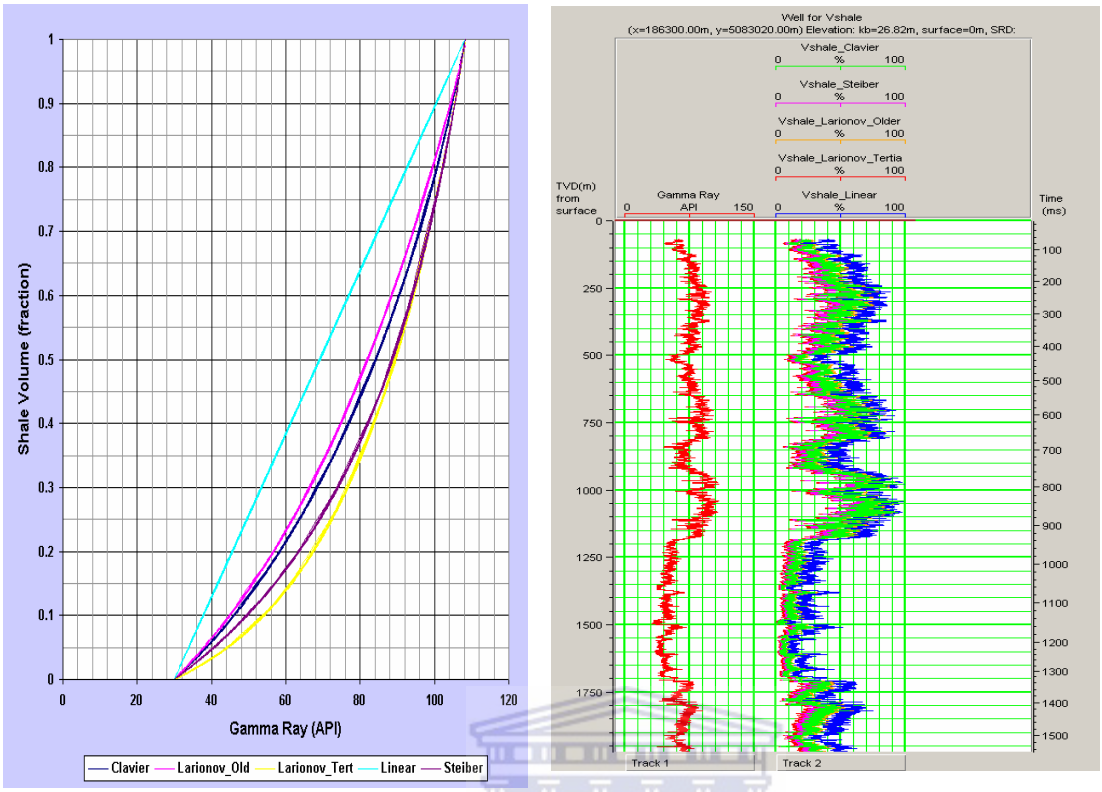

Figure 6.2: Comparison of different methods used for volume of shale determination (Saputra, 2008)

6.2 Porosity and Water saturation determination

The porosity curves were derived from the density, neutron and sonic logs. Neutron-density combination logs were used to calculate the porosity and water saturation of well E-AH1 and E-BW1 whereas density log were used for well E-L1 due to the absence of neutron log. The following formula was used to derive the density porosity log curve: $\Phi=P_{ma}-P_b/P_{ma}-P_f$..... (6)

Where: P_b= fluid density of the mud filtrate (g/cc)

P_{ma}= matrix density (g/cc)

P_f= fluid density (g/cc); salt mud=1 and fresh water= 1

And the formula used to derive the neutron porosity log curve was as follows:

PHIN= PHIe x Sxo x PHINw…….. (7)

Where: PHIN= log reading

PHIe= effective porosity

Sxo= water saturation in invaded zone

PHINw= log reading in 100% water

The porosity from the sonic slowness is different than that from the density or neutron tool. It reacts to primary porosity only (it does not react to fractures or vugs). The basic equation for sonic porosity is the Wyllie Time Average

$\Phi=\Delta tl_{og}-\Delta t_{ma}/\Delta t_f-\Delta t_{ma}$ ..... (8)

Where Δt_f= Time taken to travel through the pore space

$\Delta t_{ma=}$ Time taken to travel through the matrix.

A cluster of different porosity and water saturation curves were plotted from the database development so as to obtain the correct curves for water saturation and porosity, the curves derived from the IP software had to be calibrated with the core data and then select the best curves that best fit the trend set by the core data. Modified Simandoux water saturation (SwModSim), Simandoux (SwSim) water saturation and Modified Indonesian water saturation (SwModind) curves were found to be the best fit curves when calibrated with the core data of well E-AH1, E-BW1 and E-L1 and were presented in appendix C. Below is the example of the calibration of log curves with the core data and the selection of the best fit curves (Figures 6.3 and 6.4).

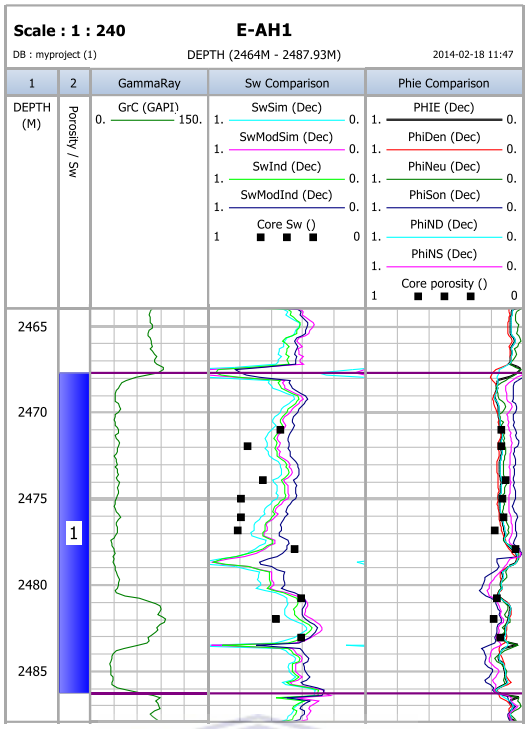

Figure 6.3: Example of the calibration of log curves with the core data.

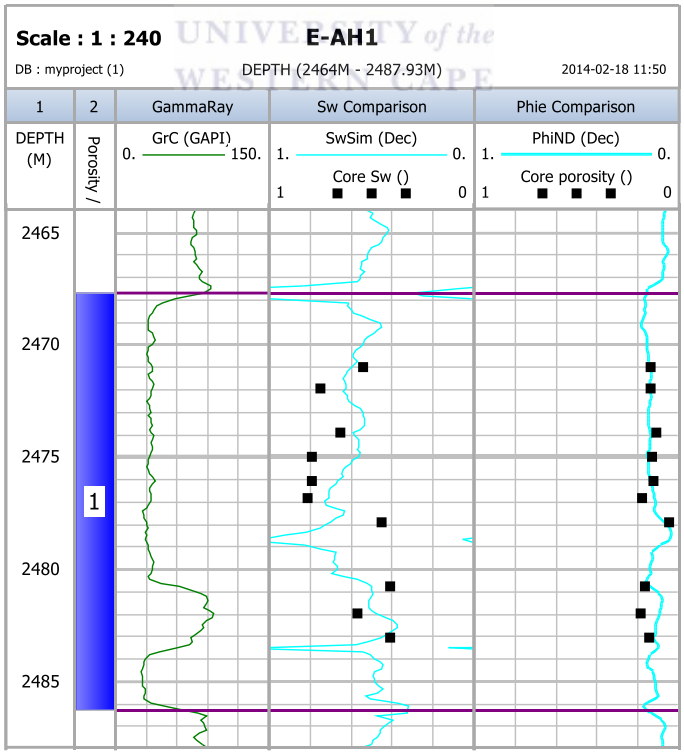

Figure 6.4: Example of the selected log curves that best fit the core data trend.

The water saturation of this reservoir rocks has been determined from the calibration of core data with the wireline logs (log derived water saturation model). The determination of water saturation from log curves can be grouped into two models namely, clean sand (shale free) and shaly sand models. The reservoir rocks in this study are shaly-sand reservoir; therefore shaly-sand water saturation model has been used to determine the water saturation. Basic log analysis parameters calculated from the standalone picket plots (appendix A) in a water bearing interval were presented in Table 6.2. The water saturation models used were simandoux, modified simandoux and Indonesia models. The models used the effective porosity as the input porosity in the water saturation model.

Simandoux (1963) proposed the following relationship:

$$\mathbf{Sw = aRw / 2\Phi m - Vsh/Rsh + \sqrt{(Vsh/Rsh)\ 2 + 4/F * Rw * Rt}} \quad \ldots\ldots\ldots\ldots (9)$$

Where:

Sw = Water Saturation

a= Equation Coefficient

Rw = Resistivity of water

Rsh = Resistivity of shale

Vsh = Volume of shale

F = Formation Resistivity factor

Rt = True formation resistivity from corrected deep resistivity log.

Φ = Effective Porosity, fraction

m= Cementation exponent

And the Indonesian formula was proposed in 1971 by Puopon and Leveaux. The relationship can be written as follows:

$$\mathbf{1/ \sqrt{Rt} = \sqrt{\Phi e^{m}/ a*Rw} + Vcl^{(1-Vcl/2)}/\sqrt{Rcl}\ ) * Swn^{/2}} \quad \ldots\ldots\ldots\ldots (10)$$

Where:

Rt = Resistivity curve from deep log reading

Rcl = Resistivity of wet clay

Φe = Effective porosity

Sw= Water saturation, fraction

Vcl = Volume of shale, fraction

Rw= Formation water resistivity

m=Cementation exponent

a=Tortuosity factor

n= Saturation exponent

6.3 Determination of initial fluid saturation parameters

Fluid saturation parameters were determined in a water bearing zones of the studied wells.

6.3.1 Water saturation exponent (n)

The water saturation exponent value is a function of both pore framework geometry and formation wettability (Bennion et al., 1996). The water saturation exponent is generally thought to be 2.0 however this varies relying upon the formation and may bring about overestimation and underestimation of water saturation in many situations (Bennion et al., 1996. The "n" value measurement is generally conducted from samples from the range of permeability, porosity and lithology which may be available in the formation; this is because of the way that the "n" values contrast with both lithology and wettability. The standard "n" value of 2.0 is utilized so generally in the oil and gas industry. In this study the saturation exponents of each of the three wells (E-AH1, E-BW1 and E-L1) were measured to be 2 from the standalone picket plots (Appendix A) in which porosity is plotted against the resistivity in a water bearing zone.

6.3.2 Tortuosity factor (a)

Tortuosity values are measured experimentally for a sequence of formation factors that are determined on a range of porosity value samples for a given lithology that is expected to exist in a specific formation (Bennion et al., 1996). The degree of consolidation controls the Archie constant because generally the lower the degree of consolidation the lower the value of the tortuosity constant and vice versa. The value of 1.0 is found for compacted sands, and a value as low as 0.62 for poorly consolidated sands and it may exceed 1.0 as the degree of compaction becomes extreme (Bennion et al., 1996). The tortuosity constant value was calculated to be 1.0 for all three wells from the standalone pickets plot (Appendix A). The 1.0 value shows that the sands for all three wells are compacted.

6.3.3 Cementation exponent (m)

The value of the cementation exponent depends on the degree of cementation and the type of cementation in the pore system. Generally a value of 2.0 is used, but this value can vary depending on the degree of cementation (Bennion et al., 1996). For example, for a poorly cemented rock "m" value may be less than 2.0 and for a highly cemented or ooliclastic rock "m" values may be as high as 3. The cementation values of 1.97, 1.98 and 2 were measured for well E-AH1, E-BW1 and E-L1 from the standalone picket plot (Appendix A) respectively. Well E-AH1 and E-BW1 are poorly cemented as compared to well E-L1 which is highly cemented with carbonates minerals (Carbonates and Dolomites).

6.3.4 Formation water resistivity

Formation water resistivity is a very important factor in the initial water saturation calculation due to the fact that the ionic composition of the water affects its overall conductivity and hence resistivity. This factor is controlled by the type of water that is present in the formation. Fresh water exhibit high resistivity while saline brine exhibit low resistivity. Standalone picket plots (Appendix A) was used to calculate the water resistivity (Rw) and the values of 0.0606, 0.0844 and 0.0605 for well E-AH1, E-BW1 and E-L1 were obtained.

Table 6.2: Basic log analysis parameters calculated from the standalone picket plots.

Well Name	Top Depth(M)	Bottom Depth (M)	Rw	m	n	a
E-AH1	2467.7	2486.3	0.0606	1.97	2	1
E-BW1	2113	2252.2	0.0844	1.98	2	1
E-L1	2205	2303	0.0605	2	2	1

6.4 Permeability determination from well logs

In simple terms, permeability is the ability of the rock to allow fluids (gas, water or oil) to flow through the pore spaces. Permeability is very essential when calculating the storage and flow capacity of the fluid in the reservoir. Permeability is the most difficult property to

determine and predict (Mohaghegh et at., 1997). Different methods are used to predict permeability. In this study only two methods (Empirical models and multiple variable regressions) are discussed and only multiple variable regression method was used. Empirical models are based on the correlation between porosity, permeability and irreducible water saturation and they are consisted of four models, namely: Tixier, Timur, Coates and Dumanoir, and Coates (Mohaghegh et at., 1997). Three of these models (Tixier, Timur and Coates) assume values of cementation (m) and saturation exponent (n) and can be applied to clean sand formation where residual water saturation exists. These methods use core and log data to calculate common exponent *w* for both n and m. However, they may not work if the reservoir is heterogeneous (Mohaghegh et, at. 1997). The second method is called multiple variable regressions; this is the method that was used to predict permeability in this study. Old wireline logs were run in the well and permeability was not determined directly from the wireline log. However, permeability (predicted K) was estimated from the regression equation obtained from the porosity versus permeability cross plots (Figures 6.5-7). The following regression equations were used to predict the permeability of the respective wells:

$K_{E\text{-}AH1}$ = 10^ (0.960613+4.45783*PhiND)…… (11)

$K_{E\text{-}L1}$= 10^ (-2.30885+19.4339*PhiSon)……..… (12)

$K_{E\text{-}BW1}$= 10^ (-2.93045+24.5867*PhiDen)……..…. (13)

Where,

PhiND= Neutron-Density porosity

PhiSon= Sonic porosity

PhiDen= Density porosity

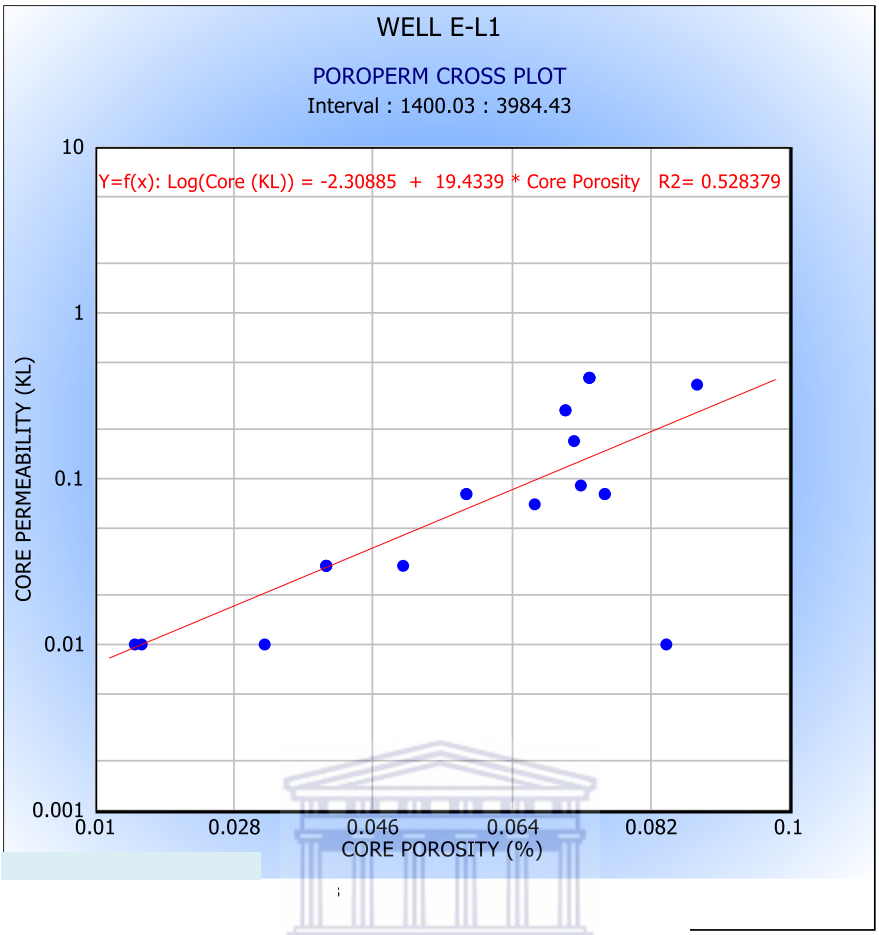

Figure 6.5: Porosity versus Permeability cross plot for well E-L1.

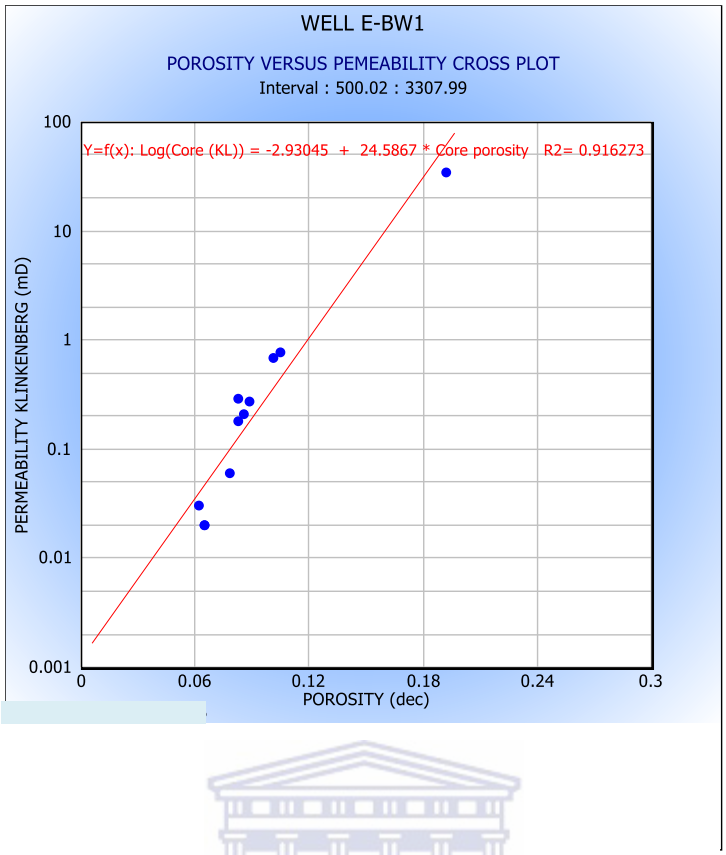

Figure 6.6: Porosity versus Permeability cross plot of well E-BW1.

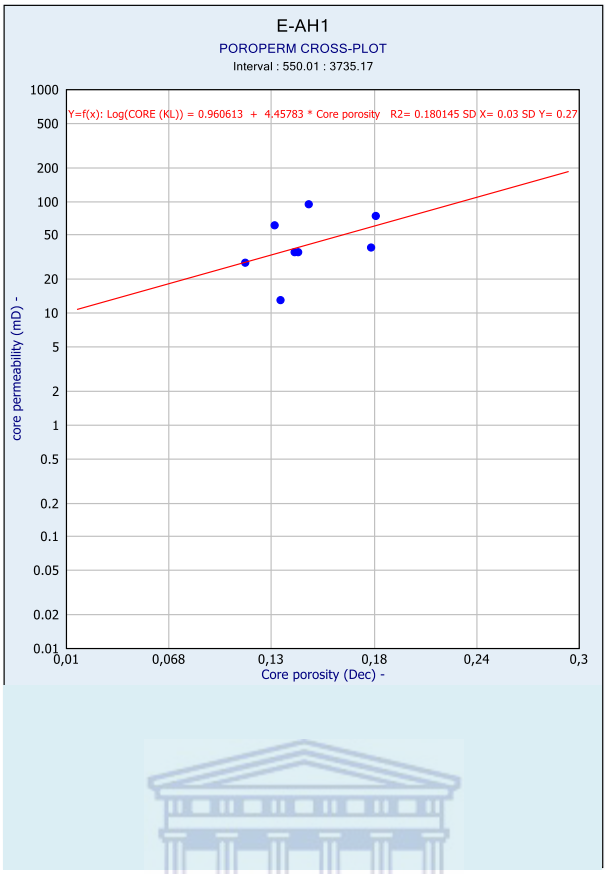

Figure 6.7: Porosity versus Permeability cross plot of well E-AH.

The IP interpretation calculator was used to generate the predicted permeability (Predicted K) as log curve and then displayed in one of the log track to estimate the average permeability at the specific depth based on the given scale. Below is the predicted permeability of selected reservoirs for each well displayed as log curves (Figures 6.8-13).

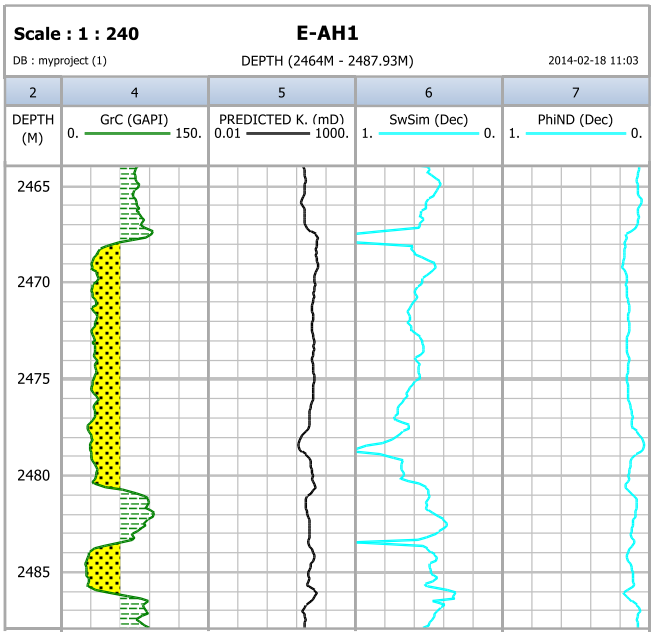

Figure 6.8: Log curves plot displaying predicted (track 5) permeability of well E-AH1.

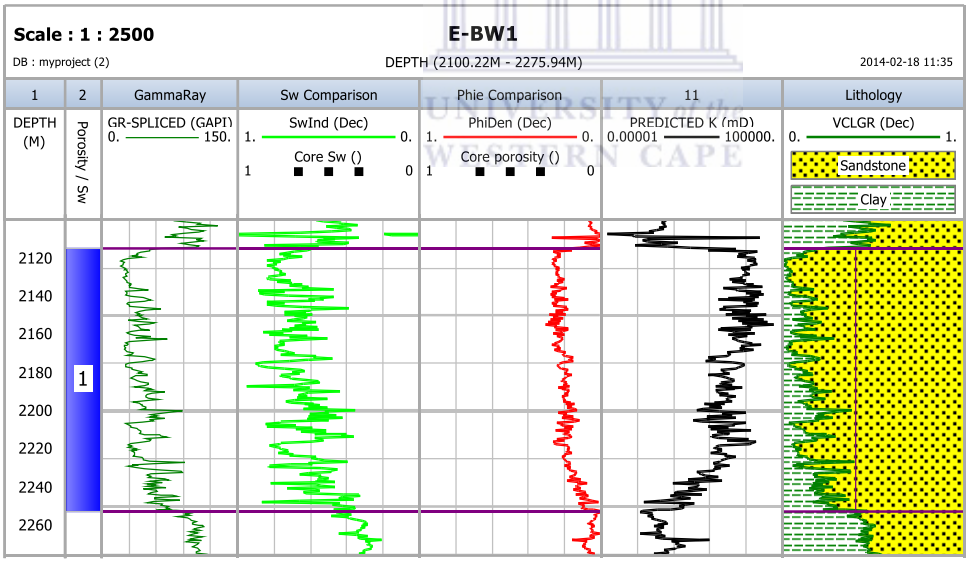

Figure 6.9: Log curves plot displaying predicted permeability (track11) of well E-BW1, reservoir 1.

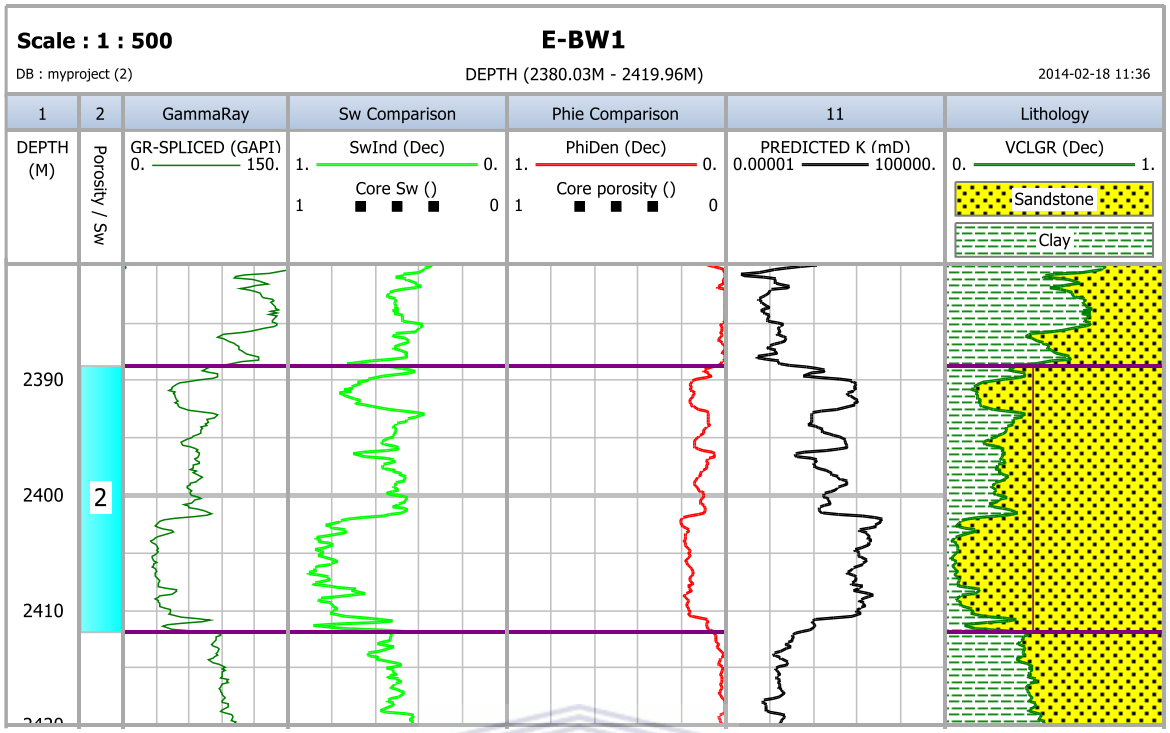

Figure 6.10: Log curves plot displaying predicted permeability (track11) of well E-BW1, reservoir 2.

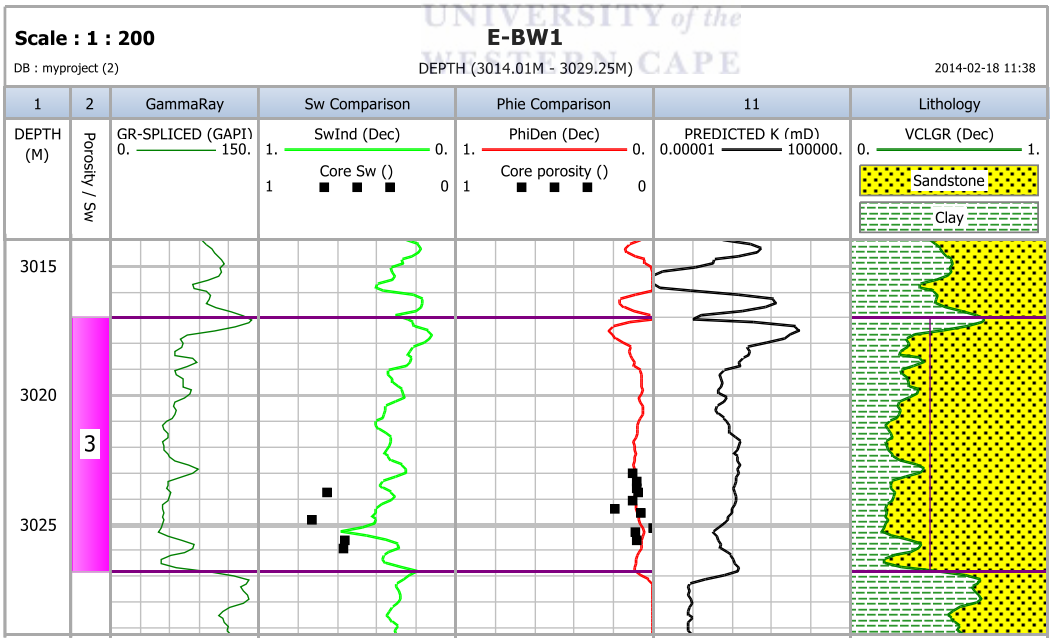

Figure 6.11: Log curves plot displaying predicted permeability (track11) of well E-BW1, reservoir 3.

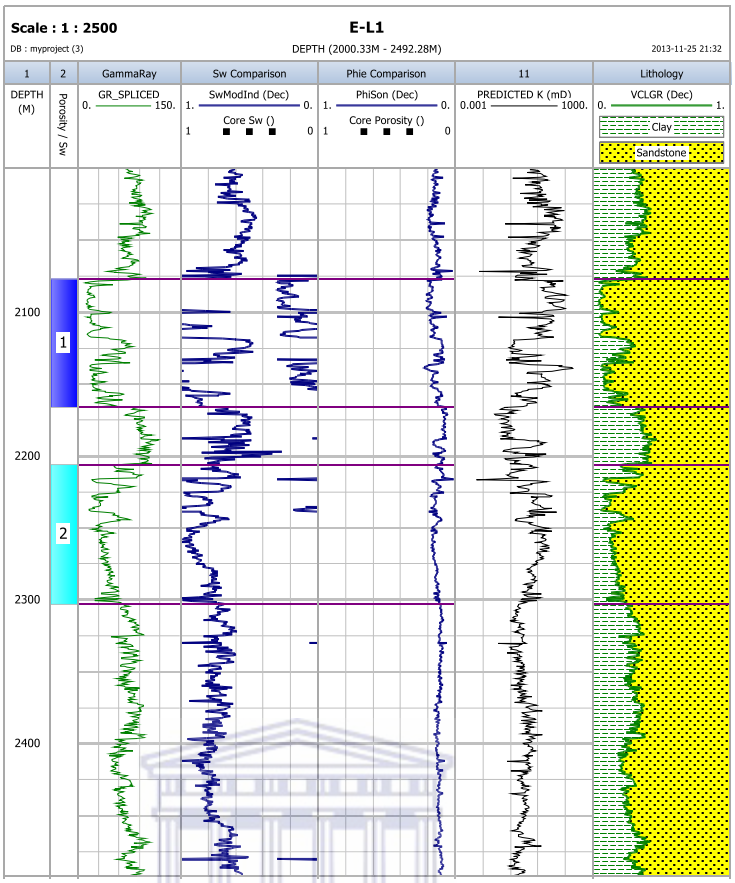

Figure 6.12: Log curves plot displaying predicted permeability (track11) of well E-L1, reservoir 1 and 2.

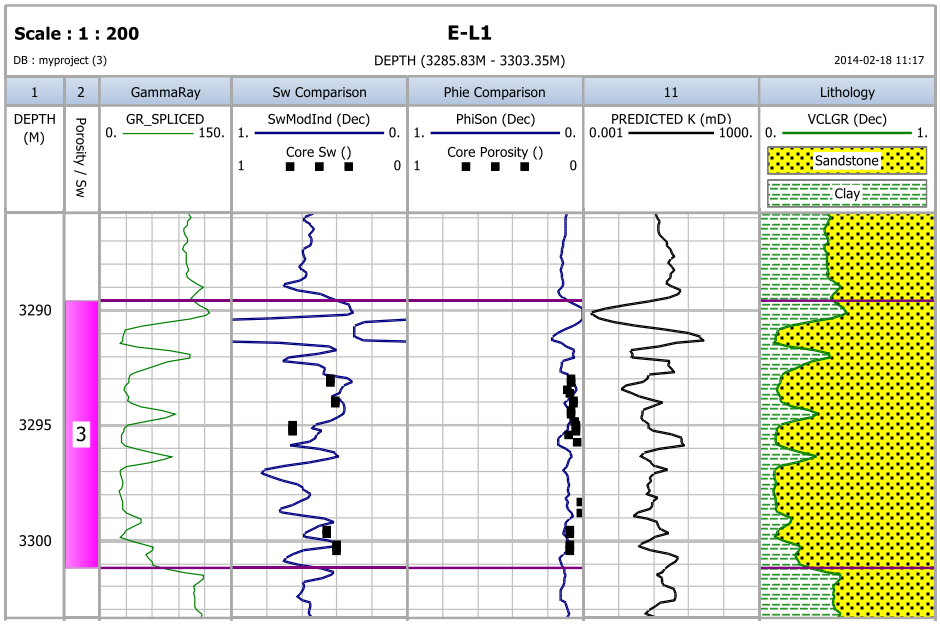

Figure 6.13: Log curves plot displaying predicted permeability (Track 11) of well E-L1, zone 3.

Chapter 7

7 Cut-off determination

The cut-offs are the limit values of formation parameters that remove non-contributing intervals. This concept is aimed at determining the effective petrophysical properties of a rock in the presence of poor reservoir zones (Worthington, 2008). Cut-off parameters can be determined by identifying reference parameters that allow us to differentiate between the intervals that have the reservoir potential and those that do not have. There is no specific or single approach to determine the cut-off parameters (Worthington and Caseation, 2005). Cut-off is normally applied to each calculated result to eliminate poor quality or non-productive zone. Non-productive zones/ non-reservoir rock may have the porosity and permeability that is too low and no hydrocarbon saturation (Opuwari, 2010). Rocks with sufficient permeability to flow hydrocarbons at commercially significant rates are classified as net sandstone or net reservoir. If they produce hydrocarbon at commercially acceptable hydrocarbon/ water ratio, they are classified as pay reservoir (Suzanne and Robert, 2004). To separate pay sand from non-pay sand there are typical cut-off values for formation parameters that are used, where maximum volume of shale is between 0.25 and 0.40, minimum porosity between 0.03 and 0.16, maximum water saturation between 0.30 and 0.70 and also the permeability between 0.1mD and 5.0mD. The permeability cut-off is usually set at 0.1mD for gas reservoir net pay and 1.0mD for oil reservoir net pay. In this study the cut-offs were applied to shale volume, porosity, water saturation and permeability respectively.

7.1 Porosity and permeability cut-off determinations

Generally, a cut-off of 1mD is applied to oil reservoirs and a cut-off of 0.1mD is applied to gas reservoir, below which the rock is not considered a reservoir rock. The reservoirs in this study were gas reservoirs, so a cut-offs values of 0.1mD and porosity of 0.68 were applied. The Φc on the x-axis and Kc indicate the porosity cut-off and permeability cut-off respectively (Figure 7.1). That is, any reservoir interval with effective porosity of less than 0.068 (6.8%) and permeability of less than 0.1mD was regarded as a non-reservoir and any interval with values above that was regarded as a potential reservoir. The permeability and porosity frequency distribution histogram plots also indicate the cut-offs of porosity and permeability (Figures 7.2 and 7.3). The predicted permeability values derived from the regression equations were also presented (Table 7.1).

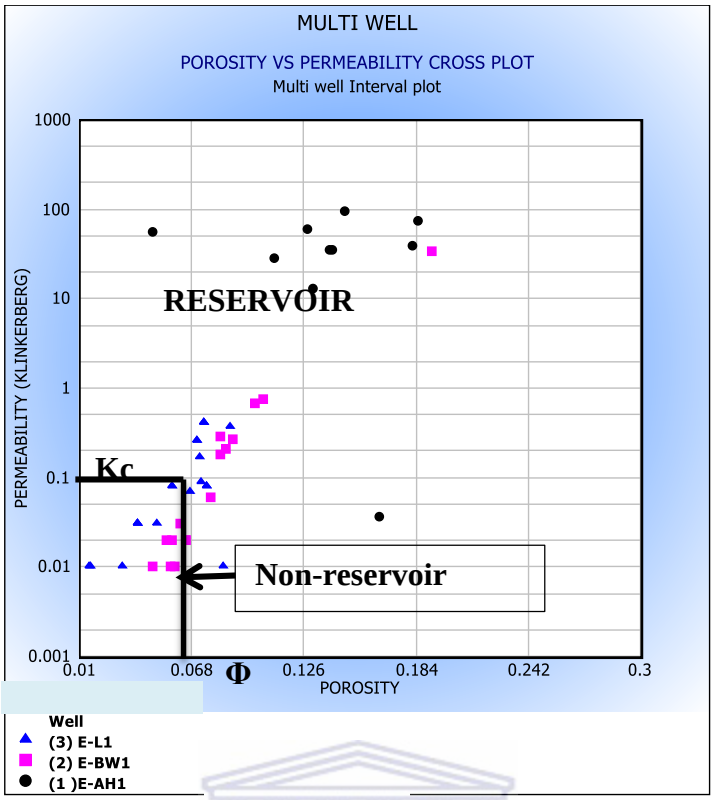

Figure 7.1: Porosity versus permeability cross plot for cut-off determination.

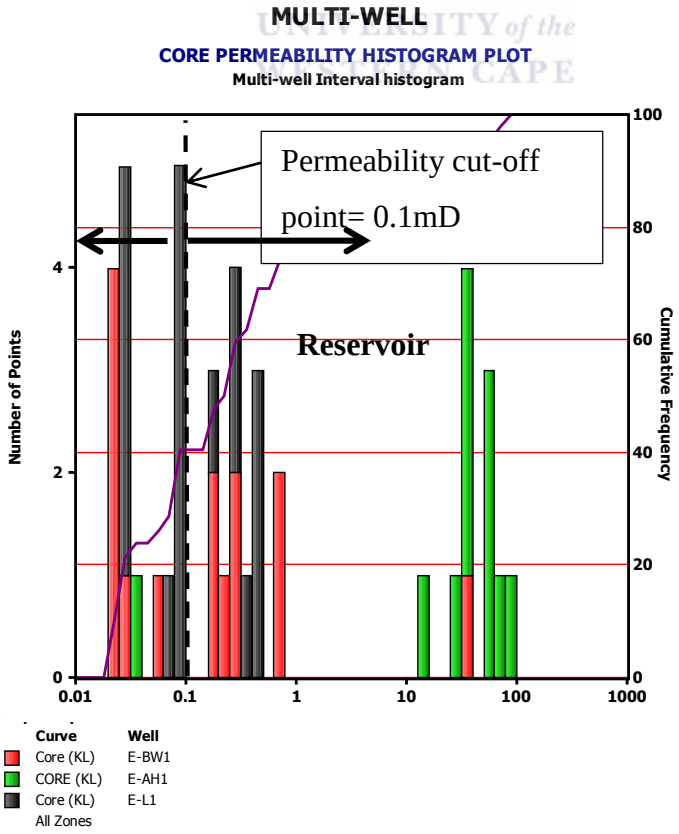

Figure 7.2: Core permeability histogram plot for all study wells.

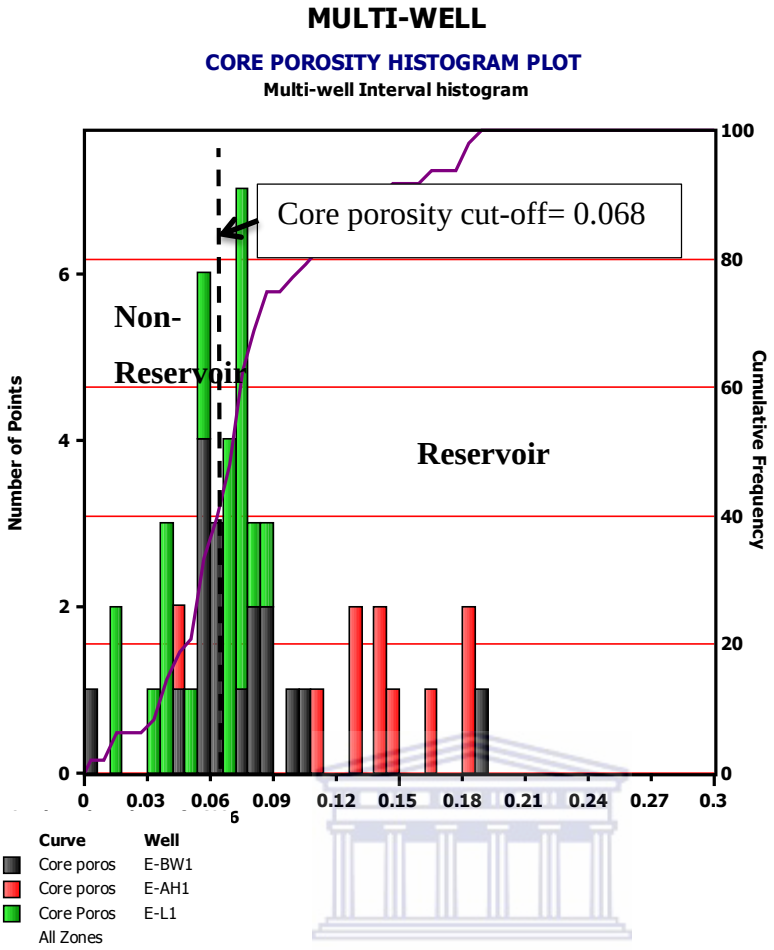

Figure 7.3: Core porosity histogram plot for all wells.

Table 7.1: Predicted permeability of the evaluated reservoirs for each study well

Top Depth (M)	Bottom Depth (M)	Well Name	Reservoir Name	Permeability value (mD).
2467.7	2486.3	E-AH1	1	33
2114.5	2411.9	E-L1	1	79
2388.7	2411.9	E-L1	2	1.95
3017	3026.8	E-L1	3	0.14
2077.1	2166.1	E-BW1	1	3.95
2205.8	2303.2	E-BW1	2	2.27
3289.6	3301.2	E-BW1	3	0.21

The permeability presented in Table 7.1 above is the predicted permeability obtained from the average readings of the permeability log within the selected interval. The permeability of well E-L1 ranges from 0.14mD to79mD. This simply means that the permeability ranges from poor (0.14mD) to good (79mD). Well E-AH1 has the permeability of 33mD (moderate) and E-BW1 had permeability ranging from 0.21mD (poor) to 3.95mD (fair).

7.2 Volume of shale cut-off determination

The volume of shale cut-off is used to discriminate between reservoir interval and non-reservoir interval by allowing all rocks that have a volume of shale of equal or less than a certain value of the total reservoir volume (Opuwari, 2010). The multi-well volume of shale cut-off value for reservoir and non- reservoir rock was determined at 0.4. Rocks with a volume of shale of 40% or above were assumed to be shale and regarded as non-reservoir whereas those with a volume of shale of 40% or less were classified as a reservoir. The volume of shale cut-off value is presented in the volume of shale versus porosity and gamma ray plot below (Figure 7.4). The average volume of shale was obtained from the volume of clay log curves calculated and presented in composite log track (see appendix B)

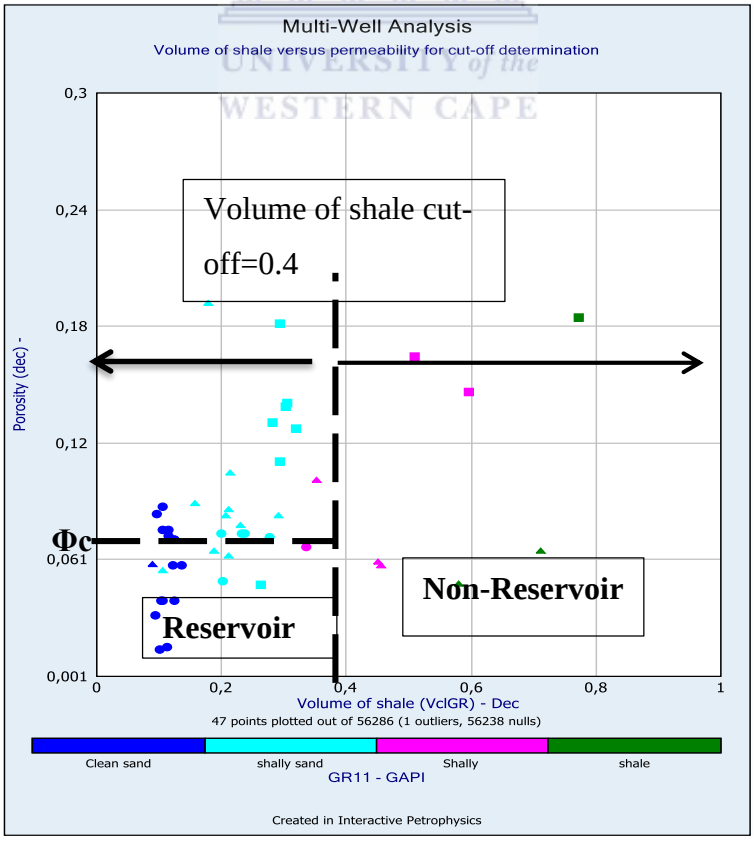

Figure 7.4: Volume of shale versus porosity and gamma ray plot.

7.3 Water saturation cut-off determination

The discrimination between hydrocarbon bearing sandstones (pay) and water (wet) bearing intervals is established by defining the water saturation cut-off of 65%. Intervals that have a water saturation of 65% or less were assumed to be hydrocarbon bearing sandstones and those that have a water saturation of greater than 65% were assumed to be wet or non-productive intervals. The water saturation versus porosity cross plot and water saturation frequency histogram plot presented below (Figures 7.5 and 7.6) represent water saturation cut-off value. The water saturation log curves used to calculate the water saturation is presented appendix B.

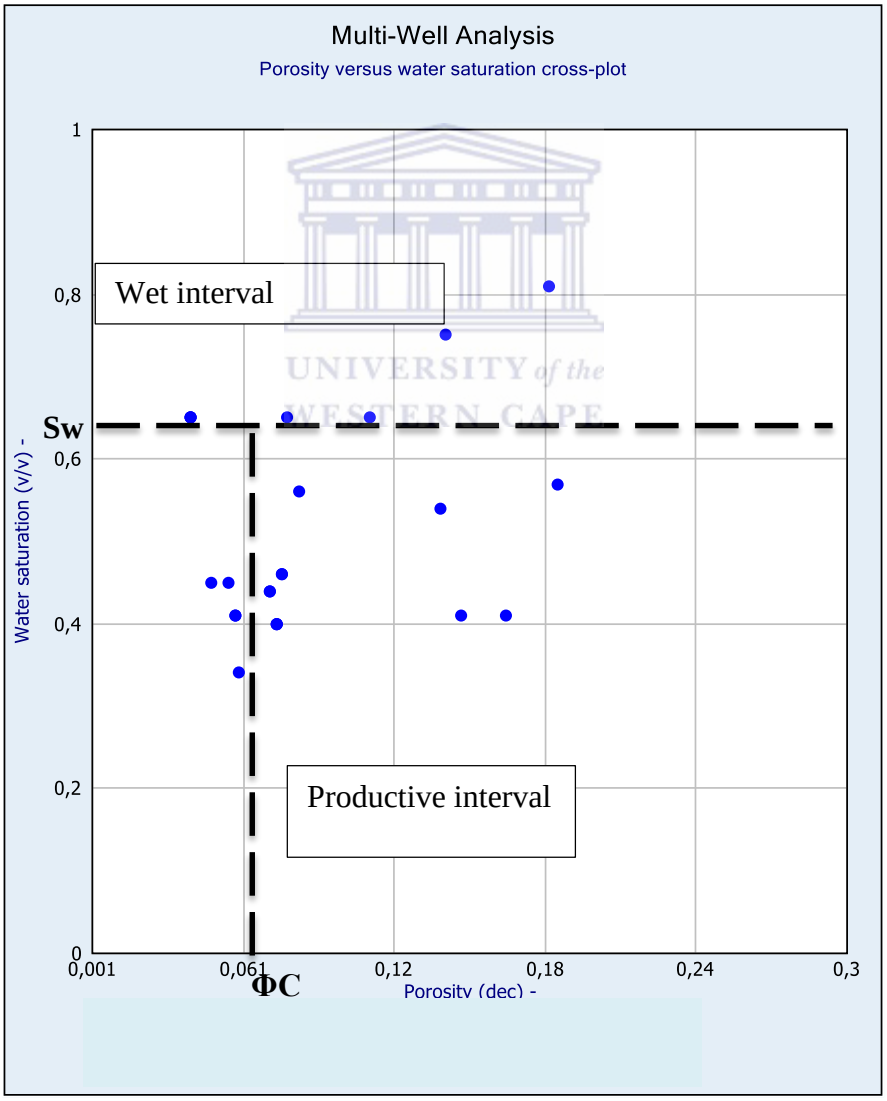

Figure 7.5: Multi-well porosity versus water saturation cross plot for cut-off determination.

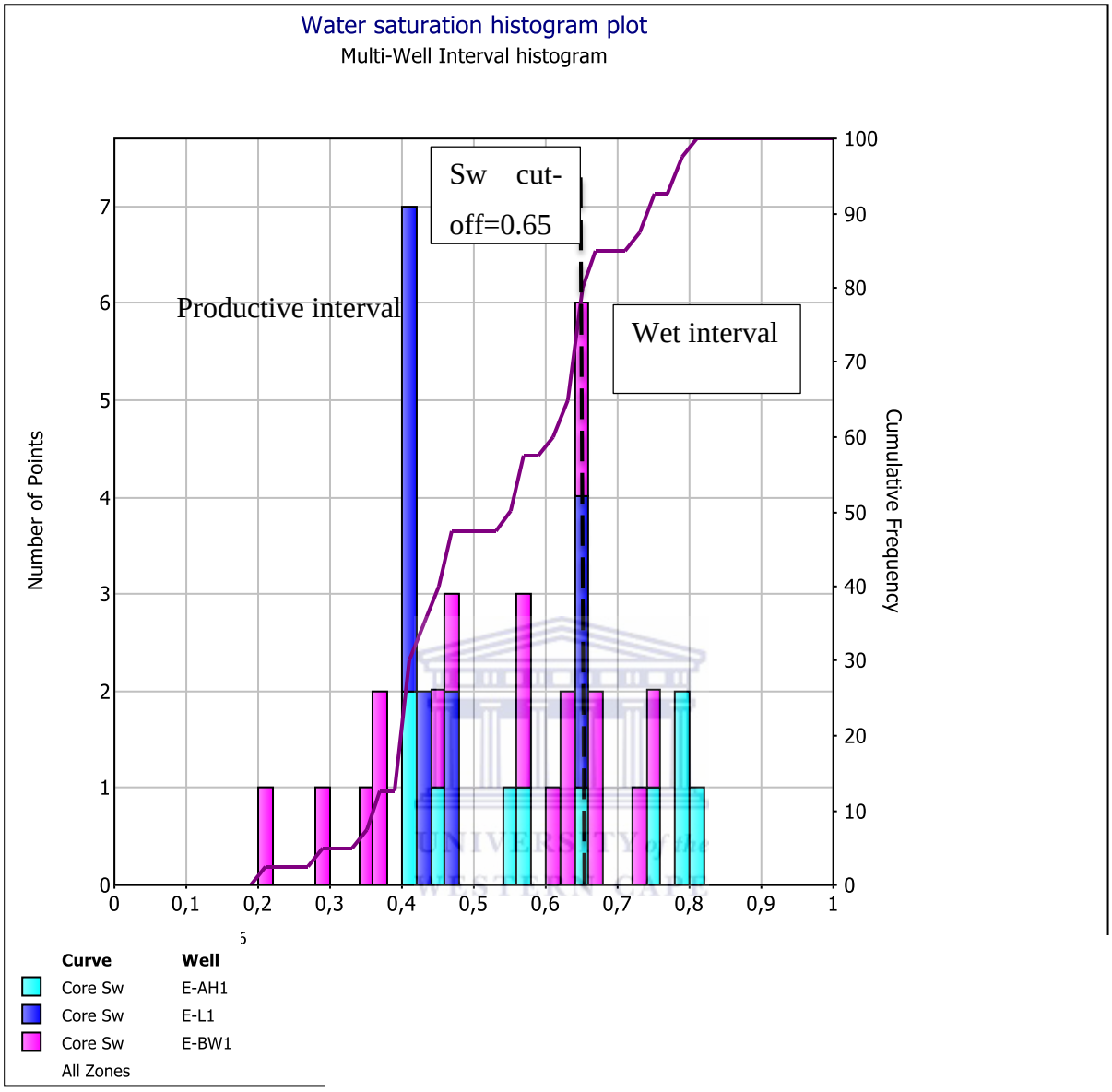

Figure 7.6: Multi-well water saturation frequency distribution cross plot.

7.4 Net-pay determination

As explained earlier, a net pay is defined as the interval of the rock that produce hydrocarbon at commercially acceptable hydrocarbon/water ratio and the gross is regarded as the reservoir interval that contains zone of which hydrocarbon can be produced and zones which does not favour the production of hydrocarbon. The determination of the net pay is required to calculate the hydrocarbon pore feet, F_{HCP} at the wellbore and also to calculate the overall

reservoir original in place (OOIP) or (OGIP) original gas in place (Cobb et al., 1998). The net to gross ratio (N/G) is the total amount of pay footage divided by the total thickness of the reservoir interval (in simplicity the well is assumed to be vertical) (Cobb et al., 1998). An N/G ratio of 1 means that the whole reservoir interval is pay footage (Cobb et al., 1998) and any interval that is considered as non-pay contributes nothing to the calculations of OOIP or OGIP reserves. The differences between gross and net pay is achieved by applying cut-off values in the petrophysical analysis. Here, cut-off values of porosity (≥ 0.068), volume of shale (≤ 0.4) and water saturation (≤ 0.65) were used to identify pay interval. That is reservoir interval with effective porosity equal or greater that 6.8%, shale volume of less or equal to 40 and water saturation of less or equal to 65 were regarded as the net pay interval. Flag curves were created in the database by using cut-off limits. Net reservoir interval was defined by red colour and gross reservoir by green colour. The averages report and flag curves interval are presented in Table 7.2-4.

Table 7.2: Petrophysical reservoir averages report

Top depth(m)	Bottom depth (m)	Gross	Net	N/G	Av phi	Av Sw	Av Vcl
2467.70	2486.40	18.71	11.28	0.603	0.143	0.551	0.234

One reservoir interval was evaluated within the E-AH1 well and the net thickness was found to be 11.28m with the average effective porosity of 14.3%, water saturation of 55.1% and volume of clay of 23.4% as presented in Table 7.2 above. Figure 7.7 below shows the reservoir and pay flags obtained.

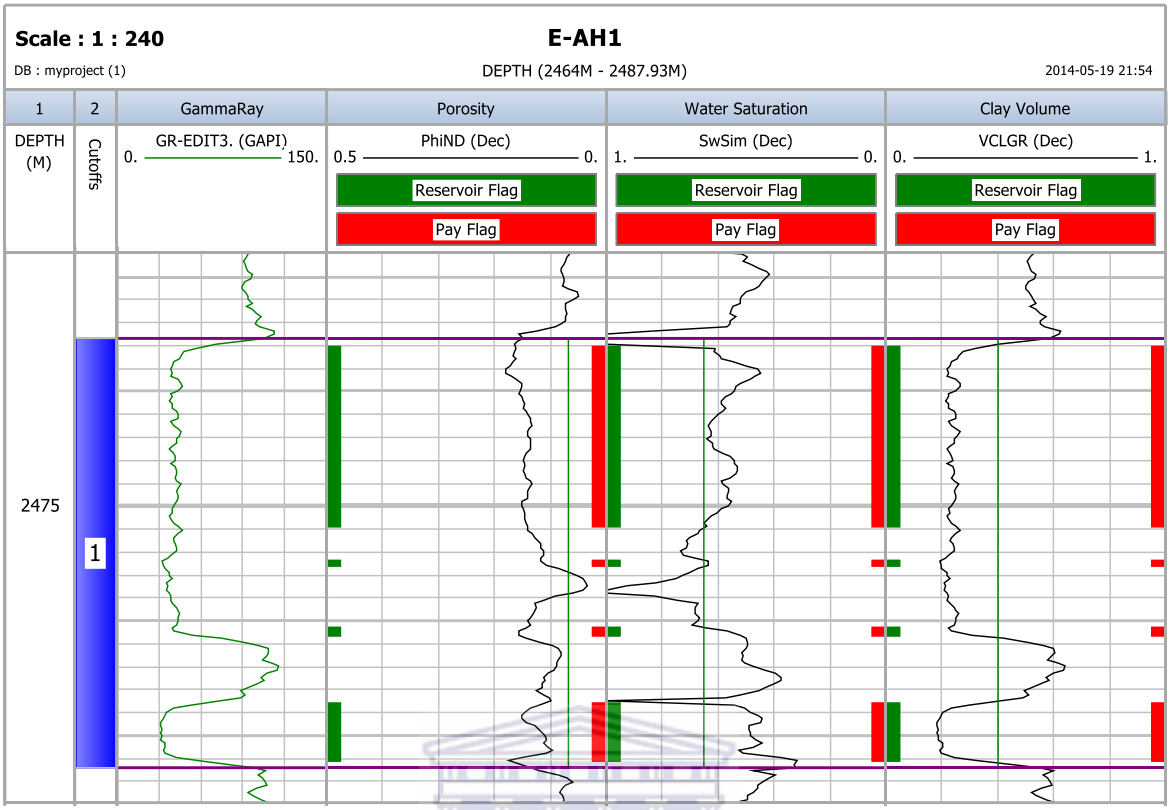

Figure 7.7: Well E-AH1 showing calculated reservoir and pay flags.

In well E-BW1 three reservoirs were evaluated and they all showed net pay potential as presented in Table 7.3. The net thickness of the producing intervals range from 8.08m to 65.35m, average effective porosity range from 10.5 to 18%, average water saturation range from 28.8% to 55.5% and average volume of clay is 19.6% to 30.5%. The implications of these parameters will be discussed later in the chapter. The net pay reservoir flags are presented in Figures 7.8-10 below.

Table 7.3: Petrophysical reservoir averages report.

Reservoir name	Top depth(m)	Bottom depth(m)	Gross	Net	N/G	Av phi	Av Sw	Av Vcl
1	2114.50	2252.50	138.00	65.35	0.474	0.180	0.555	0.196
2	2388.70	2411.90	23.20	11.28	0.486	0.107	0.519	0.261
3	3012.00	3033.00	21.95	8.08	0.368	0.105	0.258	0.305

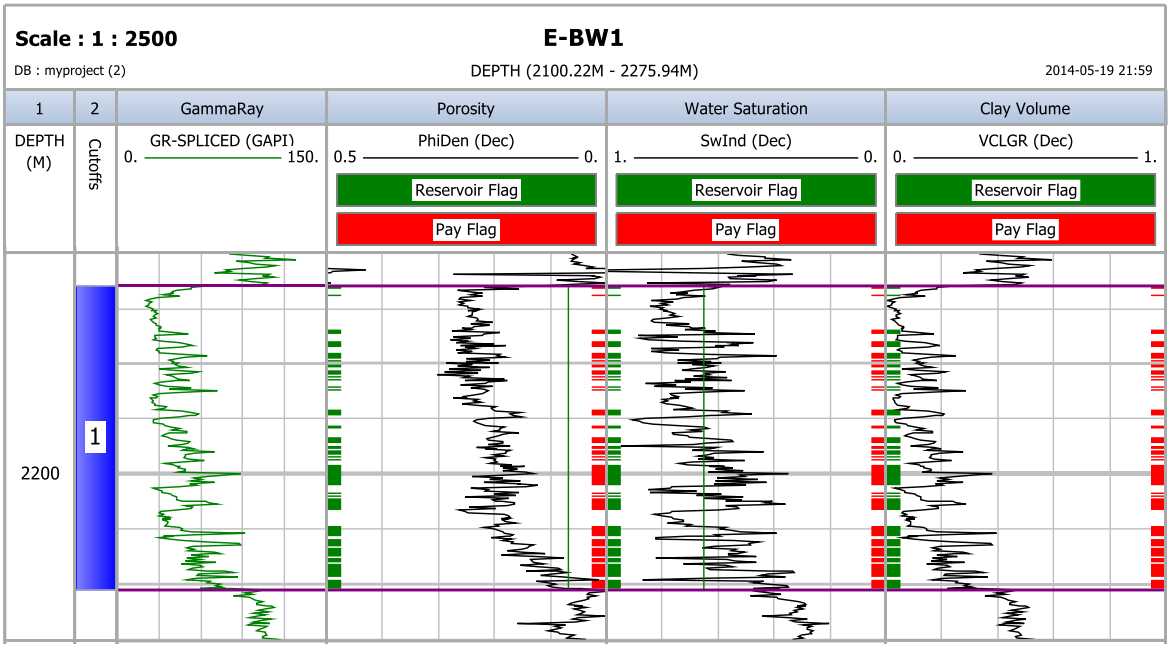

Figure 7.8: Well E-BW1 showing calculated reservoir and pay flags of reservoir 1.

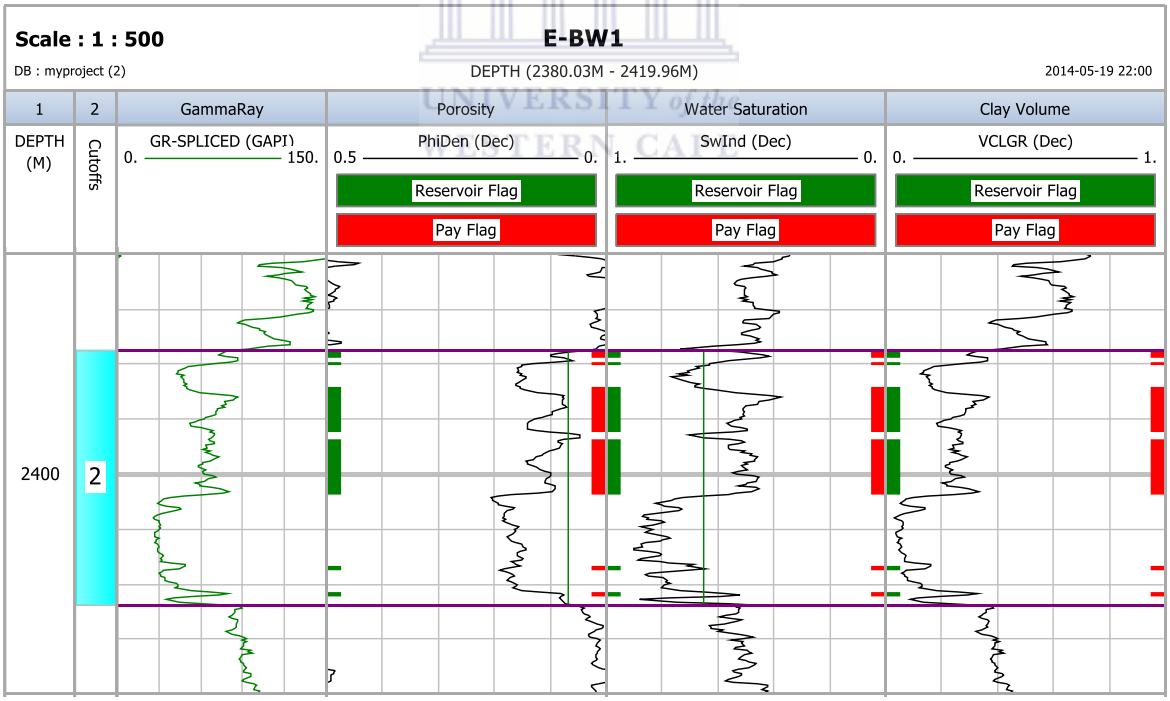

Figure 7.9: Well E-BW1 showing calculated reservoir and pay flags of reservoir 2.

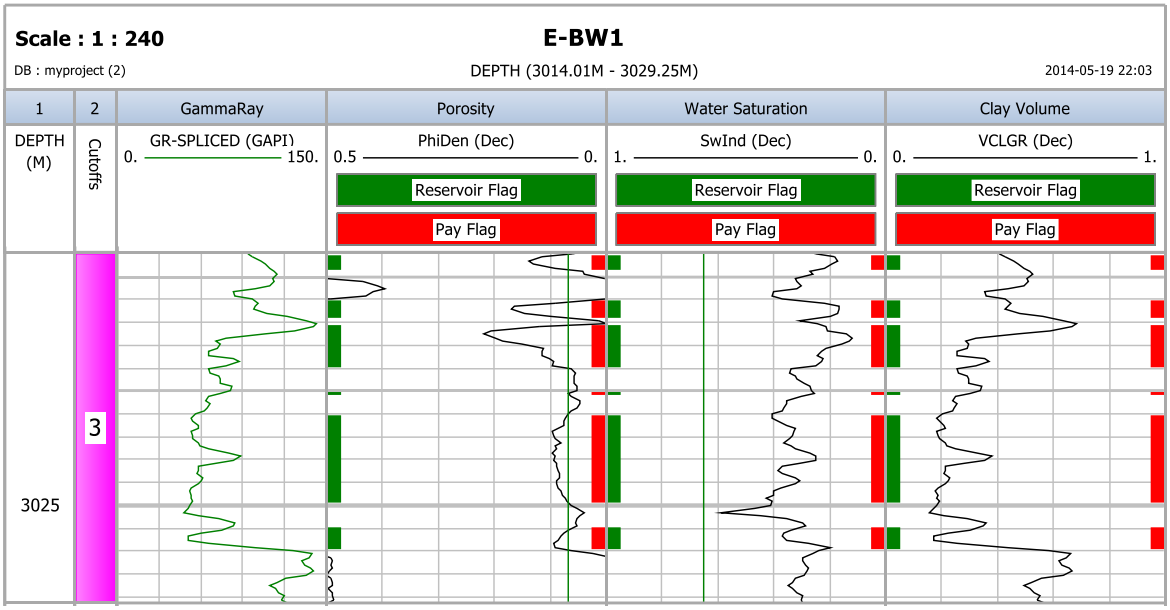

Figure 7.10: Well E-BW1 showing calculated reservoir and pay flags of reservoir 3.

Three sandstone reservoir intervals were evaluated in well E-L1 and showed pay net potential which ranges from 6m to 11.89m in thickness. The average effective porosity range from 9.3% to 9.7%, average water saturation range from 49.9% to 61.6% and average volume of clay range from 15.9% to 31.4% as presented in Table 7.4 and reservoir pay flag (Figures 11-13) below.

Table 7.4: Petrophysical reservoir averages report.

Reservoir name	Top depth(m)	Bottom depth(m)	Gross	Net	N/G	Av phi	Av Sw	Av Vcl
1	2077.10	2166.10	89.00	11.89	0.134	0.097	0.553	0.261
2	2205.80	2303.20	97.40	6.55	0.067	0.094	0.616	0.314
3	3290.40	3301.20	10.80	6.00	0.556	0.093	0.499	0.159

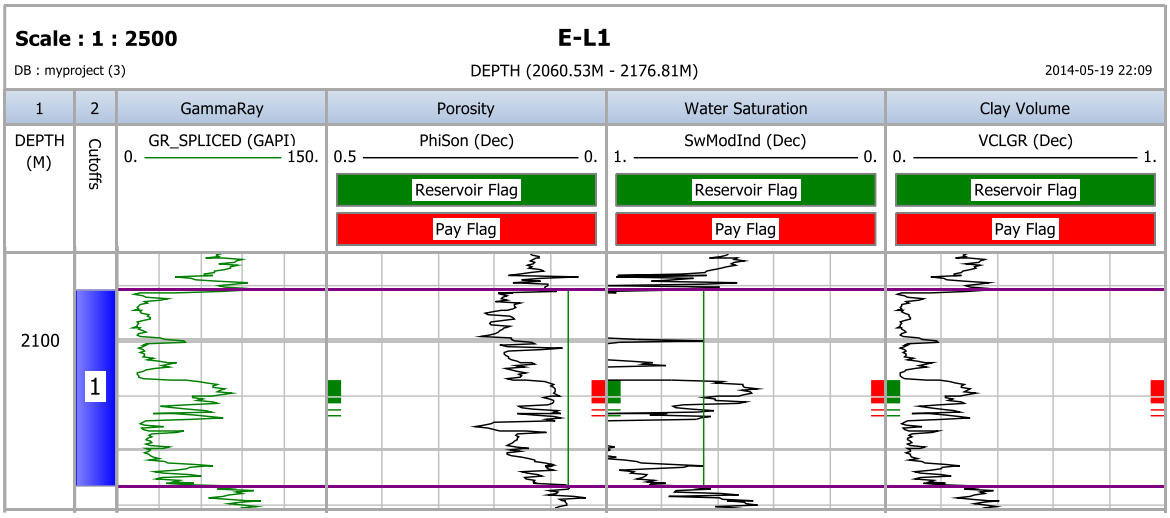

Figure 7.11: Well E-L1 showing calculated reservoir and pay flags of reservoir 1.

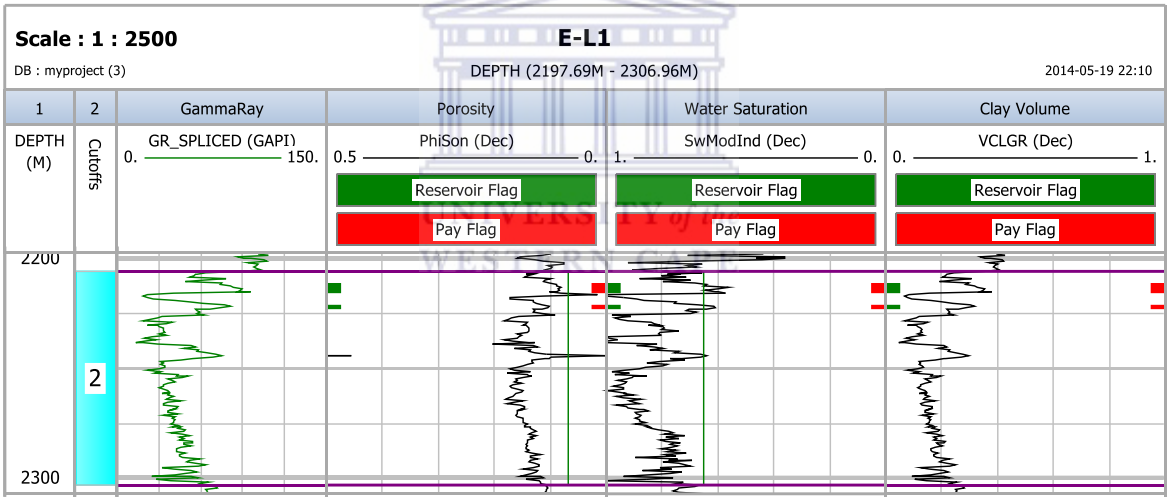

Figure 7.12: Well E-L1 showing calculated reservoir and pay flags of reservoir 2.

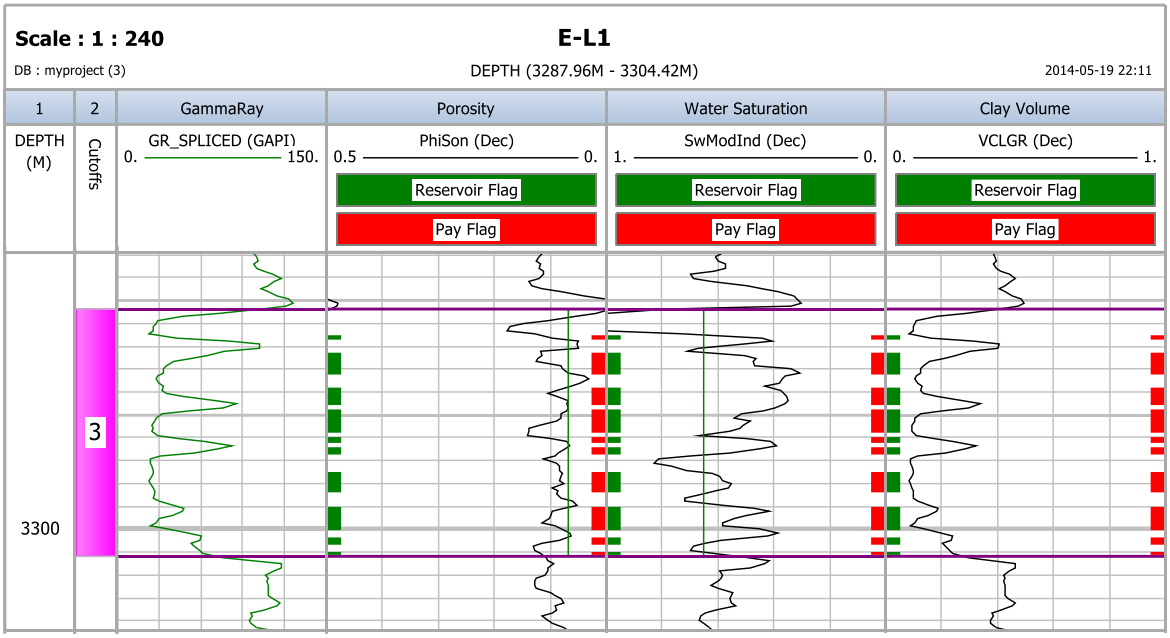

Figure 7.13: Well E-L1 showing calculated reservoir and pay flags of reservoir 3.

The results within the pay intervals of the studied wells are summarized in Table 7.2-4 above. The three studied wells are located close to each other (Figure 1.2), but most of the evaluated intervals of interest are located within different sand channels (Appendix D) and these results in very different values for the different parameters of all wells. Reservoir 1 of E-AH1 and reservoir 2 of E-L1 and E-BW1 are located within 10AT1 and 12AT1 formations. Reservoir 1 E-BW1 and E-L1 are located within the 13AMFS- 13AT1 formations and reservoirs 3 of both wells (E-BW1 and E-L1) are located between 6AT1 -8AT1 and DC1- 6AT1 respectively. Well E-AH1 showed higher average net to gross (N/G) ratio of 60.3m and E-L1 showed the lowest N/G ratio of 12.4m while E-BW1 shows N/G ratio of 46.3m. This shows that well E-BW1 on average has a large thickness that is producing hydrocarbons as compared to other wells. The average effective porosities within the pay sand for E-BW1 and E-AH1 are almost similar to one another (E-AH1=14.3% and E-BW1=13.07%) whereas E-L1 show a lower effective porosity of 9.47% as compared to others. The average water saturation within pay sands for E-L1 is 55.6 which are higher compared to 44.4% and 55.1% of E-BW1 and E-L1 respectively. The average volume of clay within the pay sand is 24.47 % for well E-L1, 25.4% for E-BW1 and 23.4% of E-AH1 this values confirm that the evaluated reservoirs are shaly-sand reservoirs (The volume of clay/shale between 10 and 35 shows that the formation is shaly-sands) (Jensen, et al., 2013).

7.5 Storage capacity, flow capacity and reservoir hydrocarbon volume calculations

7.5.1 Storage and flow capacity calculations

The calculations of the storage capacity help to give an idea of how much the producing interval is able to store the hydrocarbons. This is simply obtained by multiplying the net thickness with the porosity whereas the flow capacity is used to determine how well the hydrocarbon can flow within the reservoir, by simply multiplying the net thickness with the permeability. The calculated flow and storage capacity results are presented in Table 7.5 see appendix E for calculations.

Table 7.5: Summary results of the calculated flow and storage capacity

Well Name	Reservoir name	Storage capacity (scf)	Flow capacity (mD-ft)
E-AH1	1	529.1	1221
E-BW1	1	3852	846.9
E-BW1	2	395.9	83.99
E-BW1	3	278.25	5.6
E-L1	1	378.25	3081
E-L1	2	202.1	41.95
E-L1	3	183.21	2.76

Seven reservoir intervals evaluated from different wells proved to be producing hydrocarbons. The evaluated intervals of E-BW1 proved to have a high storage capacity with reservoir 1 showing the highest storage capacity of 3852scf. Reservoir 1 of E-L1 proved to have a highest flow rate (capacity) of 3081mD-ft as compared to the rest. The significant variation in the flow rate (capacity) and storage capacity between the evaluated reservoirs is the results of different porosities, permeability and net thickness measured within the hydrocarbon producing intervals. The highest flow rate (capacity) is caused by the high permeability measured within reservoir 1 of E-L1 and highest storage capacity is due to high porosity and net thickness of reservoir 1 of E-BW1.

7.5.2 Recoverable hydrocarbon volume determination

Rzasa and Katz (1945) proposed a method which provides a means to calculate the gas in place volume in the absence of the area and thickness on which calculations are based on one acre of reservoir volume. The calculations and the Table of the hydrocarbon volumes for all reservoirs are shown below.

The formula used is: 43.560* Φ*(1-Sw) where, Φ=Porosity, Sw= Water saturation and 43.560= Unit conversion factor.

Table 7.6: Calculated reservoir hydrocarbon volume of each reservoir

Well Name	Reservoir Name	Volume (Cubic feet)
E-AH1	1	279.69
E-BW1	1	348.92
E-BW1	2	224.19
E-BW1	3	339.38
E-L1	1	188.87
E-L1	2	157.23
E-L1	3	202.96

The productivity calculations were performed for all hydrocarbons producing intervals. Table 7.6 above present the calculated results in cubic feet for each interval. Reservoir 1 of E-BW1 shows the highest volume of hydrocarbons of 348.92 whereas reservoir 2 of E-L1 showed the lowest volume of 157.23 cubic feet. The volume of reservoir 1 of E-BW1 was always expected to be higher because of the highest net pay thickness and porosity and the opposite applies to reservoir 2 of E-L1. On average, well E-BW1 proved to be the best producing well with the total volume of 912.49 cubic feet whereas E-L1 is the less producing well with 188.87 cubic feet in total. The detailed calculations are shown in appendix F.

7.6 General trend of petrophysical properties of pay sand within the field in 3-D view

The 3-D parameter viewer was used to demonstrate the general trend of petrophysical properties within the studied field. Three parameters (average porosity, average water saturation and average volume of clay) were displayed within the view .These parameters were determined within the pay sand interval of the evaluated reservoirs, which is the interval that has the potential to produce hydrocarbon. The parameters were plotted against True Vertical Depth (TVD). The legend bar was used to distinguish different values of the parameters using different colours based on the scale. Three wells (E-AH1, E-WB1 and E-L1) were displayed together with their average pay values.

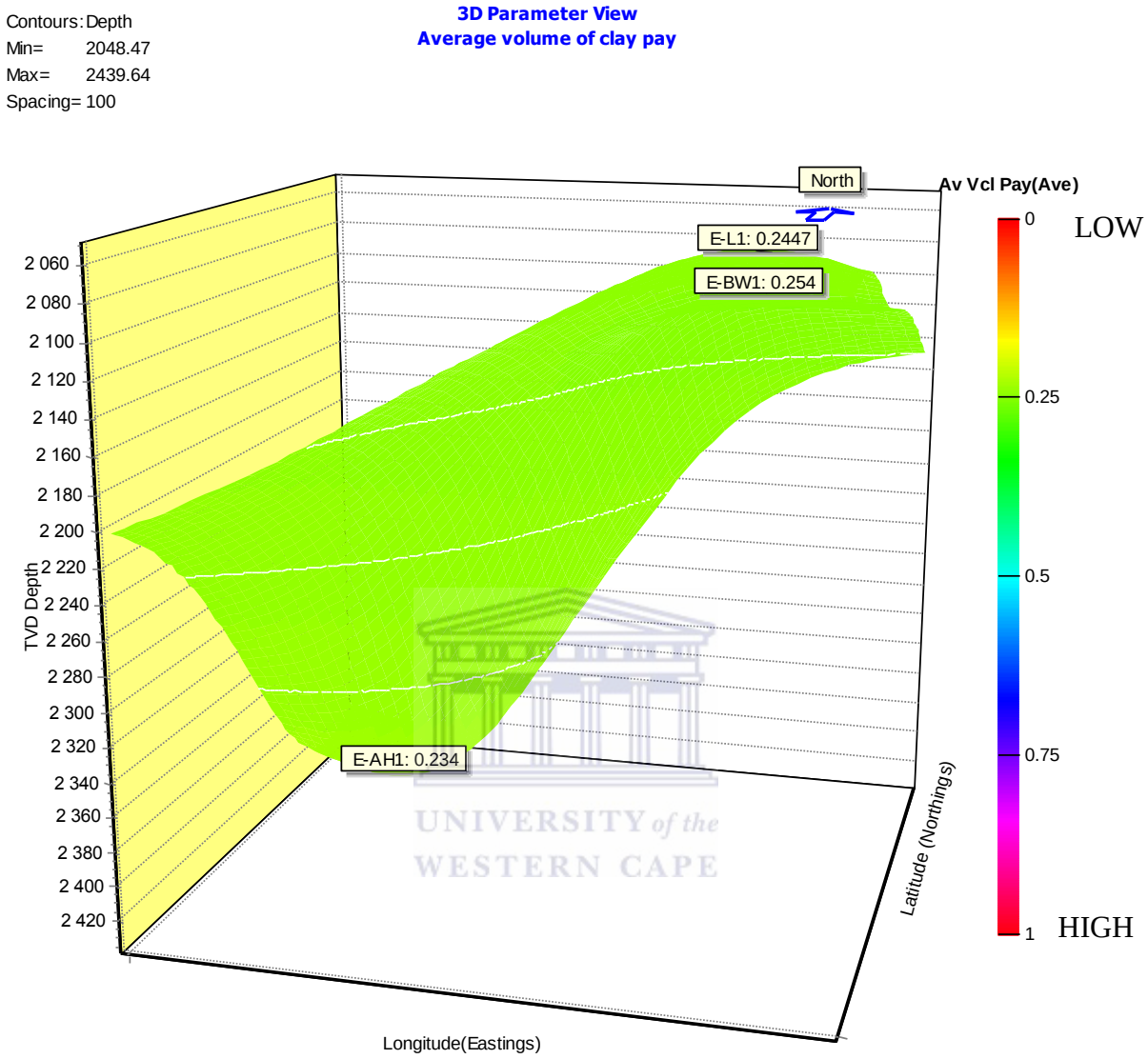

Figure 7.14: 3-D parameter view showing average volume of clay pay within the field.

The distribution of volume of clay within the field was almost the same in all directions (North, East, South and West) as shown in figure 7.14. The average volume of clay within the pay sand for E-L1 was 24.47%, 25.4% for E-BW1 and 23.41% for E-AH1. Based on the average volume of clay values presented in the figure it can be said that volume of clay slightly increases towards the Northern side of the field.

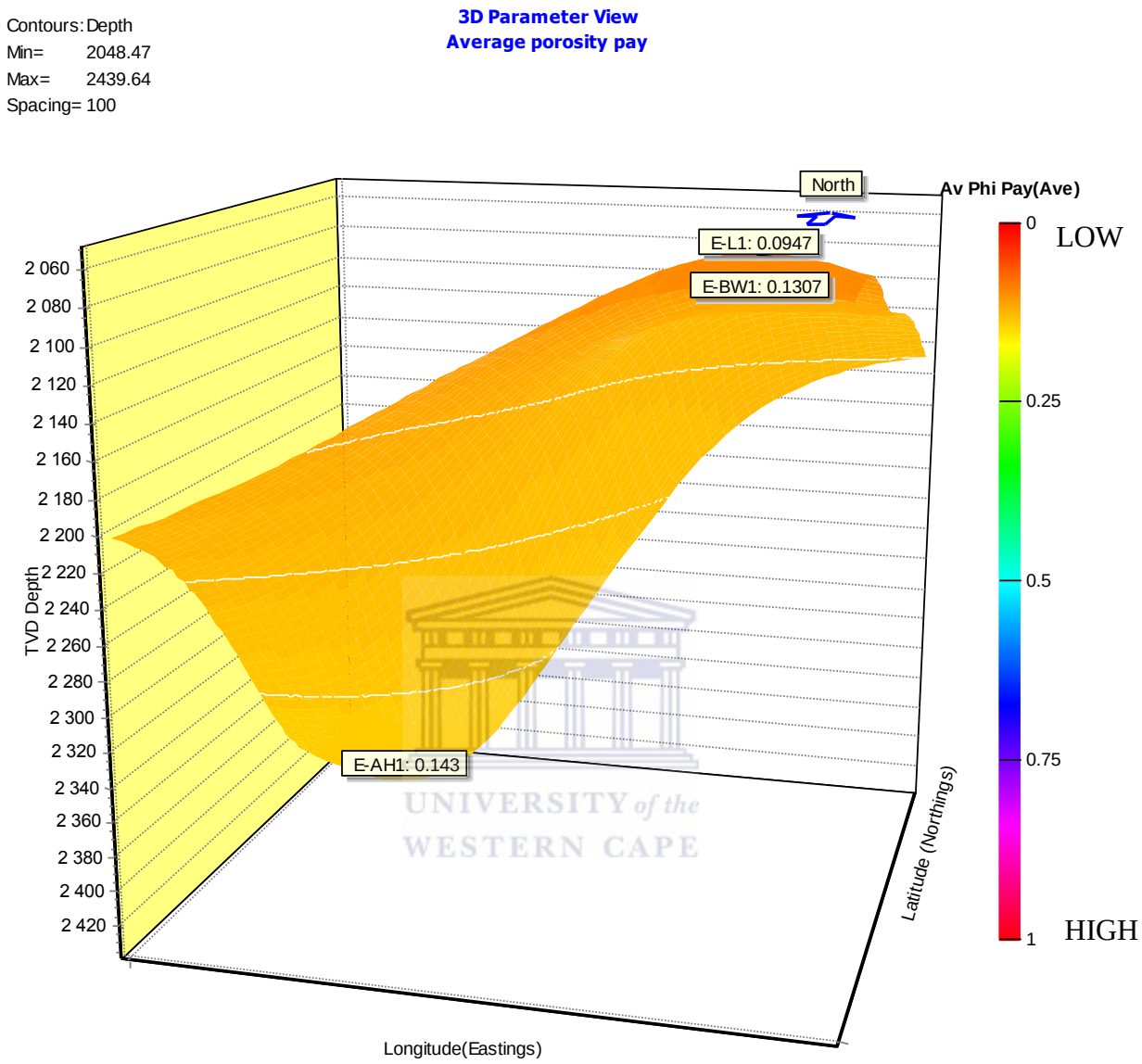

Figure 7.15: 3-D parameter view showing average pay porosity within the field.

The distribution of the effective porosity was seen clearly in figure 7.15 increasing from Northern side to the Southern side of the field. Wells E-L1 and E-BW1 shows average effective porosities of 9.47% and 13.07% respectively in the northern side of the field whereas well E-AH1 shows average effective porosity of 14.3% in the Southern side of the field. This basically means that higher effective porosity was expected in Southern side of the side and low effective porosity on the Northern side of the field.

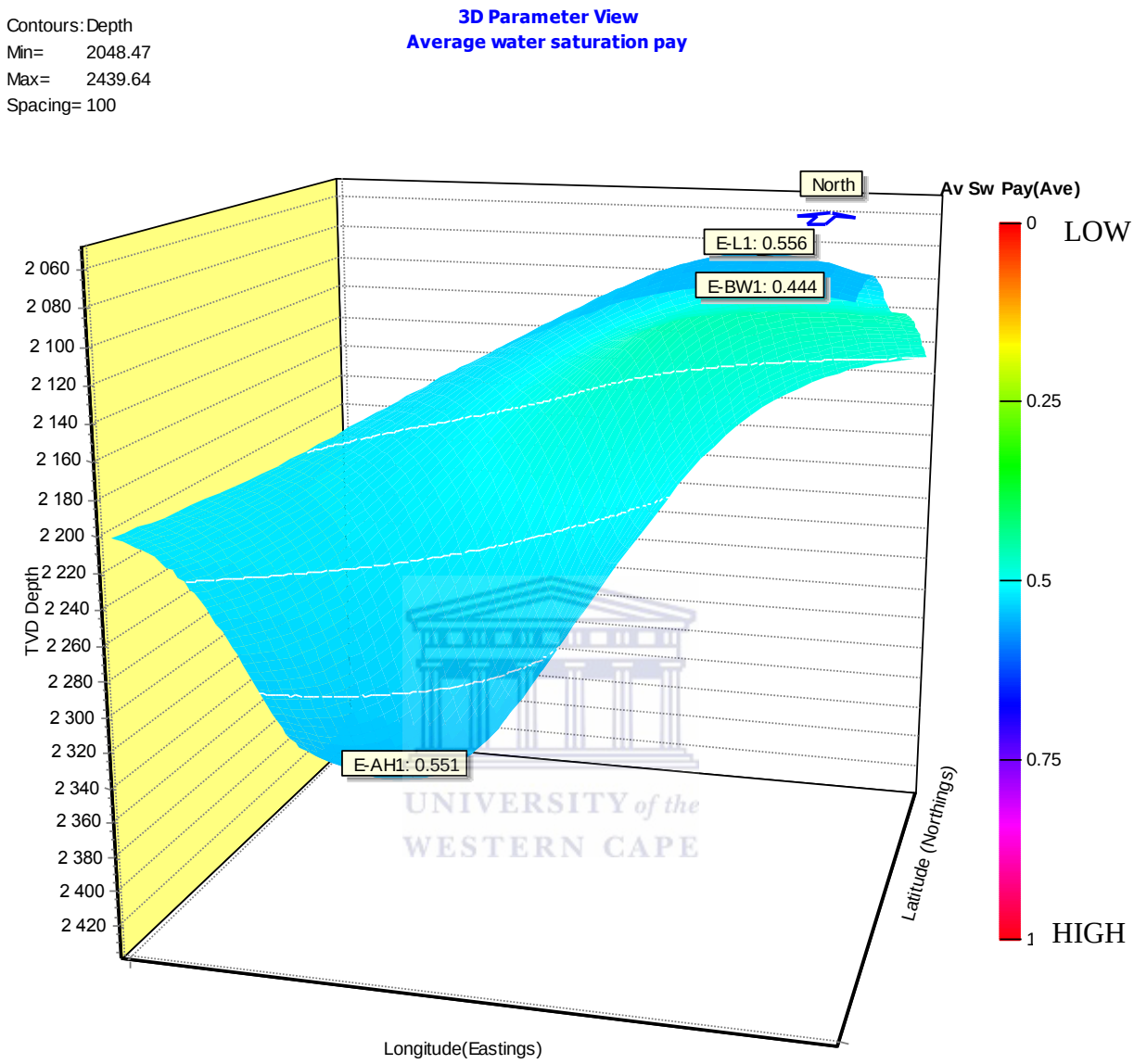

Figure 7.16: 3-D parameter view showing average water saturation clay within the field.

The trend of the distribution of water saturation pay within the field was not clearly defined, that is water saturation decreases from Southern side (E-AH1) of the field towards the Northern side of the field (E-BW1) and then increases again going further North (E-L1) (Figure 7.16). E-AH1 shows average water saturation of 55.1%, E-BW1 shows average water saturation of 44.4% and E-L1 shows average water saturation of 56.6%. That is high water saturation was expected on the Northern and Southern side of the field and low water saturation was expected in the area between E-AH1 and E-L1.

Chapter 8

8 Conclusion

The sandstone reservoir units encountered by the three central Bredasdorp Basin wells have been evaluated in this research work within the limit of the quality and amount of data available. Though the data was insufficient, necessary measures have been taken, data correction applied and every step was thoroughly explained to arrive at the presented results.

8.1 Deductions

In conclusion, the following deductions were made:

- Well E-AH1, E-BW1 and E-L1 are primary units of interest in the evaluated field. Gamma ray logs were used to identify potential reservoirs within the drilled wells. Seven potential reservoirs were identified in total across all three wells (one for E-AH1, three for E-BW1 and E-L1 each).
- Conventional core analysis results which were important for the calibration of non-cored intervals of the key wells (E-L1, E-BW1 and E-L1) were discussed. The method adopted by Nicko (1998), was used for grouping lithofacies and 4 facies were grouped according to textural features and grain sizes. Facies A was classified as a reservoir rock because their permeability and porosity values indicated good reservoir quality while facies B, C and D were classified as a non-reservoir. The high porosity values were recorded in massive sandstone and the low values in a claystone interval. Core porosity ranged from 0 to 19.2%. Core permeability ranges from 0.02mD to 94mD with a mean value of 0.49mD.
- Three wells were drilled within the field and made gas discoveries. Volume of clay, porosity and water saturation were then calculated within the pay intervals of the producing wells. Average volume of clay calculated within the pay sand interval was 24.47% for E-L1, 23.4% for E-AH1 and 25.4% for E-BW1.The average effective porosity recorded within the pay sand interval was 9.47% for E-L1, 13.07% for E-

BW1 and 14.3% for E-AH1. The average water saturation recorded within the pay sand interval was 55.6% for E-L1, 44.4% for E-BW1 and 55.1% for E-AH1.

- The storage and flow capacity was calculated for the producing (pay sand) interval of the respective wells. Storage capacity shows how much the reservoir rock was able to store hydrocarbons whereas flow capacity indicated how much the rock was able to allow fluid to flow through its pore spaces. Well E-L1 recorded a total storage capacity of 763.6 square cubic feet (scf) and total flow capacity of 3125.7mD-ft, E-AH1 recorded a total storage capacity of 529.1scf and total flow capacity of 1221mD-ft and E-BW1 recorded a total storage capacity of 4526.2scf and total flow capacity of 1034.5mD-ft.
- The estimated recoverable volume of gas for E-AH1 was 279.69 cubic feet.
- The estimated recoverable volume of gas for well E-L1 was 549.06 cubic feet.
- The estimated recoverable volume of gas for E-BW1 was 912.49 cubic feet.
- The Southern side of the evaluated field showed good porosity, and low volume of clay and water saturation compared to others which makes it a good target area for future study.

8.2 Recommendations

This study only considered the petrophysical evaluation approach by integrating core data and wireline logs for better results of static reservoir models. For future study, the following recommendations were be made:

- The new wireline logs should be run together with the new generation of logs such as NMR (Nuclear Magnetic Resonance) for better results because old data (drilled in 1989) were used for this study.
- It could be necessary to carry out an analogous outcrop base modelling in order to understand the permeability distribution and simulate flow pattern in the reservoir.
- The amount of volume of reserve estimation based on the determined petrophysical properties of the wells evaluated to quantify the gas original in place calculated in this study, can be estimated better if seismic data (preferably 3-D) can be obtained, so that the area required in the general recoverable hydrocarbon volume formula can be determined and the economic importance of the produced hydrocarbon can be discussed.

- This work could be reviewed with more data input from Petroleum Agency of South Africa (well, seismic and production data) for further studies, particularly with respect to reservoir modelling and flow simulation.

References

Bateman, R (1985). Open-hole log analysis and formation Evaluation: Boston, International Human resources Development Corporation; 647.

Bennion, D.B., Thomas, F.B. and Bietz, R.F. (1996). Determination of initial fluid saturations- A key factor in By-passed pay determination, 3-5.

Broad, (2004). South Africa Activities and Opportunities. An Unpublished Power Point Presentation to PetroChina.

Burden, P.A. (1992, December). Soekor, Partner explores possibilities in Bredasdorp Basin of South Africa. *Oil and gas Journal*, 90:51, 1-6.

Cobb, M.W and Marek, F.J. (1998). Net pay determination and waterflood depletion mechanisms, SPE 48952, in the Annual Technical Conference and Exhibition; 14.

Crain, E.R. (2013). Crain's Petrophysical handbook: URL www.spec2000.net/14-Swxplot.htm

Crain, E.R. (2014). Crain's Petrophyical handbook: URL www.spec2000.net/09-core Perm.htm

Davies, C.P.N. (1997). Hydrocarbon evolution of the Bredasdorp Basin, Offshore South Africa: From Source rocks to reservoir. Ph.D. thesis, University of Stellenbosch, South Africa.

Djebbar, T and Donaldson, E.C. (1999). Theory and practice of measuring reservoir rock and fluid transport properties.Butterworth-Heimann, USA.

Glover, P. (2009). Petrophysics M.Sc. Course notes, University of the Aberdeen, Scotland.

Haq, B.U., Hardenbohl, J. and Vail, P.R (1987). The new chronostratigraphic basic of cenezoic and Mesozoic sea level cycles, Cushman foundation forum, Res.Spec, Publ, and No.24.

Houston, J.E. (1986). Dynamic core-hole screening effects in the C-KVV Auger line shape of graphite.

Gluyas, J. and Swabrick, R. (2004). Petroleum Geoscience, p3

Jensen, J.L., Ayers. W.B. and Blasingane, T.A. (2013). Introduction to shally sand analysis. Department of petroleum Engineering. Texas A and M University.

McAloon, W., Barton, K., Egan, J., and Frewin, J. (2000). Pre-development characterisation of a marginal deep-marine channel/lobe-system reservoir, block 9, The Bredasdorp Basin, offshore South Africa. *Journal of African Sciences*, **31**(1), 47.

Mohaghegh, S., Balan, B. and Ameri, S. (1997). "Permeability determination from well log data", Paper SPE 30978 first presented at the 1995 exhibition in Morgantown, West Virginia, 17-21 September.

Moore, R.C. (1949). Meaning of facies . Memoir Geological Society of America 39.
Nieto and Rojas, N. (1998). Geological and petrophysical reservoir in Apiay K2, Freedom Fields Suria and characterization. Ecopetrol, Internal report.

Olajide, O. (2005). The petrophysical analysis and evaluation of hydrocarbon potential of sandstone units in the Bredasdorp Central Basin. Unpublished M.sc. thesis, University of the Western Cape, South Africa, 7-10

Opuwari, M. (2010). Petrophysical evaluation of the albian age gas bearing sandstone reservoir of the O-M field, Orange Basin, South Africa, Ph.D. thesis, University of the Western Cape, South Africa.

Petroleum Agency of South Africa. (1989). Core description report.

Petroleum Agency of South Africa. (2004/005). Petroleum Exploration Information and Opportunities: *Petroleum Agency SA Brochure*, 2004/2005, 16-18.

Petroleum Agency of South Africa. (2009). Western Bredasdorp basin: *Petroleum Agency SA Brochure.*

Poupon, A. and Leveaux, J. (1971). Evaluation of water saturation in shaly formations; Trans. SPWLA 12th Annual Logging Symposium; 2.

Rzasa, M.J. and Katz, D.L. (1945). Calculations of static pressure gradients in gas wells: Transaction AIME, 160, p. 100.

Rider, M. (2002). The Geological interpretation of well logs. Second edition, p1

Schalkwyk, H. J. (2005). Assessment controls on reservoir performance and the effects of granulation seam mechanics in the Bredasdorp Basin South Africa. M.Sc. thesis, University of the Western Cape, South Africa, p28.

Schlumberger Ltd (2013): Grain density classification: Houston, Texas.

Saputra, I. (2008). Shale volume calculations. HRS Jakarta; CE8R2.

Serra, O. (1984). Fundamental of well logging Interpretation. Elsevier Science Publisher, BV; 142.

Simandoux, P. (1963). Dielectric Measurements on Porous Media: Application to measurement of water saturation. Study of the behaviour of argillaceous formation. SPWLA, Houston, vol; 97-124.

Suzanne, G.C. and Robert, M.C. (2004). Petrophysics of the Lance Sandstone Reservoirs in Jonah Field, Sublette County, Wyoming. AAPG Studies in Geology 52 and Rocky Mountain Association of Geologists 2004 Guidebook; 226-227.

Turner, J.R., Grobbler, N. and Sontundu, S. (2000). Geological modelling of the aptian and albian sequences within Block 9, the Bredasdorp basin, Offshore South Africa: *Journal of African sciences,* 31 (1), 80.

Worthington PF, Cosentino (2005): The role of Cut-Offs in Integrated Reservoir Studies. SPE Reservoir Evaluation and Engineering (4). SPE 84387.

Worthington PF (2008): The Application of Cut-Offs in Integrated Reservoir Studies. SPE Reservoir Evaluation and Engineering (SPE 95428).

Appendices

Appendix A. **Standalone pickets plots for wells**

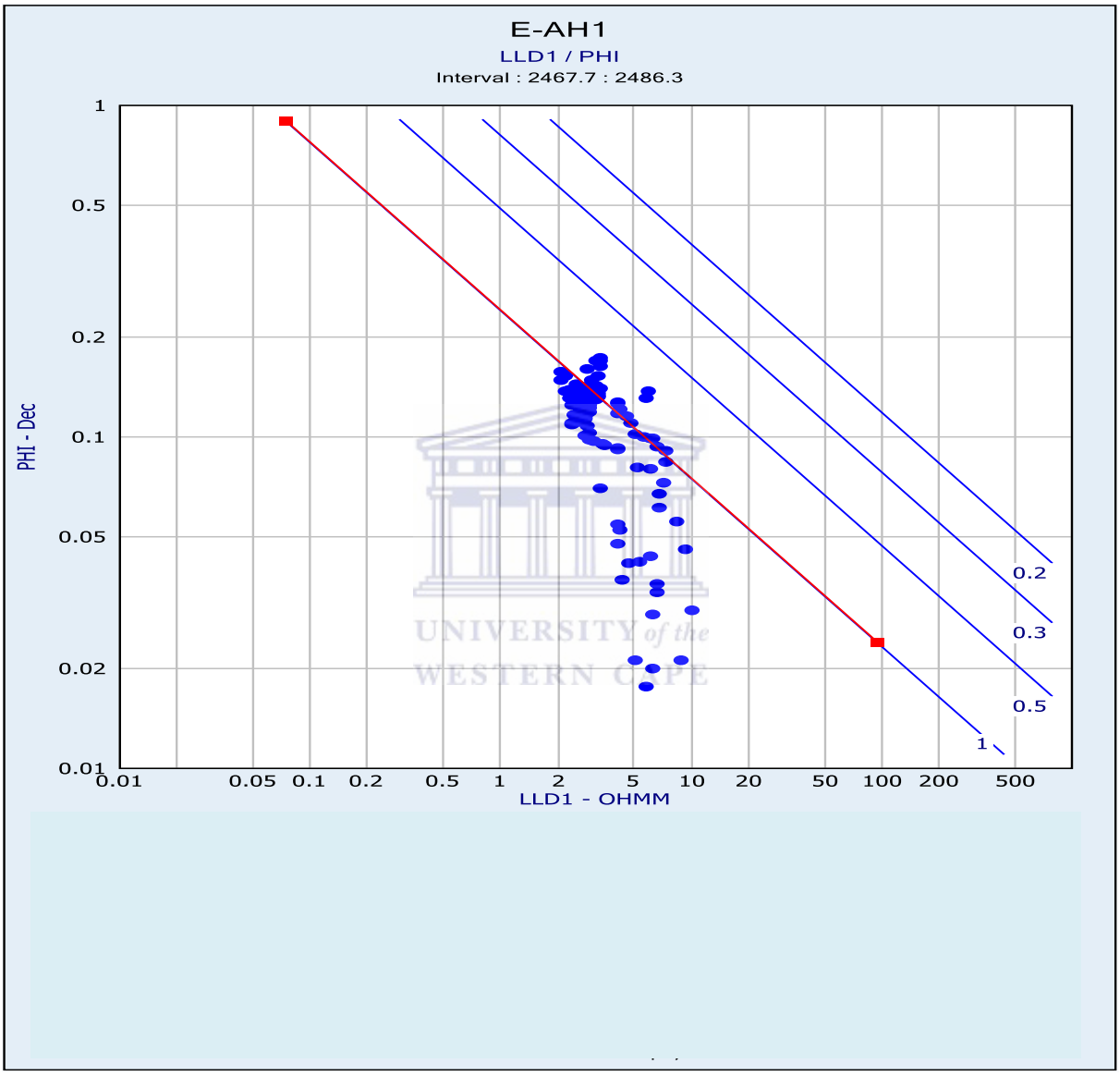

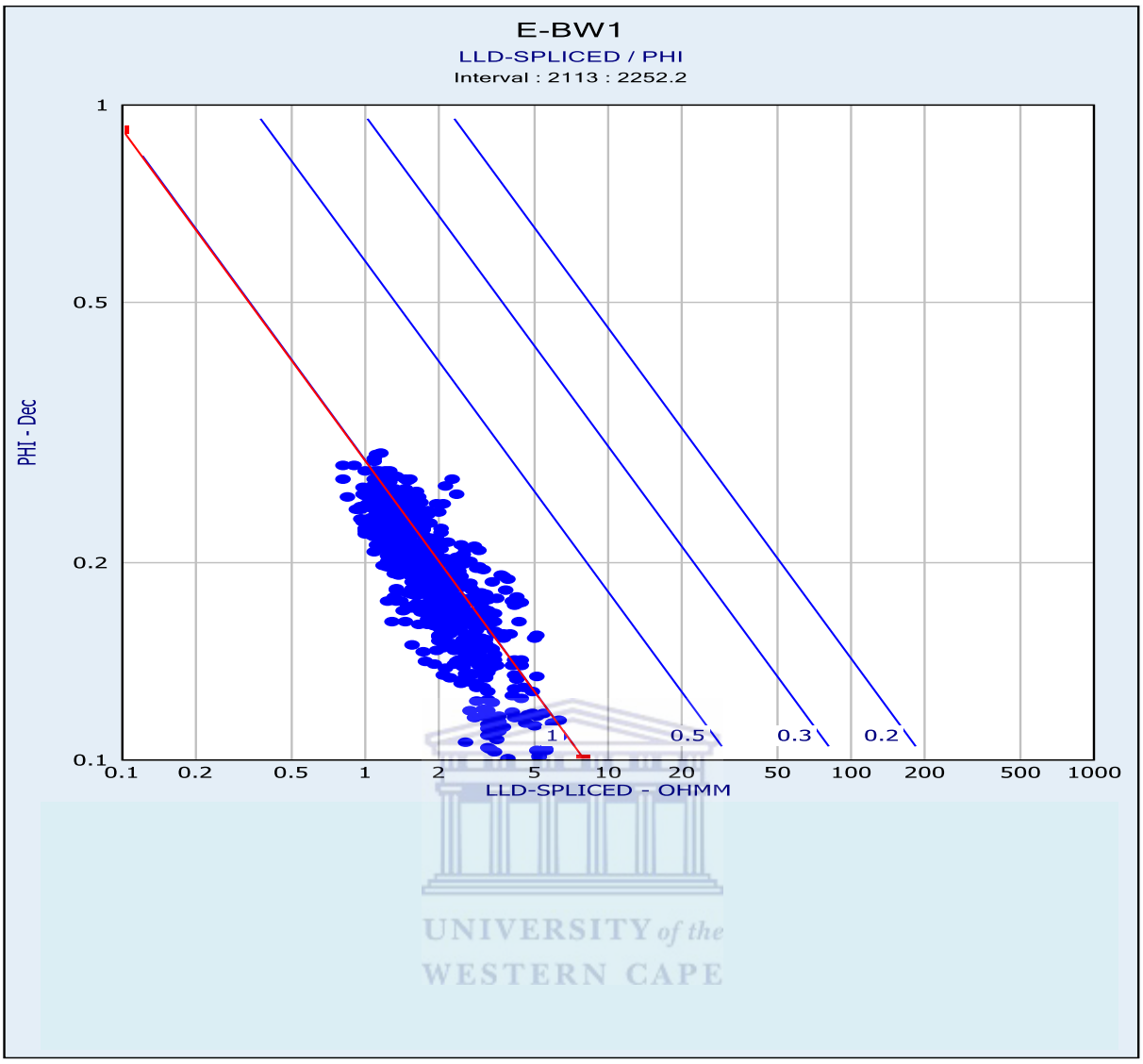

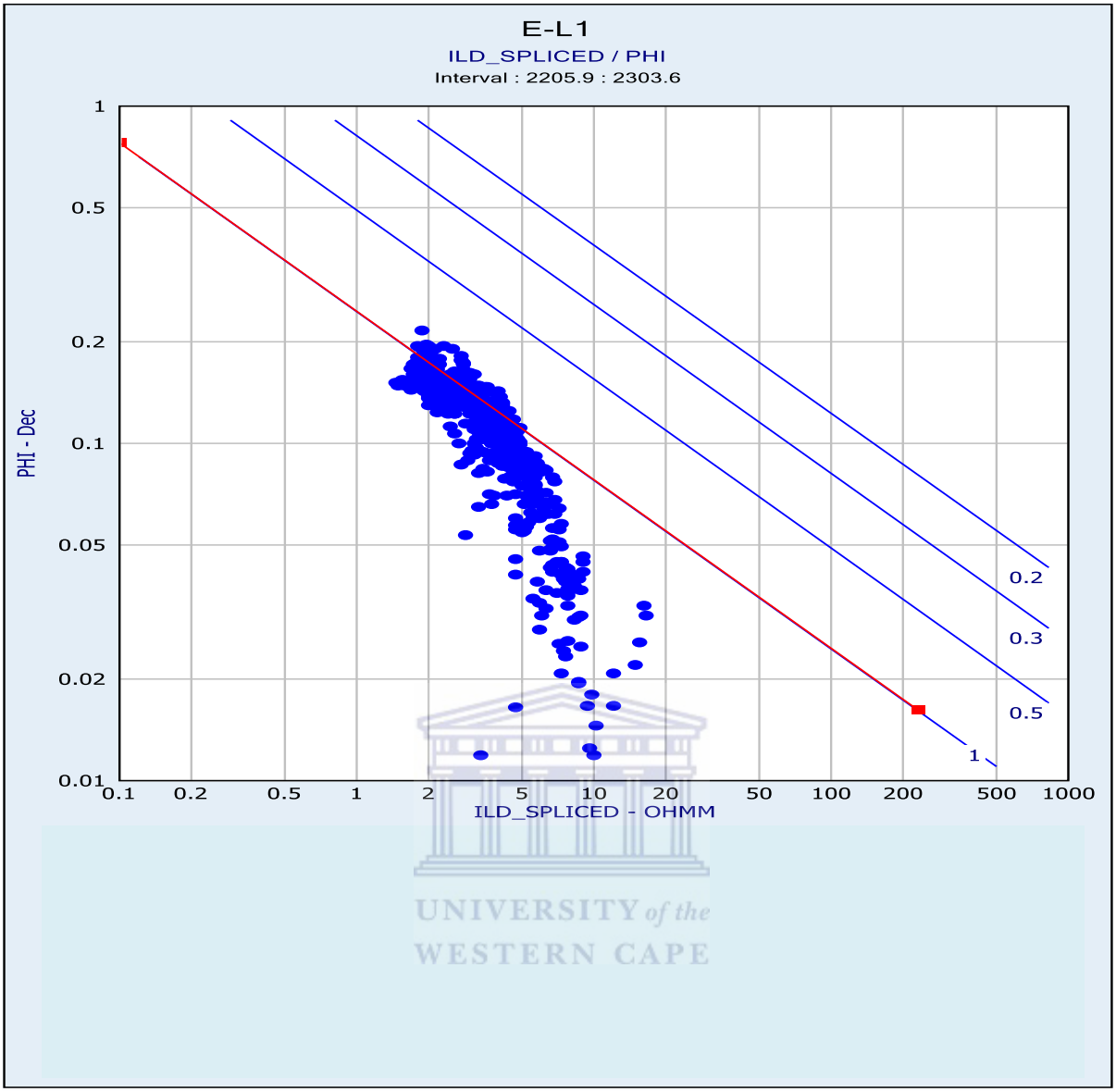

Appendix B. **Gamma ray histogram plots**

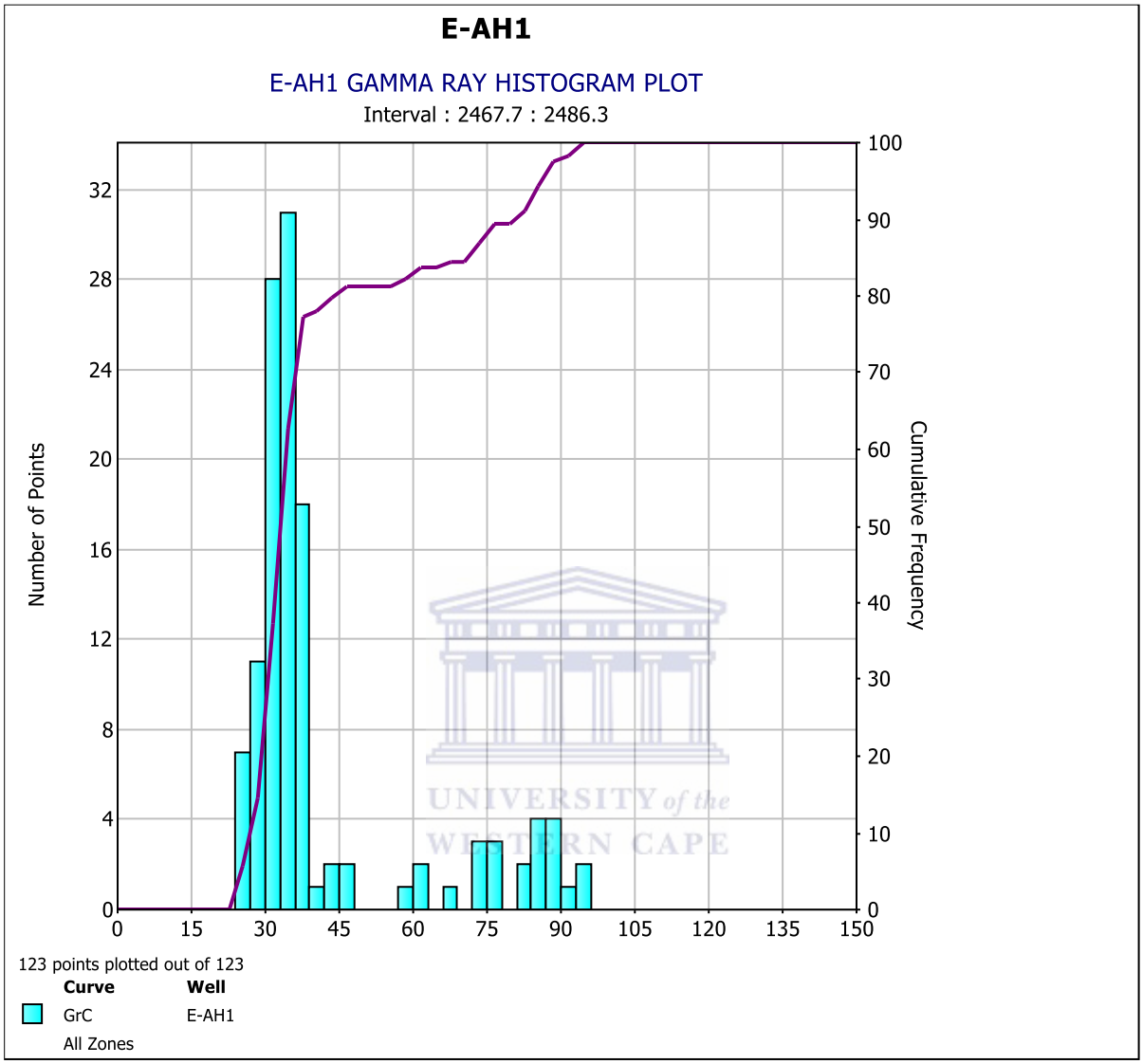

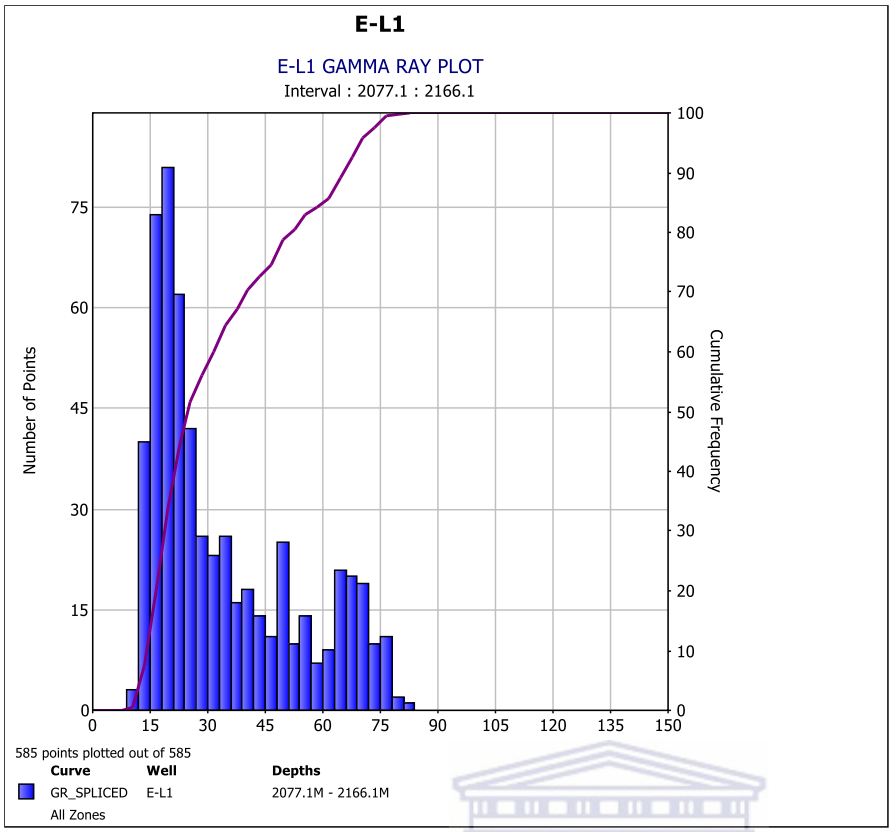

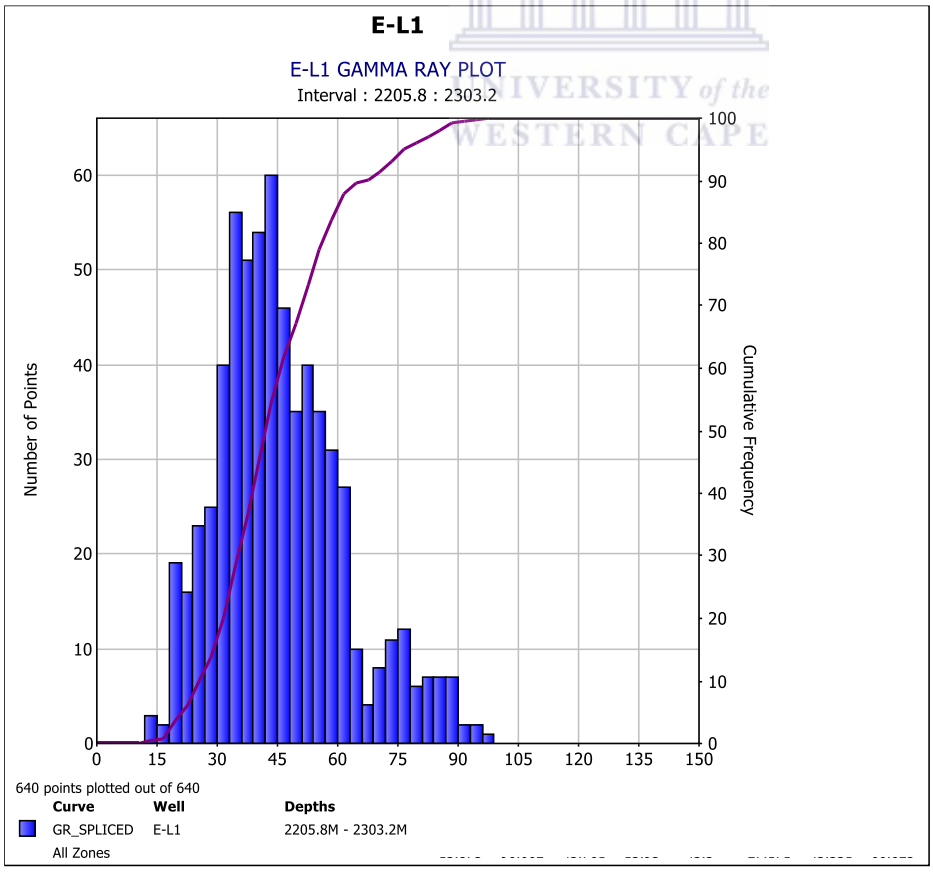

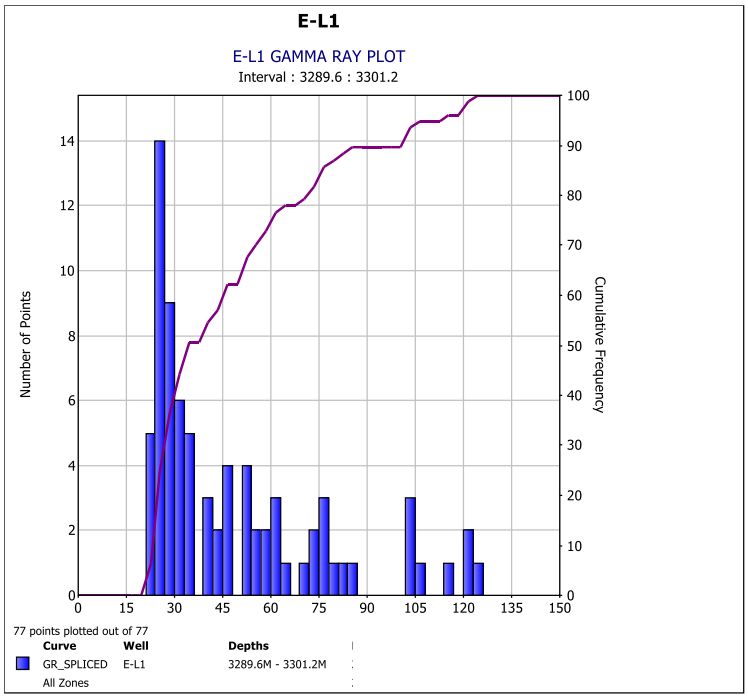

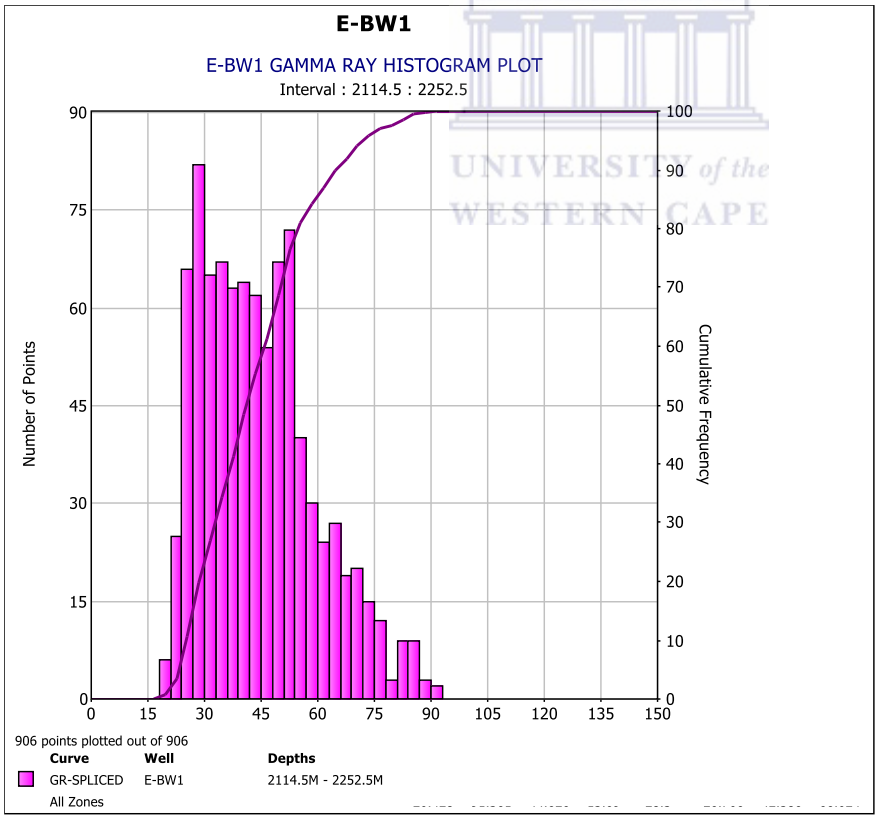

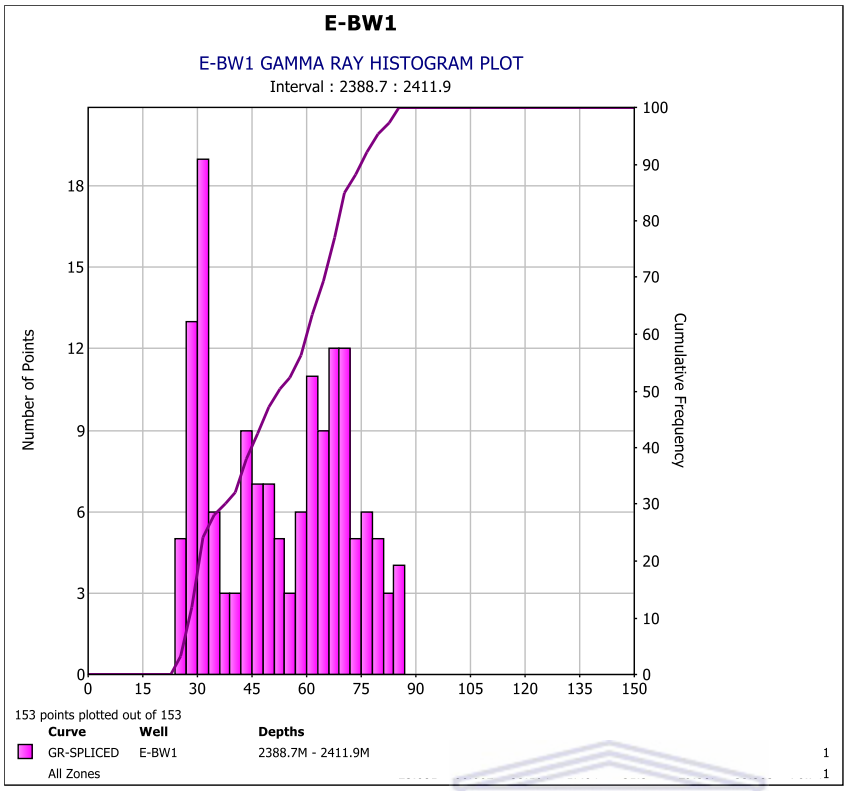

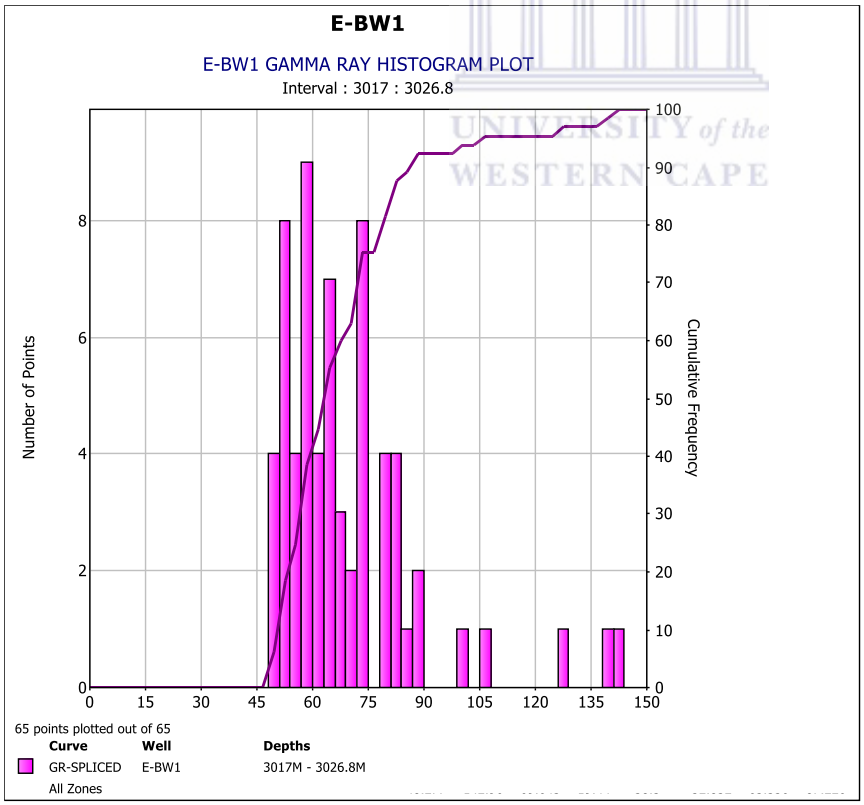

Appendix C. **Calculated volume of clay, Porosity and Water saturation curves**

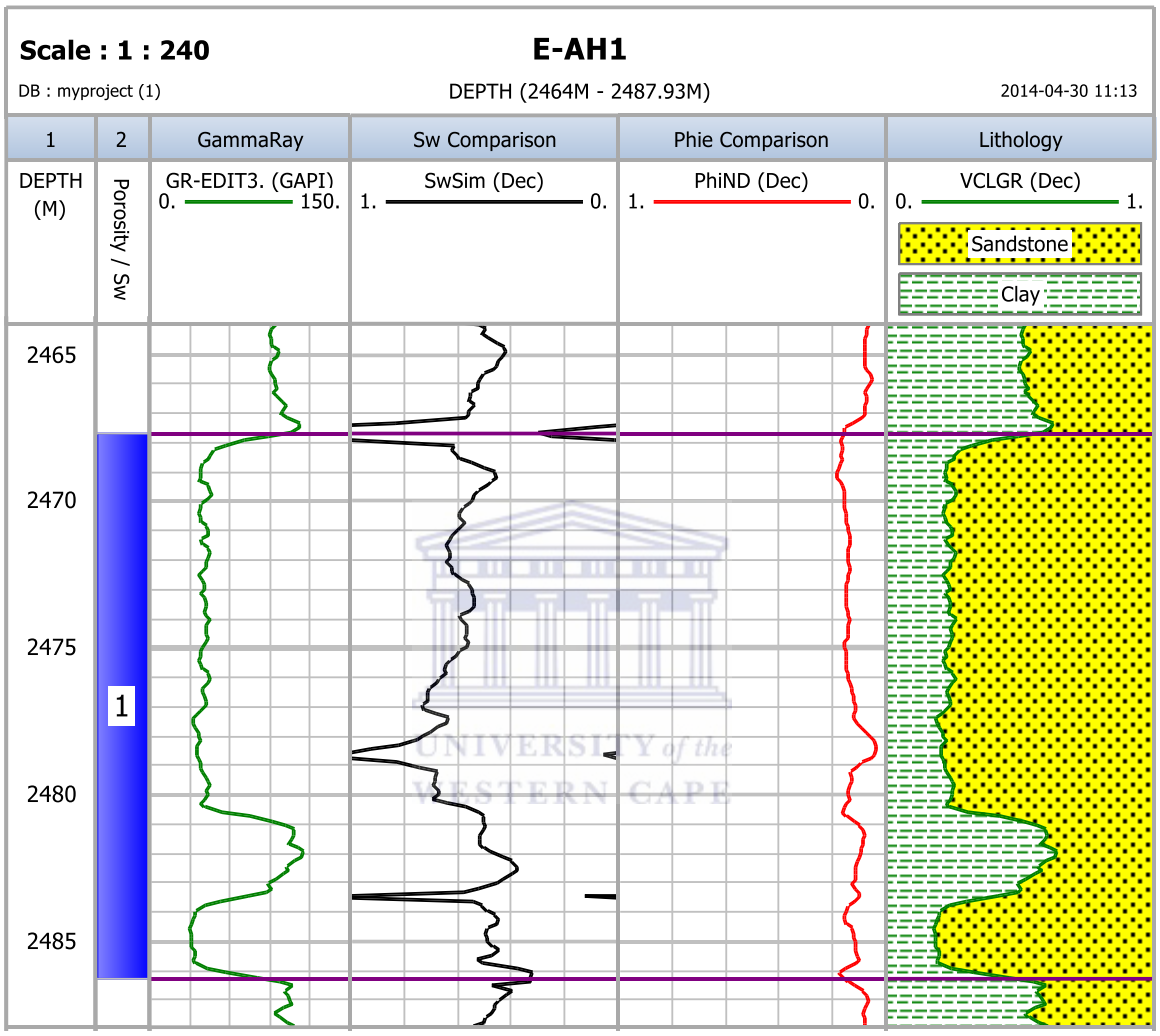

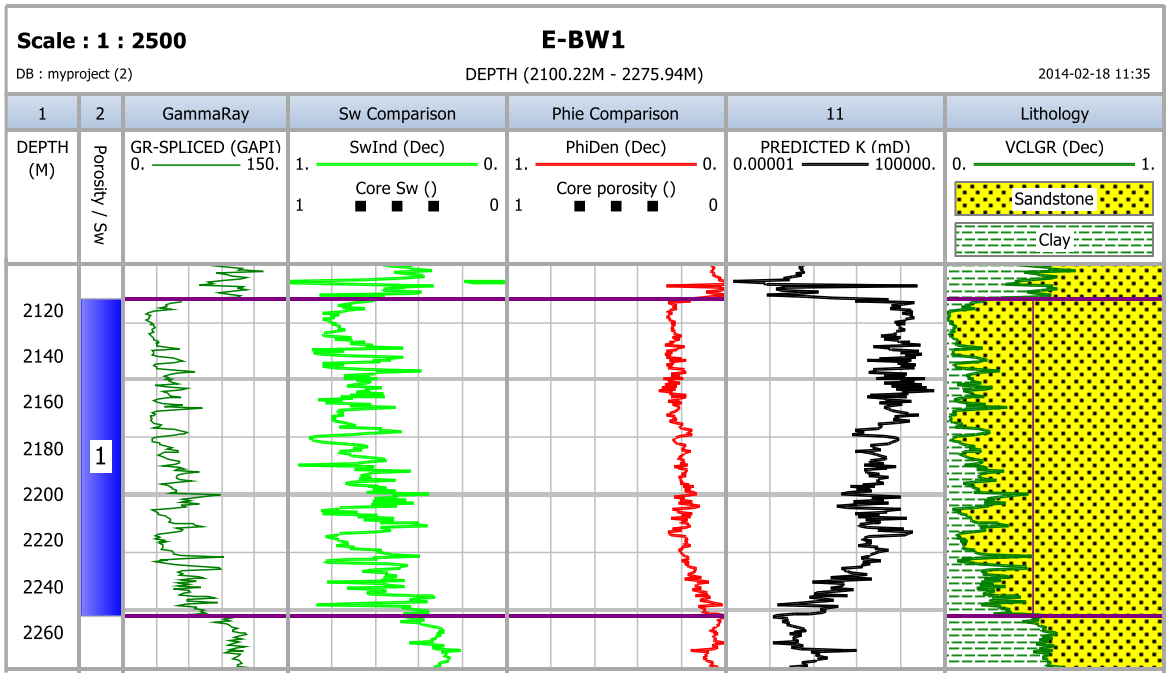
Scale : 1 : 2500
E-BW1
DB : myproject (2)
DEPTH (2100.22M - 2275.94M)
2014-02-18 11:35
1
2
GammaRay
Sw Comparison
Phie Comparison
11
Lithology
DEPTH (M)
Porosity / Sw
GR-SPLICED (GAPI)
0.
150.
SwInd (Dec)
1.
0.
Core Sw ()
1
0
PhiDen (Dec)
1.
0.
Core porosity ()
1
0
PREDICTED K (mD)
0.00001
100000.
VCLGR (Dec)
0.
1.
Sandstone
Clay
2120
2140
2160
2180
2200
2220
2240
2260
1

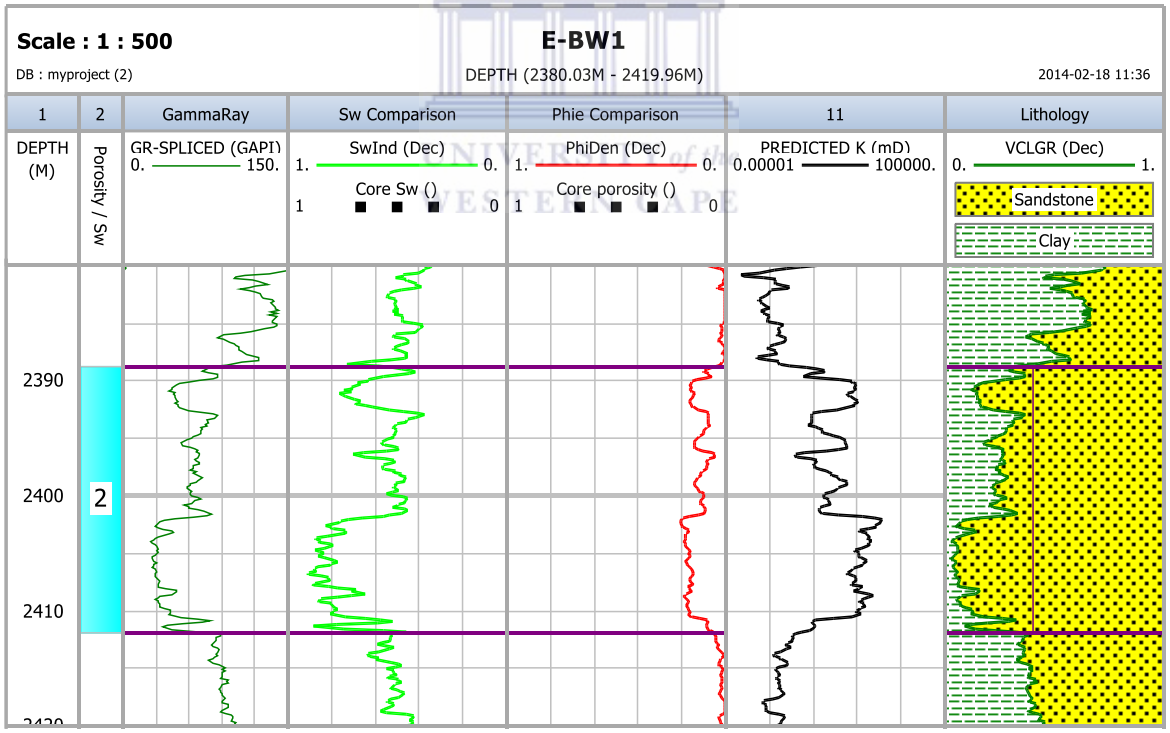
Scale : 1 : 500
E-BW1
DB : myproject (2)
DEPTH (2380.03M - 2419.96M)
2014-02-18 11:36
1
2
GammaRay
Sw Comparison
Phie Comparison
11
Lithology
DEPTH (M)
Porosity / Sw
GR-SPLICED (GAPI)
0.
150.
SwInd (Dec)
1.
0.
Core Sw ()
1
0
PhiDen (Dec)
1.
0.
Core porosity ()
1
0
PREDICTED K (mD)
0.00001
100000.
VCLGR (Dec)
0.
1.
Sandstone
Clay
2390
2400
2410
2
UNIVERSITY of the
WESTERN CAPE

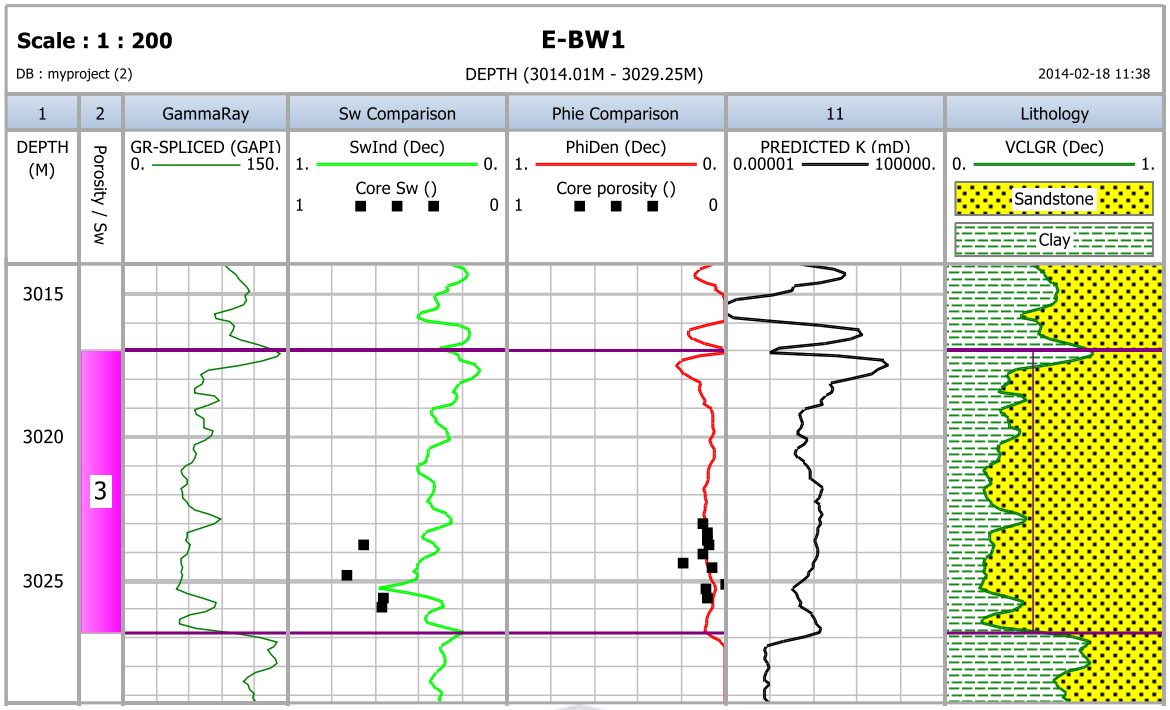

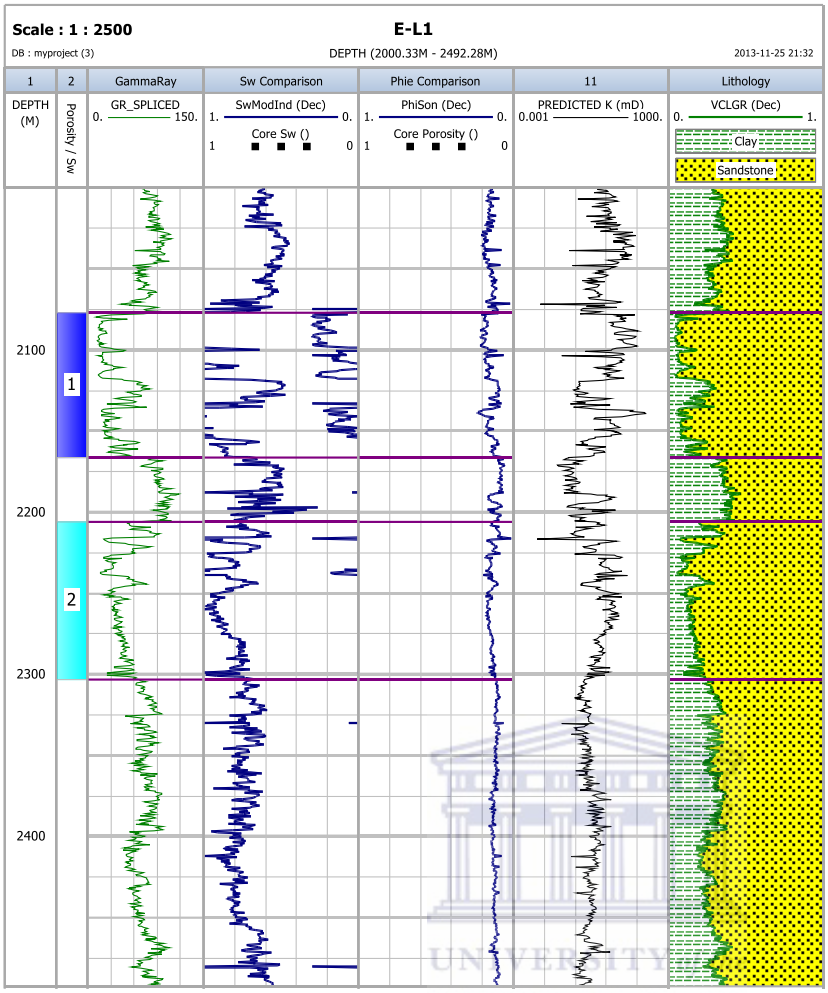

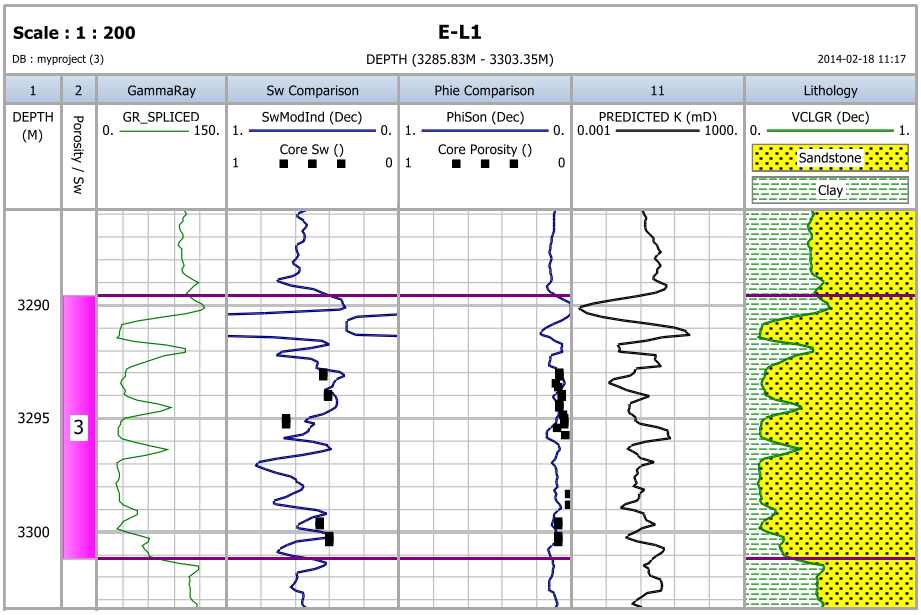

Appendix D. **Wells corelation**

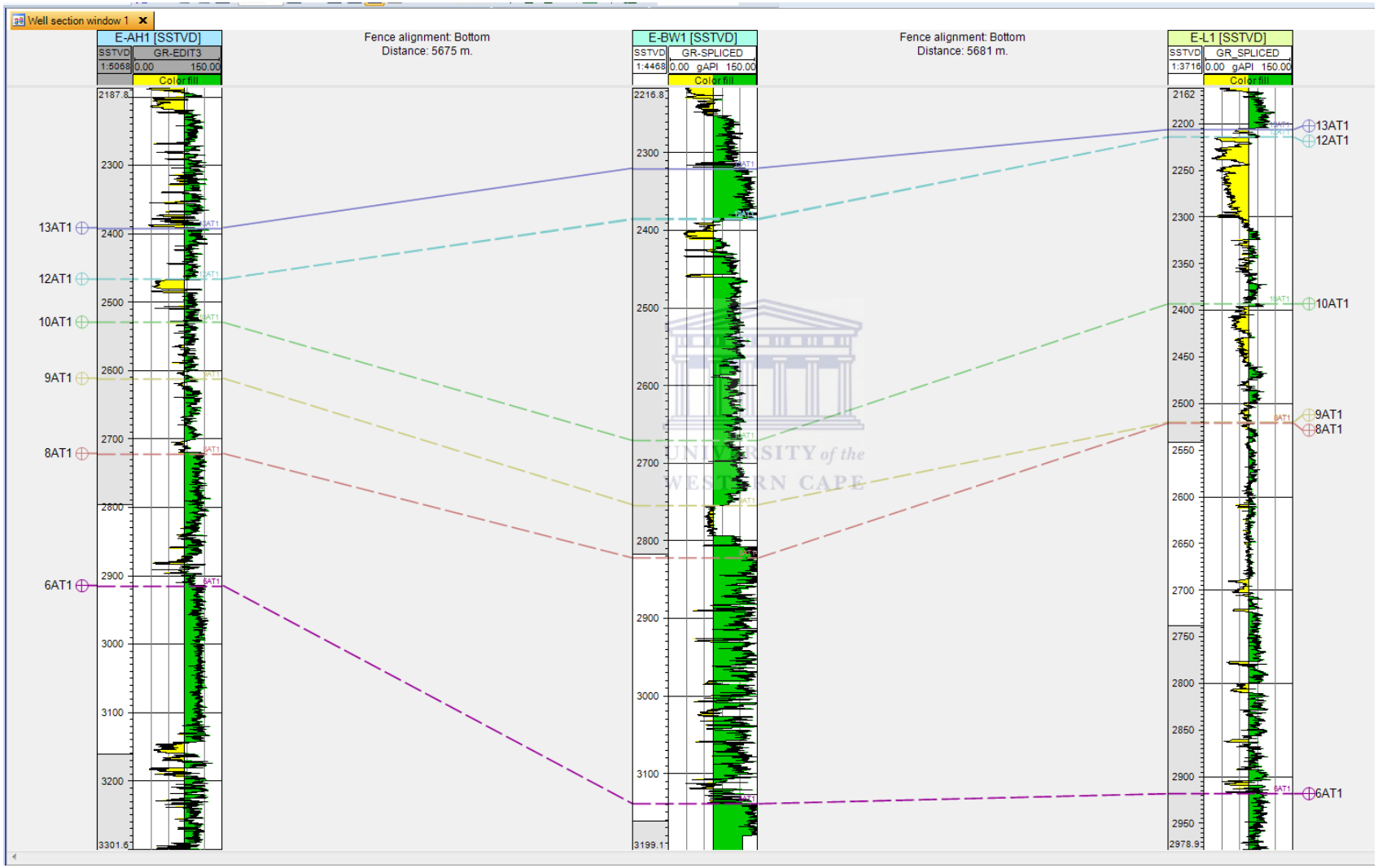

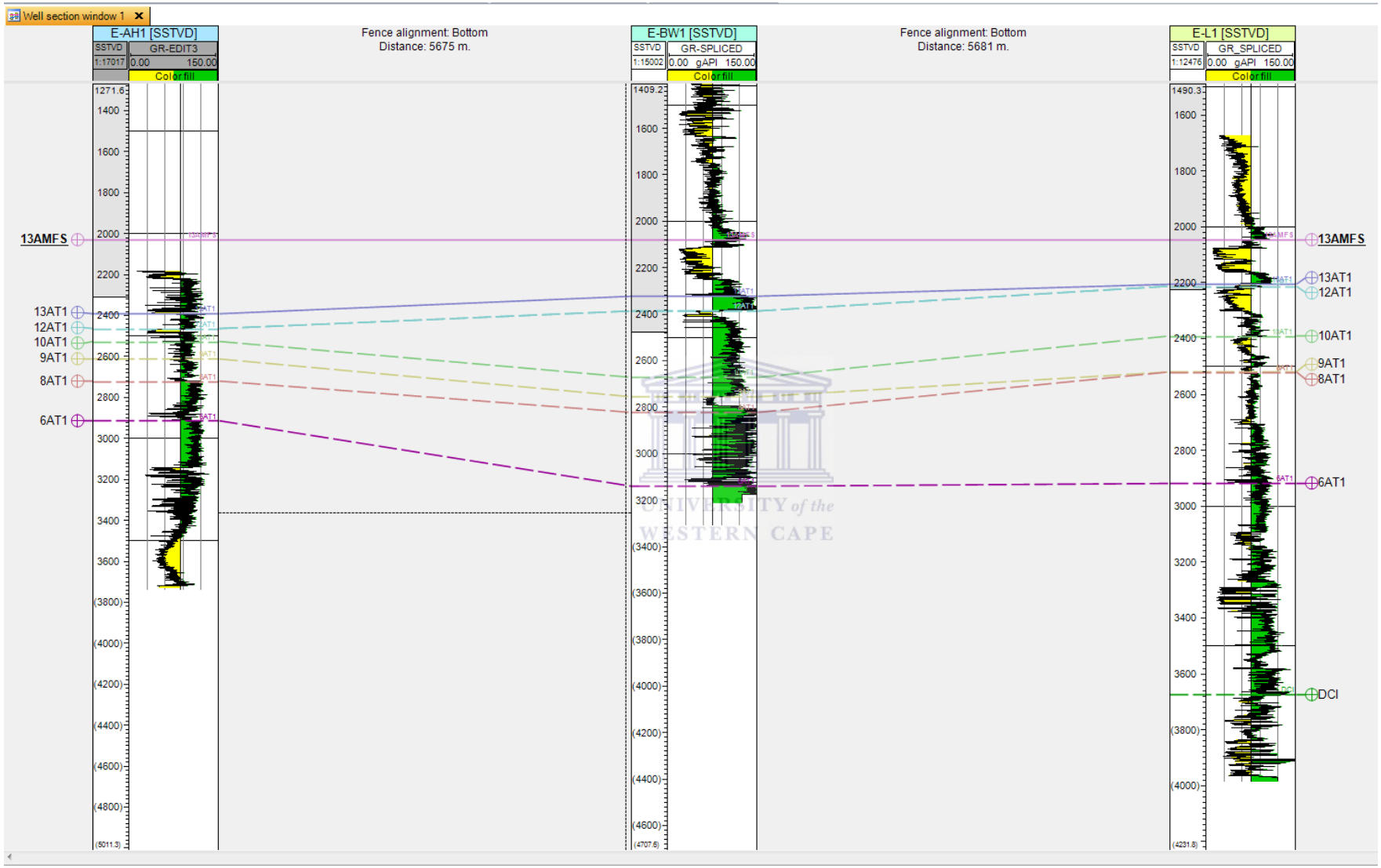

Appendix E. **Storage and flow capacity calculations**

Well E-AH1.

Storage capacity = net thickness *porosity = 37*14.3= 529.1scf

Flow capacity =net thickness * permeability =37*33=1221mD-ft

Well E-BW1.

Reservoir 1

Storage capacity = net thickness *porosity= 214.4*18.0=3852scf

Flow capacity= net thickness * permeability=214.4*3.95=846.9mD-ft

Reservoir 2

Storage capacity = net thickness *porosity= 37*10.7= 395.9scf

Flow capacity= net thickness * permeability=37*2.27=83.99mD-ft

Reservoir 3

Storage capacity = net thickness *porosity= 26.5*10.5= 278.25scf

Flow capacity= net thickness * permeability=26.5*0.21=5.6mD-ft

Well E-L1

Reservoir 1

Storage capacity = net thickness *porosity= 39*9.7= 378.3scf

Flow capacity= net thickness * permeability=39*79=3081mD-ft

Reservoir 2

Storage capacity = net thickness *porosity= 21.5*9.4= 202.1scf

Flow capacity= net thickness * permeability=21.5*1.95=41.925mD-ft

Reservoir 3

Storage capacity = net thickness *porosity= 19.7*9.3=183.21scf

Flow capacity= net thickness * permeability=19.7*0.14=2.758mD-ft

Appendix F. Reservoir hydrocarbon volume in acre foot of rock calculations

WELL E-AH1

N= 43.560*14.3* (1-0.551)

=279,685 cubic feet

WELL E-BW1

Reservoir 1

N=43.560*18.0* (1-0.555)

=348, 92 cubic feet

Reservoir 2

N=43.560*10.7* (1-0.519)

=224.19 cubic feet

Reservoir 3

N=43.560*10.5* (1-0.0.258)

= 339.38

WELL E-L1

Reservoir 1

N=43.560*9.7* (1-0.553)

=188.87 cubic feet

Reservoir 2

N=43.560*9.4* (1-0.616)

=157.23 cubic feet

Reservoir 3

N=43.560*9.3* (1-0.499)

=202.96 cubic feet

Appendix G. **Core photographs**

G.1. WELL E-AH1 CORE PHOTOGRAPH (PASA, 1989)

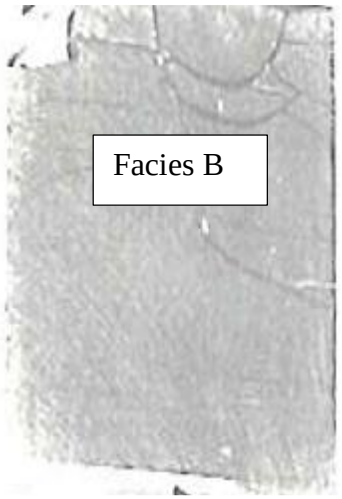

G.2. WELL E-L1 CORE PHOTOGRAPH (PASA, 1989)